The effect of the circadian clock on the mechanism of gouty inflammation

Dmitry Popov

School of Medical Sciences

Faculty of Medical and Health Science

The University of Auckland

New Zealand

A thesis submitted in partial fulfillment of the requirements for the degree of Master of Science in Pharmacology, The University of Auckland, 2022

In the loving memory of Isupov Vladimir Vasilievich

Abstract

Background: Circadian oscillators are present in every tissue of the body and synchronized by both external and endogenous signals to regulate physiological functions of the body and maintain tissue homeostasis. Multiple studies suggested that proteins encoded by circadian clock genes affect the development and/or the severity of chronic inflammation that causes a variety of diseases such as rheumatoid arthritis, atherosclerosis and colitis. However, no studies yet demonstrated involvement of circadian clocks of immune cells in development of gout attacks, despite the fact that gout attacks are known to be time-of-day dependent.

Aims: To determine whether MSU (monosodium urate crystals) crystal exposure resulted in a change in expression of circadian clock components in the THP-1 monocyte/macrophage-like cell model and whether specific components of the clock (REV-ERBa and BMAL1) influenced MSU crystal-induced NLRP3 (nucleotide-binding domain (NOD)-like receptor protein 3) inflammasome activity in THP-1 cells.

Methods: THP-1 and PMA-differentiated THP-1 macrophage-like cells were treated +/-MSU crystals over 24h time-course and the expression of the full range of core circadian genes (*CLOCK* (circadian locomotor output cycles kaput), *BMAL1* (brain and muscle Arnt-like protein-1), *REV-ERBa, CRY1/2* (cryptochrome 1/2), *PER1/2/3*) was measured by RT-qPCR. The protein levels of core circadian clock component REV-ERBα and TLR4 (Toll-like receptor 4) were measured by Western blot. The activity of NLRP3 inflammasome complex was measured by Caspase-1 Glo assay in THP-1 cells treated with heme (a REV-ERBa agonist), SR-8278 (REV-ERBa antagonist) and prednisolone in the presence/absence of MSU crystals. The assessment of cell numbers was done by using Cyquant GR dye.

Results:

Time had a significant effect on the expression of *BMAL, REV-ERBa, CRY1* and *PER1* in both cell types. The treatment with MSU crystals resulted in a time-dependent reduction of *REV-ERBα* in monocytes and altered expression of *REV-ERBα* and *CRY1* in macrophage-like cells in a time-dependent manner. Overexpression of BMAL1 led to reduction in NLRP3 inflammasome activity in both cell types in the presence of MSU crystals, yet in the absence of MSU crystals BMAL1-overexpression increased NLRP3 activity. Knockdown of BMAL1 induced the expression of NLRP3 inflammasome in both THP-1 cell lines in the presence of MSU crystals, however, NLRP3 activation was decreased in the absence of MSU crystals. Heme and prednisolone treatment demonstrated cell- and time- dependent regulation of NLRP3 activity. The effects of heme were mediated in part via alteration in REV-ERBα activity as well as other regulatory mechanisms.

Conclusions:

Our findings suggest that alternations in the expression of a core circadian components such as *REV-ERBα* produce an effect on MSU-induced inflammatory response in THP-1 monocytes/macrophages-like cells. Furthermore, the result from this study demonstrated that both REV-ERBα and BMAL1 regulate the activity of MSU-induced NLRP3 inflammasome, however, the exact mechanism of their anti-inflammatory activity is yet to be identified.

Acknowledgments

I would like to express my deepest gratitude first and foremost to my primary supervisor Dr Raewyn Poulsen for the enormous support and guidance during my Master's research project. Thank you so much for taking me on board and giving me a chance to do this research project under your supervision, you are the best supervisor.

I am also extremely grateful to my co-supervisor Dr Lekha Jain for being so supportive and encouraging. Thank you for all your support in the lab and all your valuable contribution during the writing process, it meant a lot to me. I would like to extend my sincere thanks to Mariam Alhilali who was teaching me laboratory work from the first day throughout the whole year. Thank you for helping me with experimental design and sharing my troubles and strife in the work with the THP-1 cells. Many thanks to Bianca Nijmeijer, Taryn Green and James Hearn who guided me around the lab and gave me valuable life-advice.

I am very grateful that I had such amazing and knowledgeable people who supported me throughout the entire project. I could not have undertaken this journey without you.

Finally, I must express my very profound gratitude to my parents and to my girlfriend for providing me with unfailing support and continuous encouragement throughout my years of study and through the process of researching and writing this thesis. This accomplishment would not have been possible without them. Thank you.

Table of Contents

List of Figures

List of Tables

Abbreviations

ACTB	Actine-(β)beta
ANOVA	Analysis of variance
cDNA	Complementary DNA
C_T	Threshold cycle
DEPC	Diethylpyrocarbonate
DMSO	Dimethylsulfoxide
DNA	Deoxyribonucleic acid
dNTP	Deoxynucleotide triphosphates
DTT	DL-Dithiotheitol
FBS	Fetal bovine Serum
xg	Times gravity
GFP	Green Fluorescent Protein
HBSS	Hank's Balanced Salt Solution
M	Mole
MOI	Multiplicity of infection
N	Sample size
NaOH	Sodium hydroxide
Opti-MEM	Reduced-Serum Medium
P	*p*-value
PBS	Phosphate buffered Saline
PMSF	Phenylmethylsulfonyl fluoride

RIPA	Radioimmunoprecipitation Assay
RNA, mRNA	Ribonucleic acid, messenger RNA
rpm	Revolutions per minute
RPMI	Roswell Park Memorial Institute (culture medium)
RT-qPCR	Real-time polymerase chain reaction
SEM	Standard error of the mean
siRNA	Short-interfering RNA

1.0 Literature Review

1.1 Introductory Statement

Gout is one of the most common, debilitating forms of inflammatory arthritis in the world. Acute gout is a disabling and painful condition that is associated with an increased risk of serious chronic conditions such as renal and cardiovascular diseases (Ragab et al, 2017). Gouty arthritis is an increasing public health problem in Aotearoa/New Zealand with the highest prevalence in the world (Dalbeth et al., 2018). There is a high prevalence particularly in Māori and Pacific Island men as approximately one-third of Māori men and a quarter of Pacific Island men aged 65 years and over have diagnosed gout (Dalbeth et al., 2018). Although there are pharmacological treatments that help limit the progression of the disease, gout still remains incurable. The pathogenesis of gouty inflammation is relatively well understood, however, there is a clear need for a better understanding of the reason and mechanism of sudden gout flares in order to develop novel treatment strategies or improve existing ones.

Gout flares are episodes of acute inflammation, characterized by activation of the NLRP3 (nucleotide-binding domain (NOD)-like receptor protein 3) inflammasome by urate crystals in the joint cavity and subsequent release of pro-inflammatory cytokines (Kingsbury et al., 2011). Gout flares are frequently initiated during early morning or at night. The timing of gout flares could potentially provide a clue to their origin. It is now known that the activity of NLRP3 inflammasome, synthesis of inflammatory cytokines and trafficking of immune cells normally differ rhythmically over the course of a day (Pick, He, Chen, & Scheiermann, 2019). This rhythmic pattern is driven by a cell signalling circuit known as the circadian oscillator. The circadian oscillator is present in almost every cell in the body, including immune cells. It has recently been demonstrated that the loss of circadian oscillations in NLRP3 inflammasome signalling triggers inflammasome activation and release of pro-inflammatory cytokines such as IL-1β (interleukin 1 beta) and IL-6 (interleukin 6) , potentially contributing to the development of chronic inflammatory diseases (Pourcet & Duez, 2020). Recent studies suggested that altered expression of proteins encoded by circadian clock genes affects the development or induces the severity of chronic inflammation that causes a variety of diseases such as rheumatoid arthritis, atherosclerosis and osteoarthritis (Buttgereit et al., 2015; Chalfant et al., 2020; Kc et al., 2015). Whether altered core circadian oscillator components in immune cells contribute to gout flares is yet to be determined. Therefore, the focus of this thesis is to determine whether or not an alteration in circadian oscillator components in immune cells contributes to the development of acute gouty inflammation.

1.2 Gout

Gout is an extremely painful form of arthritis. It is characterised by intermittent attacks of excruciating pain, redness, swelling and tenderness in one or multiple joints. A gout attack is a result of an innate immune reaction to monosodium urate crystals (MSU) which accumulate within affected joints ***(Figure 1.1)*** (Dalbeth & Haskard, 2005)**.** Attacks can be so painful that the victim is unable to tolerate even the touch of a bed sheet on the affected joint. The attacks can last anywhere from several hours to several weeks without the administration of anti-inflammatory medication. There are two main types of gout: acute and chronic. Acute gout is characterized as a painful condition that commonly affects 1-3 joints and symptoms only present during the attack. Chronic gout occurs if acute gout is left untreated therefore allowing the disease progresses to a chronic state. It is characterised by a higher frequency of intermittent attacks of extreme pain as well as a feeling of a low-level constant pain the majority of the time. Chronic gout could lead to the progression of severe disability due to the formation of tophi (large accumulation of insoluble MSU crystals) in the cartilage of the joints (Brook et al, 2010). The tophi cause irreparable joint damage as well as being visually distressing ***(Figure 1.2).***

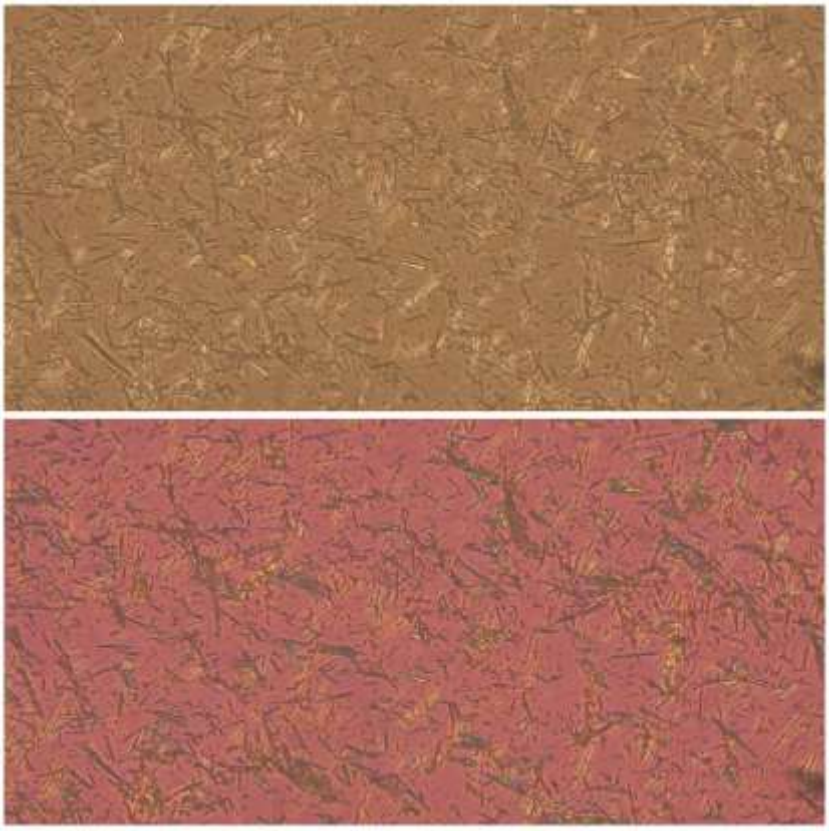

Figure 1.1 MSU crystals. Visualised under the microscope in x20 in a normal and polarised field.

Figure 1.2 Photo of chronic tophaceous gout in a toe. Obtained with informed patient consent by Prof Nicola Dalbeth.

1.2.1 History

Gout appeared in the history of medical writing several thousand years ago. The disease was first observed as early as 2640BCE by Egyptian doctor Imhotep who recorded evidence of gouty lesions within the joints (Schwartz, 2006). Gout was also described by the father of modern medicine, the Greek physician Hypocrates who referred to it as "the unwalkable disease" (Nuki & Simkin, 2006). The prominence of gout in historical medical writing is due not only to its incidence but also due to its prevalence among the famous and wealthy people at that time. Gout was known as "disease of lords and lord of diseases" as it was restricted to the circles of high society as they had a lifestyle that allowed them to have access to rich food and alcohol. Several famous historical figures such as King Henry VIII, Leonardo DaVinci and Benjamin Franklin were affected by this disease. In addition, the familial inheritance of gout also served to solidify the belief that gout was only a disease of "high living".

1.2.2 Epidemiology

In the modern age, gout is no longer restricted to the high social status and people from the full range of socioeconomic groups suffer from this common systemic disease. Recent reports of gout's incidence and prevalence vary extensively depending on the methods employed and the population studied, however, it

ranges from a prevalence of <1-6.8% and an incidence rate of 0.58-2.89/1000 person-years (Dehlin et al., 2020). The statistical reports show that some countries are affected by gout more than others. In fact, Aotearoa/New Zealand has the highest prevalence of gout in the world. The prevalence of gout in Aotearoa/New Zealand impressively increased from 3.8% to 6% in adults over 20 years old in past 7 years (2012-2019) (Dalbeth et al., 2018). Gout is over three times more prevalent in men than in women and prevalence also increases significantly with age and ethnicity (Kuo et al., 2015). Māori and Pacific people have 2-3 times higher prevalence than New Zealanders of European descent and one-third of Māori men and a quarter of Pacific Island men aged >65 years have been diagnosed with gout (Dalbeth et al., 2018). Despite increasing incidence and prevalence of gout worldwide, there is still suboptimal management of the disease.

1.2.3 Risk factors

1.2.3.1 Hyperuricemia

The greatest risk factor for the development of gout is uric acid concentration in the blood. The levels of uric acid fall into the range of 3.4-7mg/dL in men and 2.4-6.0 mg/dL in women (Crawley et al., 2022). When the levels of uric acid in blood exceed 7mg/dL, clinical hyperuricemia is diagnosed as uric acid approaches its solubility limit (Diseases & Section, 1960). Uric acid is a weak acid that has a pH of 5.8 and it's made in the body as a breakdown product of purines. There are two types of purines: endogenous and exogenous. Endogenous purines are made by the body and are essential building blocks for DNA (deoxyribonucleic acid) and RNA (ribonucleic acid) and therefore involved in the synthesis of enzymes and other proteins. The rate of synthesis or breakdown of purines can be increased due to cell damage, necrosis, surgery or alcohol consumption. Exogenous purines are obtained by the body through foods that are high in purines such as meat and seafood. Serum uric acid concentration in the body is determined by the balance of exogenous and endogenous purine production and excretion by the kidneys and gastrointestinal tract ***(Figure 1.3).*** Only 10% of gout cases are caused by overproduction of uric acid, and the remaining 90% of cases are caused by renal under-excretion of uric acid (Mandal & Mount, 2015).

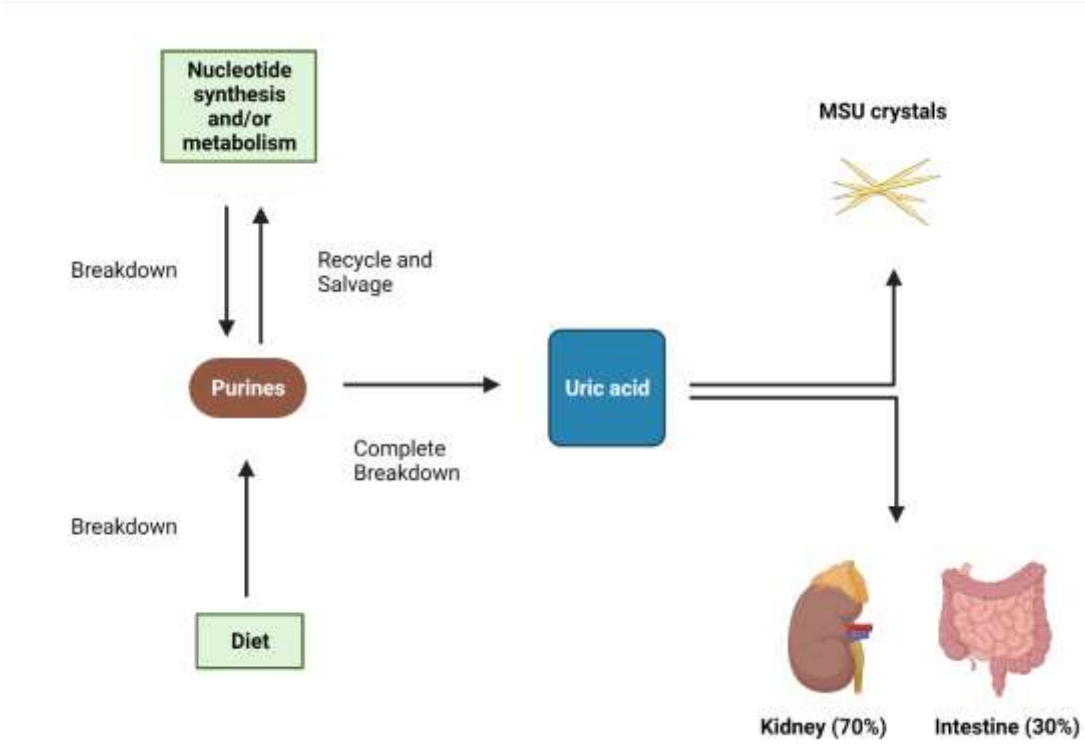

Figure 1.3 Schematic representation of simplified uric acid production and excretion. Purines obtained from both metabolic and dietary sources contribute towards the total amount of exogenous and endogenous purines in the body. The concentration of uric acid is determined by the balance between endogenous and exogenous purines and their excretion by the kidney (70%) and intestine (30%). The disruption in uric acid excretion results in the formation and accumulation of MSU crystals in the joint. Figure created by Dmitry Popov based on information in (Ragab et al., 2017) using Biorender software.

1.2.3.2 Diet

Exogenous purines that come from the diet are a significant contributor to the levels of uric acid in the blood. The intake of purine-rich foods such as cooked or processed food from seafood or animal origin could lead to elevated serum urate levels and potentially the development of gout flares (Kanbara & Seyama, 2011). Foods rich with purines include seafood (trout, sardines), red meat (beef, pork), mushrooms and beer. On one hand, multiple prospective studies demonstrated that individuals with high seafood/meat intake have significantly increased uric acid levels and are potentially at the highest risk of gout development (Zhao et al., 2016). However, on the other hand, studies also showed that hyperuricemia (>7mg/dL) is a risk factor for gout, however, it doesn't necessarily induce gout as a large proportion of individuals with hyperuricemia never experienced a gout attack in comparison to individuals with gout who have normuricemia (Zhang, 2021). Other foods associated with gout development, include alcoholic beverages and fructose. Fructose is one of the main components in soft drinks and a major contributor to serum uric acid levels due to its interference with ATP (adenosine 5'-triphosphate) recycling. Fructose causes ATP to be converted into AMP (adenosine monophosphate) and then subsequently degraded into uric acid. Intake of alcoholic

beverages also leads to an increase in purines breakdown due to high ATP turnover during ethanol metabolism (Kanbara & Seyama, 2011).

1.2.3.3Gender

Gender is another important risk factor in gout. Gout appears to be a predominantly male disease as the estimated prevalence in men is 5.9% compared to 2% in women (Singh, 2013). The incidence of gout in men 4 times higher than in women at age <20 years old. The significant difference in incidence and prevalence between the genders is believed to be due to the uricosuric effects of estrogen (Nicholls et al., 1973). Estrogen reduces the concentration of uric acid in serum by suppressing the protein levels of urate re-absorptive transporters such as URAT1 (uric acid transporter 1) and GLUT9 (glucose transporter 9) in kidney tubules. In addition, testosterone is known to induce the expression of URAT1 which further implicates the role of sex hormones in the development of gout (Takiue et al., 2011).

1.2.3.4 Genetics associated risk

Genetics play an important part in the risk of gout development. Since endogenous overproduction of purines is quite rare, genetic risks are most likely to be due to differences in uric acid renal excretion. Previous studies found two genes and their proteins (URAT1 and GLUT9) that play a crucial role in the regulation of uric acid in the blood (Preitner et al., 2009). Both of these proteins are involved in the reabsorption of uric acid following glomerular filtration in the kidney. *SLC22A12* (solute carrier family 22) gene encodes for the renal tubular transporter URAT1 on the apical membrane of renal tubules, while the *SLC2A9* gene encodes for transporter protein GLUT9 in the membrane of renal tubules. Polymorphism in both these genes has been associated with abnormal excretion of uric acid which leads to the development of hyperuricemia and subsequently increases the risk of gout (Kolz et al., 2009). The genetic variations in genes related to uric acid excretion significantly modulate the individual's susceptibility to gout development. Distinctive prevalence and incidence rate of gout across racial populations have indicated that there is indeed a risk factor associated with genetics. However, large scale epidemiological and genetic studies across ethnic populations are yet to be done.

1.2.4 Acute gout pathogenesis

Acute gout is clinically characterized as intermittent episodes of joint inflammation which often affects a single joint. Attacks are scattered by symptom-free periods that have varying duration. High levels of serum uric acid and subsequent accumulation of uric acid in the joint cavity is the cause of gout development. Uric

acid is a ubiquitous and endogenous compound that mostly possesses anti-inflammatory properties. However, accumulation of uric acid in the blood leads to its precipitation within joints where it forms crystals of monosodium urate. MSU crystals are a characteristic feature of gouty joints as their presence stimulates acute inflammation in the joint ***(Figure 1.4)*** (Cronstein & Sunkureddi, 2013). Prior to the first gout attack, MSU crystals precipitate within the joint cavity and trigger activation of local monocytes via TLRs (Toll-like receptors). During the initiation stage, MSU crystals are phagocytosed by monocytes. However, the crystals are resistant to cellular lysis causing damage to lysosomal membranes, and rupture of the phagolysosome triggering oligomerization and assembly of the NLRP3 inflammasome complex. The NLRP3 inflammasome is a crucial component of the innate immune system that controls the activation of the caspase-1 enzyme which mediates activation and secretion of the pro-inflammatory cytokines IL-1β and IL-18 (interleukin 18) in response to cellular damage or microbial infection. NLRP3 inflammasome activation is responsible for the pivotal mechanism of gouty arthritis. Activated NLRP3 inflammasome promotes cleavage of caspase-1 and subsequent activation and release of crucial pro-inflammatory cytokine IL-1β. During the amplification stage, active IL-1β released by the resident monocytes binds to IL-1 (interleukin 1) receptors on the surface of local macrophages and endothelial cells. This induces vasodilation and coordinates the recruitment of neutrophils to accumulated MSU crystals, therefore it drives an episode of an acute gout attack (Liu et al., 2000). There is still little known about the precise mechanisms involved in the recruitment of monocytes and macrophages as well as the mechanisms of NLRP3 activation during gout flares. The acute gout attacks are self-limited and can resolve within a few hours or a few days. Our understanding of the underlying mechanism leading to the resolution of gout flare still remains unclear. Self-limitation is believed to be based on the shutdown of inflammatory response by regulatory events such as apoptotic cell clearance, crystal coating, production of TGFβ1 (transforming growth factor β1) and switching secretion pattern of an inflammatory mediators with maturating macrophages which phagocytosed MSU crystals (Dalbeth & Haskard, 2005). Phagocytosis is considered to be an important mechanism for the resolution of acute inflammation due to the ability of well-differentiated mature macrophages to engulf, digest MSU crystals and express the anti-inflammatory TGF-β1. However, recent studies showed that phagocytosis of crystals by less-differentiated macrophages is associated with the initiation of sterile inflammation and subsequent pro-inflammatory cytokine release (Landis et al., 2002).

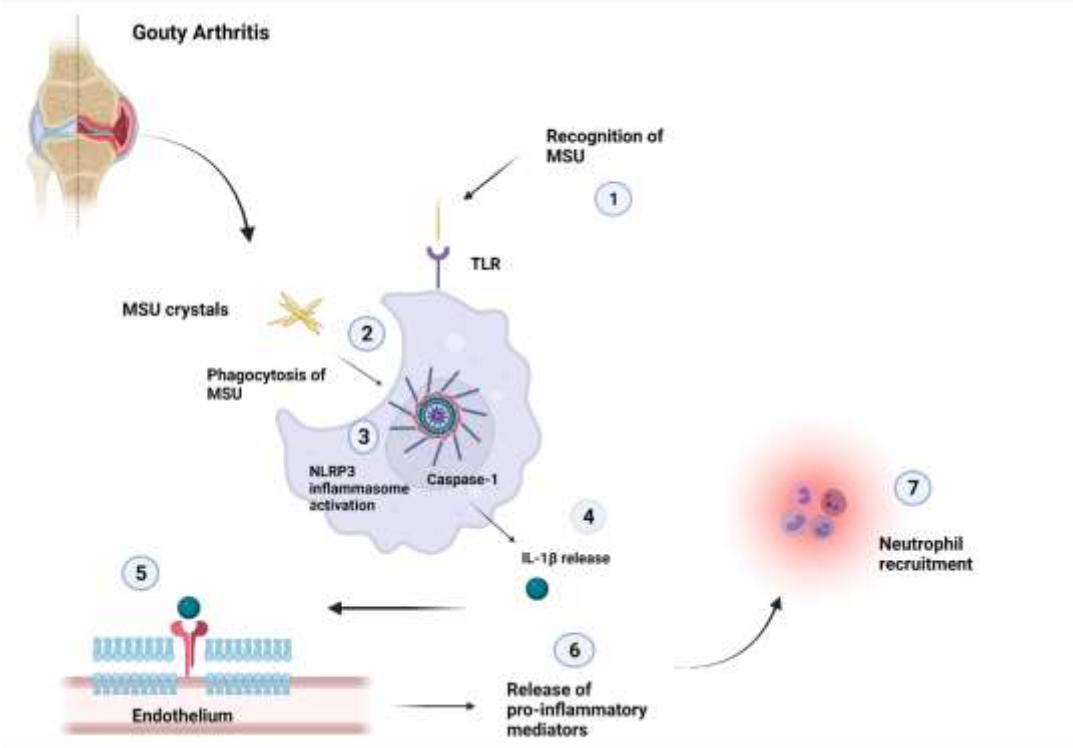

Figure 1.4 Schematic representation of gouty arthritis. Multiple steps are required for the development of acute gout attack. (1) MSU crystals accumulate within the joint cavity and trigger activation of local monocytes via monocyte's expressed extracellular Toll-like receptors. (2) Phagocytosis of MSU crystals. (3) Activation of NLRP3 inflammasome complex. (4) Extracellular release of the crucial pro-inflammatory cytokine IL-1β. (5) Binding of IL-1β to the endothelial receptor to modulate cell adhesion. (6) Release of other pro-inflammatory mediators from leukocytes. (7) Recruitment of neutrophils to accumulated MSU crystals. Figure created by Dmitry Popov based on information in (Busso et al., 2010) using Biorender software.

1.2.5 Chronic gout pathogenesis

Gout is a complex disease and chronicity is one of its features. Individuals with acute gout who experienced periodical gout flares for several years may develop chronic gout. It is characterised by more frequent and serious flares as well as chronic inflammation of the joints. Clinical manifestation of chronic gout is described as a development of cartilage damage, synovitis and the formation of nodules, called tophi (Schlesinger, 2013). Tophi are stone-like deposits of MSU crystals inside synovial tissues, bones and soft tissues. The formation of tophi is caused by the presence of crystals in the synovium which triggers the production of nitric oxide, pro-inflammatory cytokines and metalloproteases by chondrocytes and results in severe cartilage damage. Clinical complications of tophi include extreme pain, joint deformation, and destruction as well as soft tissue damage (Schlesinger, 2013). People with chronic gout can never

experience complete freedom from continuous pain and inflammation of the joints which makes it a debilitating disease.

1.3 Gout and NLRP3 inflammasome

Background

Despite the fact that gout is an ancient disease and that MSU crystals were identified to be a causative agent back in the early 1800s, the underlying mechanism by which MSU crystals initiate acute inflammation and sudden gout flares have only recently begun to be understood. It is now known that the initiation of gout occurs when a variety of cells recognise and respond to accumulated MSU crystals and subsequently induce the inflammation process (Ragab et al., 2017). The nature of the response depends on the type of cells that have recognized the MSU crystals and the cells that were recruited to the inflammation site. The formation of MSU within the joint triggers the activation of inflammatory cells such as mast cells, synoviocytes and monocytes that release inflammatory molecules: IL-6, IL-1β, TNFα (tumor necrosis factor alpha) and proteins S100 (Cronstein & Sunkureddi, 2013). Together these inflammatory mediators promote the subsequent recruitment of leukocytes and neutrophils from the blood into the inflammation site. Neutrophil invasion of the joint cavity and interaction with phagocytosed MSU crystals triggers the production of reactive oxygen species (ROS) which also contribute to massive inflammatory response during gout flares (Davidsson et al., 2020).

The most well-known pro-inflammatory cytokine which has a pivotal role in orchestrating the inflammatory response to MSU is IL-1β (Chung et al., 2016). This key regulatory proinflammatory cytokine is thought to promote an influx of neutrophils into the joint cartilage and synovial fluid which causes ROS formation and is a classic hallmark of a gout attack. Studies in animals and humans provide compelling evidence for IL-1β role in gouty arthritis. In vivo gout model study showed that inflammation caused by an injection of MSU crystals into the joint was significantly reduced in mice treated with an IL-1β inhibitor (Mariotte et al., 2020). Phase II clinical studies also demonstrated similar results when patients with gout were treated with anti-IL-1β monoclonal antibody, thus supporting the crucial role of IL-1β in gout pathogenesis (Tran et al., 2013). Proinflammatory cytokine IL-1β is produced in an inactive form by innate immune cells such as monocytes, dendritic cells and macrophages and then cleaved and activated by caspase-1 which also exists in an inactive form until the induction of immune response. The understanding of a mechanism that is responsible for the activation of caspase-1 and IL-1β has been a priority for multiple high-profile studies (Kingsbury et al., 2011; Mao et al., 2018). The results of these studies showed the involvement of macromolecular complexes called “inflammasomes”. Since the discovery of the NLRP3 inflammasome

complex a decade ago, it has been implicated in the pathogenesis of several inflammatory diseases including rheumatoid arthritis, atherosclerosis, colitis, and gout (Pourcet & Duez, 2020).

The following section will describe the molecular mechanisms and pathophysiology of the NLRP3 inflammasome complex, in particular its implication in MSU-associated inflammatory immune response.

1.3.1 Structural and molecular mechanisms involved in activation of NLRP3 inflammasome

The first line of defence against foreign substances including bacteria and viruses is the innate immune system. It plays a crucial role in the recognition and subsequent clearance of a variety of pathogens (bacteria, viruses) as well as endogenous molecules released by the host as the consequence of infections, damage to membrane, necrosis or pathological conditions (MSU crystals, dsDNA). Immune cells detect and eliminate exogenous pathogen-associated molecular patterns (PAMPs) which are obtained from foreign agents and also endogenous danger-associated molecular patterns (DAMPs) which are obtained from dead or damaged cells (Gong et al., 2020). First, these motifs are recognized by innate immune cells such as macrophages, neutrophils, dendritic cells and mast cells that express receptors termed pattern-recognition receptors (PRRs). The PRRs families are classified depending on the cellular location and the ligands that bind to them. PRRs family members include Toll-like receptors that are located within extracellular membranes (TLRs: 1,2,5,6,10) and endosomal membranes (TLR: 3,7,8,9). NOD-like receptors (NLRs) and RIG-like helicase (RLHs) receptors are located at the cytoplasmic membrane (Evavold & Kagan, 2019).

TLRs are membrane receptors expressed on a variety of cell types. They recognise and respond to a range of PAMPs and DAMPs and upon activation trigger a series of signalling cascades to produce transcriptional factors that will in turn induce transcription of pro-inflammatory cytokines (interleukins and TNF) to drive immune-inflammatory response. As an example, TLR-4 and TLR-2 in the membrane of the cell are bound by PAMPs such as Gram-negative liposaccharides (LPS) and this triggers signalling cascades that stimulate the production of transcription factors such as NF-κB, IRF-3 and AP-1 which in turn activate the adaptive immune system (Ciesielska et al., 2021).

The intracellular NLRs have been a focal point for the investigation of the immune response in inflammatory diseases. NLRs are the major class of PRRs that are able to recognise both DAMPs and PAMPs from a variety of endogenous and exogenous signals and initiate a sterile inflammation (Pourcet & Duez, 2020). The most studied and characterized NLRs is NLRP (contains Pyrin domain), in particular NLRP3. NLRP3 recognition of DAMPs and PAMPs leads to the formation of an inflammasome complex that mediates the activation of inflammatory caspases and subsequent release of pro-inflammatory

cytokines ***(Figure 1.5)***. NLRP3 protein is a sensor protein that is characterized by 3 domains: a pyrin domain (PYD), a leucine-rich repeat (LRR) motif and NACHT domain (***Figure 1.5***). The PYD interacts with the pyrin domain of the apoptosis-associated speck-like protein (ASC) that contains the caspase recruitment domain (CARD). The CARD domain of adaptive protein ASC recruits an unprocessed pro-caspase 1 which is then cleaved to its active form activating the NLRP3 inflammasome complex (Vajjhala et al., 2012). Subsequently activated caspase-1 cleaves and therefore activates pro-IL-1β converting it into IL-1β allowing it to be released from the cell (Grebe et al., 2018).

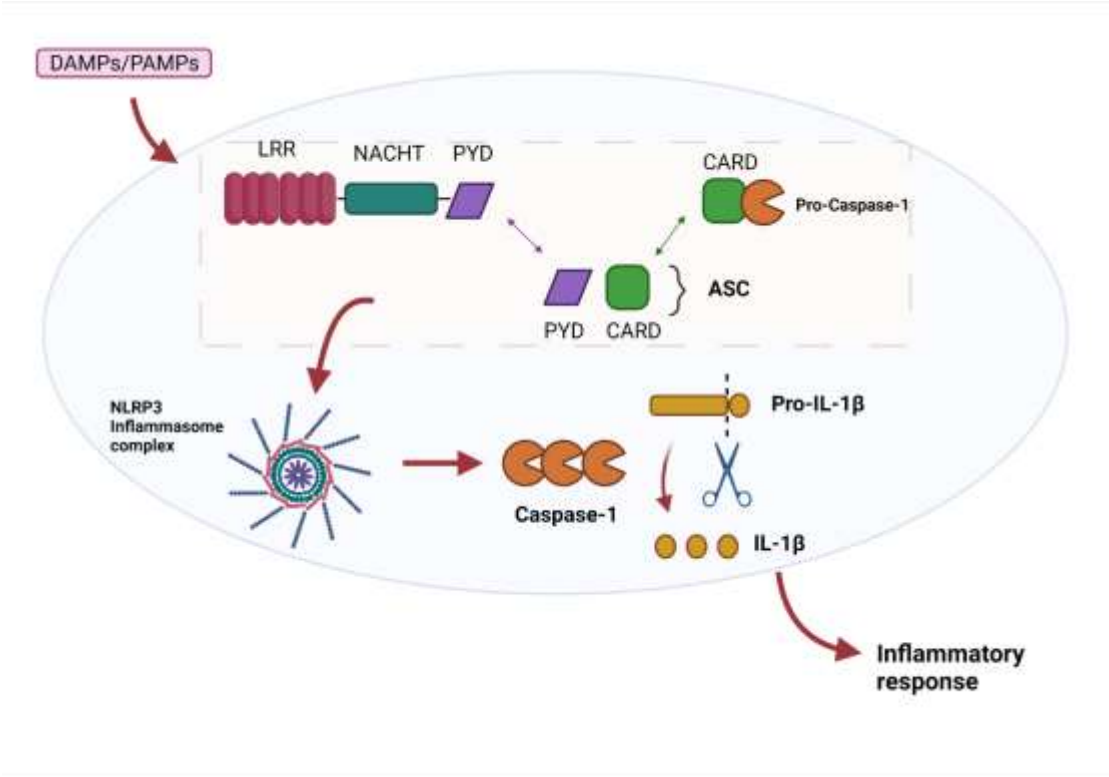

Figure 1.5 The structure of NLRP3 inflammasome complex. The NLRP3 inflammasome complex consists of ASC, NLRP3 and pro-caspase 1. NLRP3 protein is characterized by 3 domains: LRR, NACHT and PYD. When DAMPs/PAMPs activate the upstream signalling pathways, it leads to oligomerization and assembly of NLRP3 inflammasome. The PYD interacts with the caspase recruitment domain (CARD) and it results in the recruitment of unprocessed pro-caspase 1 which is then cleaved to its active form caspase 1. Caspase-1 induced cleavage and secretion of crucial pro-inflammatory cytokine IL-1β, which in turn causes the inflammatory response. Figure created by Dmitry Popov based on information in (Busso et al., 2010) using Biorender software.

1.3.2 The role of the NLRP3 inflammasome in acute and chronic gout

Although the role of NLRP3 inflammasome in gout pathogenesis has been well described in the literature, there are still many unknown aspects of the underlying mechanisms of NLRP3 inflammasome activation by MSU crystals. The NLRP3 inflammasome involvement can be divided into a two-step process: priming and activation (***Figure 1.6***).

Priming, also known as the initiation phase, regulates the gene and protein expression of all inflammasome complex components which are necessary for NLRP3 assembly and activation. It is controlled at the transcriptional level by the activated transcriptional factors NF-κB. The priming step is achieved as a result of signalling cascades mediated by PRRs on the surface of innate immune cells. The most known of the TLR family, TLR2 and TLR4 have been shown to play an important role in gout inflammation. It's been proposed that there is a direct interaction between TLR4 & TLR2 and MSU crystals as modified macrophages with downregulated TLRs were found to not engulf MSU crystals as efficiently as wild-type macrophages (Liu-Bryan et al., 2005). The data from the studies on TLRs indicates that the gouty inflammation could be regulated by TLRs recognition of ligands that can prime macrophages and monocytes to release an active form of IL-1β (Qing et al., 2014). Endogenous ligands of TLR4 include MRP8 and MRP14 which are released after phagocyte activation. In a murine model of gout, genetic downregulation of MRP14 significantly reduced immune response to MSU crystals (Holzinger et al., 2014). Moreover, other factors such as cluster of differentiation 14&36 (CD14 and CD36) which serve as co-receptors for TLR2 and TLR4 demonstrated engagement in the mediation of MSU crystal inflammation (Mendonça-Natividade et al., 2019). Phagocyte-expressed PRRs CD14 and CD36 functionally interact with both TLR4 and TLR2 and modulate their signalling. An in vitro study in bone marrow-derived macrophages demonstrated that downregulation of CD14 and CD36 impaired phagocytosis of MSU crystals as well as attenuated NLRP3 inflammasome activation, caspase-1 cleavage and as a result IL-1β production (Chung et al., 2016). The priming step is compulsory for the assembly of the NLRP3 inflammasome complex, however, this step is known to be non-specific and may result from different signals that induce an inflammatory response. Priming provides an inflammatory milieu for NLRP3 inflammasome engagement, but it is not enough to induce an inflammasome pathway (Bauernfeind et al., 2009).

The second step is the activation of the inflammasome complex. This step is known to be more specific as it directly guides the post-transcriptional and translational assembly of the NLRP3 inflammasome complex (Swanson et al., 2019). The assembly of the NLRP3 complex enables recruitment of apoptosis-associated speck-like (ASC) proteins and cleavage of pro-caspase 1 to produce caspase-1 which results in caspase-1 mediated activation of the pro-inflammatory cytokines IL-1β and IL-18. Although the precise molecular mechanisms of NLRP3 inflammasome complex activation by MSU crystals are yet to be elucidated, current evidence suggests that there are three signalling pathways that mediate agonist recognition and activation of the inflammasome (Kelley et al, 2019). First, the phagocytic pathway appears to be involved in the activation of NLRP3 inflammasome by crystals. The uptake of the particles by immune cells disrupts the phagolysosome acidic compartment and results in a release of cathepsin B (Hornung et al., 2008). Secondly,

the generation of reactive oxygen species can lead to activation of NLRP3 inflammasome in response to different stimuli (Cruz et al., 2007). Finally, recent research suggests an important role for P2X7 receptor-mediated K+ and Ca+ efflux in NLRP3 activation (Piccini et al., 2008). The prevention of efflux of these ions resulted in inhibition of NLRP3 inflammasome complex assembly. Furthermore, the activation of NLRP3 inflammasome complex is highly dependent on the availability of inflammasome components. In vivo studies demonstrated that macrophages derived from mice with a deficiency in several inflammasome components such as ASC and caspase-1 were not able to trigger cleavage and release of IL-1β in response to MSU phagocytosis (Martinon et al., 2006). Moreover, this study also found attenuation in neutrophil influx in mice injected with MSU. These findings suggest that NLRP3 plays an important role as a link between the pivotal stimulus of gout and pathological hallmark of a gout flare.

Overall, the NLRP3 inflammasome complex is a stress sensor that can recognise a loss of tissue homeostasis and the presence of abnormal endogenous substances that produce 'danger signals' due to infection, tissue damage or metabolic abnormalities.

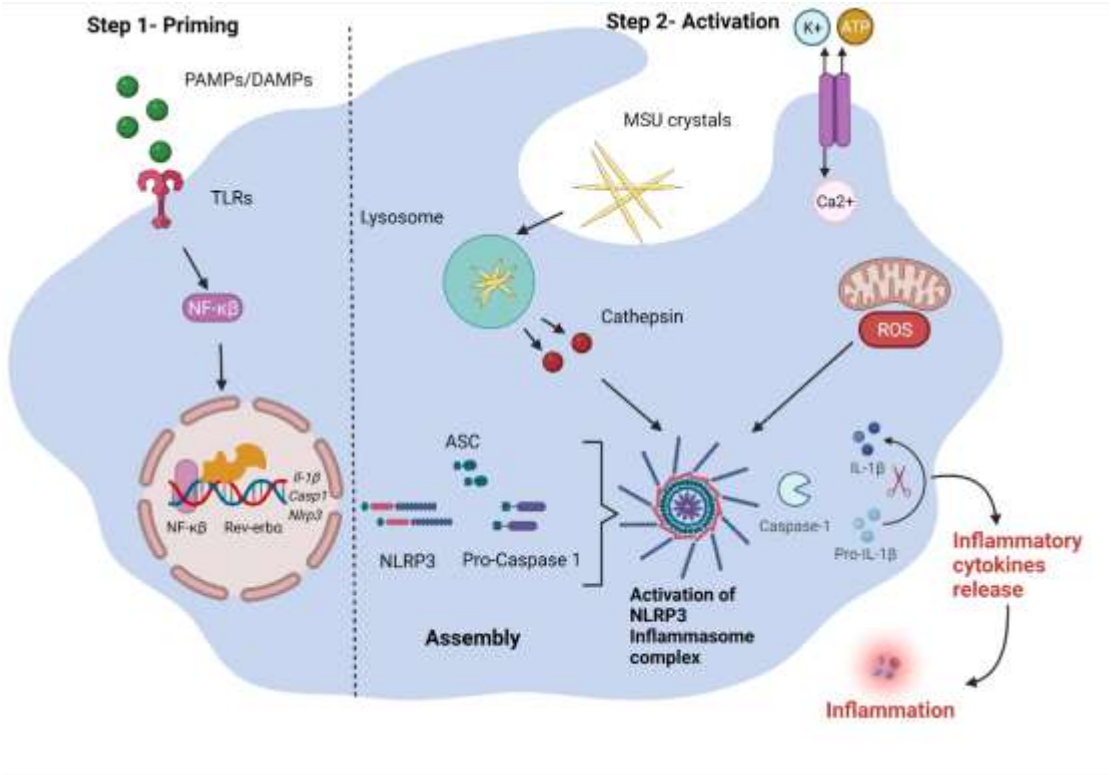

Figure 1.6 NLRP3 inflammasome two-step activation process. The priming step (step-1) occurs upon binding of DAMPs/PAMPs TLRs on the surface of monocytes and macrophages, thus triggering nuclear factor- κB (NF-κB)-dependent transcription of NLRP3 inflammasome components as well as transcription of IL-1β in its pro-active form. The activation of NLRP3 inflammasome (step-2) is the result of phagocytosis of DAMPs (MSU crystals) and subsequent lysosomal damage, formation of ROS due to mitochondria dysfunction which leads to alternation of K+ and Ca2+ fluxes. The assembly of the NLRP3

complex enables cleavage of pro-caspase 1 to produce caspase-1 which results in caspase-1 mediated activation and secretion of the pro-inflammatory cytokines IL-1β, which in turn triggers recruitment of leukocytes to the site of inflammation. Figure created by Dmitry Popov based on information in (Pourcet & Duez, 2020) using Biorender software.

1.4 Introduction to the Circadian Clock

1.4.1 Background

Every single organism on Earth is continuously exposed to daily and seasonal changes in the external environment. While some of the changes are distinctive, there are many events that repeat over time: day and night cycle, tidal shifts and changes in seasons. In order to survive and adapt it was crucial for organisms to develop an internal clock mechanism that enabled them to anticipate and respond to these cyclic changes. One of the most rudimental cyclic changes experienced by living organisms is a light-dark cycle. Almost every organism on the planet, from simple prokaryotes to mammals has developed an endogenous clock that is synchronized with Earth's 24-hour solar time. This internal clock is called the circadian clock as the majority of functions and physiological pathways are controlled in a circadian manner (from circa diem, "about a day") (Patke et al., 2020). Circadian oscillators are present in every tissue of the body and synchronized by both external and endogenous signals to regulate physiological functions such as body temperature, immunity, blood pressure, sleep-wake cycle and hormone level ***(Figure 1.7)***.

In the 1960's chronobiologist Franz Halberg demonstrated the three key components that are known to be fundamental to the circadian clock today. The first component is a self-sustaining circadian oscillator that is able to sustain rhythmic outputs even if isolated from external signals. Therefore, when a clock is isolated from the external environmental cues, the system can run at its own pace which is termed "free-running". The second component is linked to external cues such as light that cause synchronisation of the clock and it is named "zeitgebers" (German name for time-giver). The process that synchronizes the internal clock to a zeitgeber's period is called "entrainment". The third component is the ability of rhythms maintain a 24-hour pace despite the change in the body temperature. Those rhythms are known to control an organism's physiology, behaviour, cell biology and gene expression (Kuhlman et al., 2018).

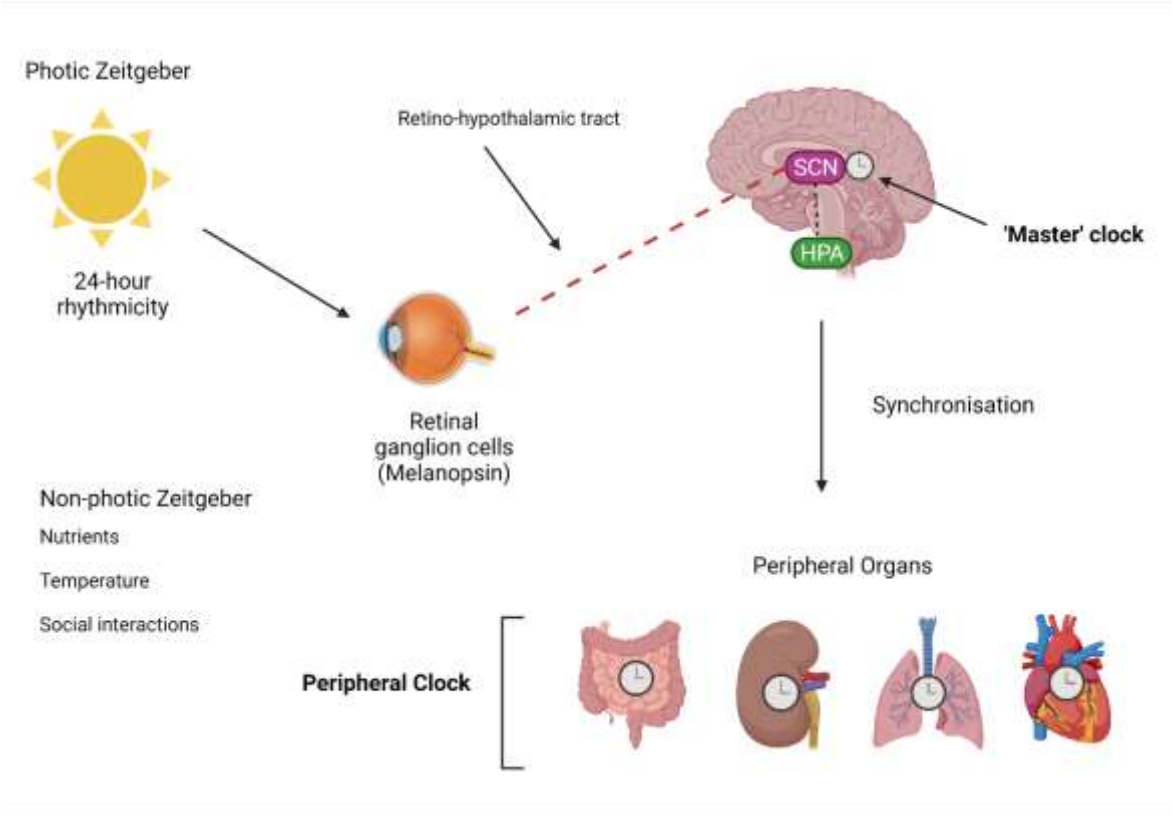

Figure 1.7 Schematic diagram of a hierarchical organisation of the mammalian circadian clock entrainment. The circadian clock consists of the master pacemaker, located in the suprachiasmatic nucleus (SCN) and peripheral oscillators that are found in all cell types in the body. The specific photoreceptors that express melanopsin receive photic signals and transfer them into the SCN via the retino-hypothalamic tracts. The hypothalamus pituitary adrenal gland (HPA) transmits time cues from SCN master clock to non-SCN peripheral clock. The SCN master clock synchronizes and entrains the peripheral clock in a variety of tissues via endocrine and neural pathways. The local clocks can work independently from the master clock as they rely on non-photic signals such as temperature, nutrients and social interactions. Figure created by Dmitry Popov based on information in (Kondratova & Kondratov, 2012) using Biorender software.

1.4.2 "Master" clock

Circadian rhythms in mammals are orchestrated by a central pacemaker which is known to be neural. It plays a major role in the regulation of circadian rhythms by synchronising the activity of peripheral oscillators all over the body, therefore it allows to maintain general circadian synchrony. The central circadian clock is located in the suprachiasmatic nuclei (SCN) which is in turn located within the hypothalamic region of the brain (Mieda, 2020). The SCN is presumed to consist of multiple autonomous oscillating cells which are all connected with each other to form the Master clock. These cells communicate through various neurotransmitters including vasoactive intestinal peptide (VIP) which is secreted from one SCN cell and recognised by the neighbouring cell's vasoactive intestinal peptide receptor (VPAC2) receptors (Mieda, 2020). This signalling between SCN cells allows synchronisation of all the cells in the

tissue to one rhythm. The master clock is synchronized with external environmental rhythms, primarily light signals received by the retina of the eye (***Figure 1.7***). The variation in light intensity acts as a zeitgeber entraining the SCN clock leading to 24-hour rhythmicity. The SCN integrates the light input from the retino-hypothalamic tracts via intrinsically photosensitive retinal ganglion cells (ipRGCs). The ipRGCs are mammalian photoreceptors that express melanopsin which is vitamin A-based light-sensitive opsin photopigment that plays an important role in the photo-entrainment of the master clock (Li & Androulakis, 2021). The light-activated master clock in SCN orchestrates rhythmic release of glucocorticoids and melatonin by directly controlling the activity of hypothalamus pituitary adrenal gland (HPA) axis through efferent connections from SCN to hypothalamus. The creation of diurnal oscillations by a master clock is crucial for the regulation of physiological and behavioural processes on a daily basis (Robinson & Reddy, 2014). Moreover, the master clock plays important role in the modulation of glucocorticoids and catecholamines release from the adrenal glands in HPA independent manner by modifying the sensitivity of the adrenal cortex to adrenocorticotropic hormone (ACTH) through SCN activation of the autonomous nervous system (ANS). Glucocorticoid and catecholamine signalling are directly involved in the synchronization of circadian rhythms in peripheral clocks (Li & Androulakis, 2021).

1.4.3 Peripheral clock

The peripheral clocks play an essential and unique role in each of their respective peripheral tissues, operating the expression of specific circadian genes involved in an array of physiological functions. The interplay between master clock in the brain and local clocks in the peripheral tissues establishes correct oscillations throughout the body. Although the exact mechanism of interaction is not well understood, it is believed that SCN synchronises external cues with peripheral clocks via the release of hormones which act as a zeitgeber for peripheral clocks. There are two main models which explain the relationships between master clock and peripheral clocks. The first model is “master-slave” model which states that master clock has complete synchronization power and therefore peripheral clocks are synchronized exclusively by master clock and not affected by internal or external stimuli. The second model is referred to as “orchestra” model in which master clock plays the role of conductor, with each peripheral clock as a member of an orchestra. In this model, each peripheral clock can adapt to its own internal or external stimuli such as feeding cues, but it would be ultimately “conducted” by the light-dark cues transmitted from the master clock (Richards et al., 2012). The evidence from multiple studies showed that peripheral clocks are also capable of acting autonomously to the SCN which allows them to maintain circadian rhythmicity even in isolation from master clocks. SCN-lesion studies demonstrated that the local clock in peripheral tissues continues to function even in the absence of the SCN clock (Cui et al., 2001). In addition, circadian rhythms

in peripheral tissues like lung, kidney and liver have been observed to persist for several days ex-vivo (Okubo et al., 2013). It is now known that virtually every cell in the body has an internal biological clock, therefore it is believed that cell-to-cell communication plays a crucial role in the maintenance of synchronisation between individual oscillators (***Figure 1.7***) (Kowalska & Brown, 2007). The peripheral clock is shown to be entrained not only by cues from the SCN but also by regular feeding times. In vivo study showed that food restriction can entrain animals to anticipate food. The change in feeding pattern caused a change in behaviour, the sleep-wake cycle and the expression of clock genes in peripheral organs, while the master clock in SCN remained unchanged (Hirota et al., 2002). Therefore, change in nutrient availability could be more important zeitgebers for the peripheral clocks than entraining cues from the master clock. Another non-photic entraining signal for peripheral clocks is a change in body temperature. This was clearly shown in vitro studies when a change in temperature with only one degree resulted in re-synchronization of circadian oscillation in fibroblast cells (Tsuchiya et al., 2003).

1.4.4 Molecular basis of a circadian oscillator

The molecular machinery of circadian oscillation is increasingly well understood. In mammals, the circadian clock consists of a core transcription/translation feedback loop and stabilizing feedback loops. The core transcriptional/translation feedback activators and suppressors are organized into positive and negative limbs (***Figure 1.8***) (Shearman et al., 2000). The genes *BMAL1 (ARNTL)* (Brain and Muscle ARNT-like-1) and *CLOCK* (Circadian Locomotor Output Cycles Kaput) are the central genes in the positive limb, and they encode for BMAL1 and CLOCK proteins respectively. CLOCK and BMAL1 heterodimerize and activate transcription of Cryptochrome *(CRY1/2)* and Period *(PER1/2/3)* genes via binding to E-box elements (Cermakian & Sassone-Corsi, 2000). Translated CRY1/2 and PER1/2 form a dimeric complex and act as the negative limb of the clock. Once a sufficient quantity of these proteins in the cytoplasm is reached, PER and CRY translocate into the nucleus and inhibit CLOCK/BMAL1 activity. Therefore, further transcription and translation of *CRY* and *PER* genes cease. The degradation of CRY and PER proteins is dependent on post-translational mechanisms. The degradation of CRY proteins is controlled by the intracellular ubiquitination process, while PER protein degradation is regulated by phosphorylation (Robinson & Reddy, 2014). Subsequent degradation of CRY1/2 and PER1/2 proteins allows for a new cycle of transcriptional activation by CLOCK/BMAL1. It takes about 24 hours for the full BMAL1: CLOCK and PER: CRY cycle to occur.

The core transcriptional/translational loop is finely tuned by auxiliary stabilizing feedback loops. The primary stabilizing loop consists of nuclear receptors such as *REV-ERBα* and retinoic-acid receptor-related orphan receptor alpha (*RORα*) which bind to ROR response elements (ROREs) on the promoter site of

BMAL1 to regulate its transcription (Preitner et al., 2002). While REV-ERBα acts as a transcriptional suppressor of BMAL1, the nuclear receptor activator RORα competes with REV-ERBα for binding to RORE response elements on the BMAL1 promoter antagonising the repressive effects of REV-ERB. The competition for the promoter site of *BMAL1* is rhythmic and contributes to driving the circadian oscillation in *BMAL1* expression. *BMAL1* is a transcription factor and other clock components such as *REV-ERB* are transcriptional repressors, one of the best understood mechanisms is through time-of-day dependent regulation of target gene expression (Shearman et al., 2000). This series of transcriptional-translational feedback loops (TTFLs) work in a self-sustaining cycle to control degradation and production of BMAL1 and CLOCK in anti-phase with that of PER and CRY. The circadian clock molecular machinery ultimately controls circadian oscillation in cell biology, tissue homeostasis, metabolism and gene expression in all the tissues in the body (Cermakian & Sassone-Corsi, 2000).

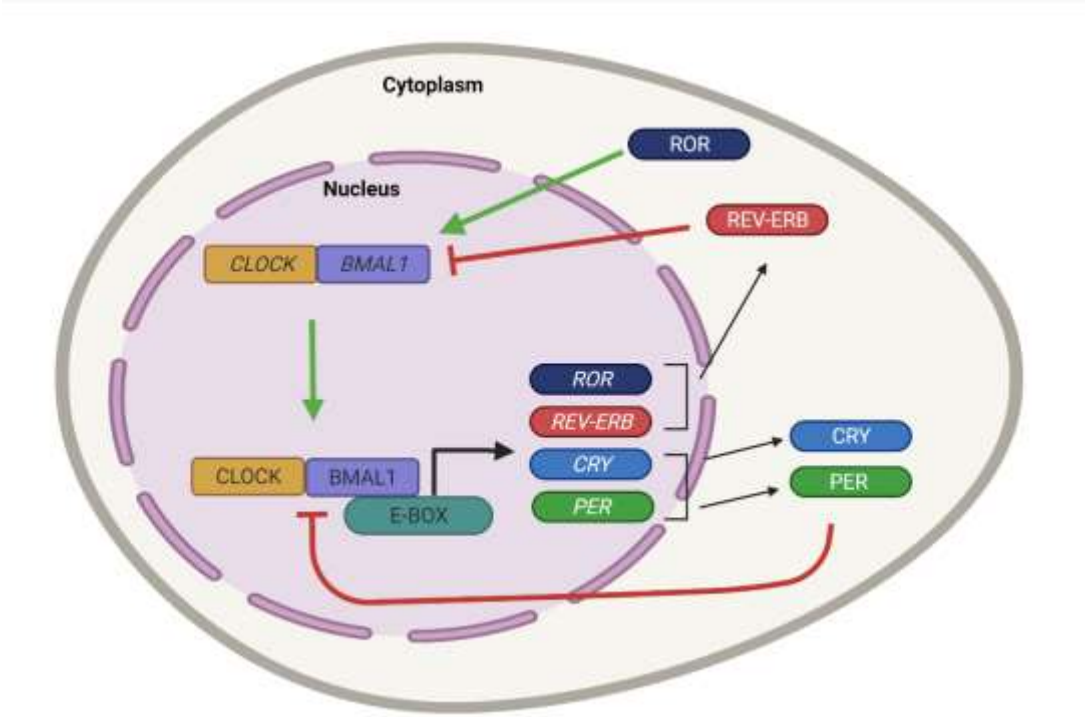

Figure 1.8 Schematic diagram of the transcriptional/translational feedback loops (TTFL) in the circadian oscillator of the mammalian cells. The core clock genes *BMAL1* and *CLOCK* heterodimerize and bind to the E-BOX element to activate transcription of PER (1,2,3 homologs) and CRY (1,2 homologs), ROR and REV-ERBα, constructing the positive limb of TTFL. PER and CRY translocate into the nucleus and bind to BMAL1-CLOCK heterodimers, inhibiting CLOCK/BMAL1-driven activation and transcription and thus their own expression, constructing the negative feedback loop. REV-ERBα and ROR also act as a stabilising feedback loop that controls the activity of the core positive and negative TTFL via inhibiting or inducing BMAL1 gene expression, respectively. Figure created by Dmitry Popov based on information in (Robinson & Reddy, 2014) using Biorender software.

1.5 Circadian clocks and immune system

The mammalian immune system has been adapting and evolving for a long period of time to be able to effectively combat invading bacteria, viruses and parasitises. There is a large body of literature highlighting the contribution of circadian oscillations to the adaptive and innate immune responses (Pourcet & Duez, 2020). Firstly, various immune cells possess the clock machinery and demonstrate daily variation in their normal function. Secondly, alteration of the biological clock has a crucial effect on the function of the adaptive and innate immune systems. Finally, there is multiple evidence that deletion or knockout of core clock genes can affect immune responses and cause a variety of diseases (Buttgereit et al., 2015; Chalfant et al., 2020; Kc et al., 2015).

1.5.1 Role of internal circadian clocks in individual components of immune system

Various studies revealed that cells of the immune system such as neutrophils, macrophages and lymphocytes that activate and perpetuate inflammatory pathways have circadian clocks. These clocks control a number of immune functions such as phagocytosis, cytokine release, and response to pathogens throughout the day and night cycle. The number of leukocytes in circulation changes throughout the day, peaking during the rest phase (night for diurnal animals) because of circadian variations in haematopoietic cells leaving the bone marrow. Previous studies showed that leukocyte number also varies across the day due to alterations in their adhesion to endothelium and infiltration into tissues which occurs at the beginning of an animal's active phase (day for diurnal animals) (Muller, 2012). In addition, in vivo studies also demonstrated circadian oscillation in macrophages (Keller et al., 2010.). Interestingly, it appears that macrophages not only have molecular expression of clock genes but also possess functional changes in phagocytotic activity which depends on the time of the day, with activity greater at night (Timmons et al., 2021). Moreover, ex vivo studies in rats showed that enriched natural killer cells (NK cells) also demonstrated circadian clock gene expression as well as a time of the day dependant cytolytic activity (Stawski et al.,, 2015).

The majority of immune cells demonstrate internal circadian oscillations as well as time-of-day dependent differences in their numbers in circulation. In humans, naïve T cell levels are known to be the lowest at midday, however, CD4+ and CD8+ T cells are shown to peak in circulation at midday (Dimitrov et al., 2009). In addition to intrinsic clocks, the central clock in the SCN is able to control the level of immune cells in circulation by utilising hormonal regulators (Li & Androulakis, 2021). The circadian rhythm in naïve T cell levels has shown to be negatively correlated with cortisol rhythms. Thus, the level of naïve T cells peaks during the night while the level of cortisol is at its peak in the morning (Dimitrov et al., 2009). Cortisol

sensitivity of T cells is related to the oscillation in chemokine receptor CXCR4 expression as well as rhythmic expression of its ligand CXCL12, which controls the migration of T cells into the bone marrow in response to a rise in serum cortisol level. The immune response such as cytokine production is also known to be controlled by circadian rhythms and has been linked to rhythms of glucocorticoids (a hormone with known anti-inflammatory activity) and melatonin which are regulated by the master clock in SCN. Furthermore, the immune responses such as cytokine production and phagocytosis of foreign substances showed oscillations during the 24h days which led to time-of-day dependent dissimilarities in the susceptibility to infection or injury (Gibbs et al., 2012). A recent study demonstrated that *CRY1/CRY2* double knockout mice had up-regulated pro-inflammatory cytokine levels of IL-6 and TNFα due to an increase in NF-kB signalling and subsequent NLRP3 inflammasome activation (Narasimamurthy et al., 2012).

These examples show that circadian rhythms play an important role in the immune response. Such rhythms occur by controlling multiple components of the immune system, either by peripheral internal circadian clocks or by the hormonal regulation from the master clocks in the SCN. The combination of both those factors, immune cell internal rhythms and hormones influence diurnal control of the immune response.

1.5.2 Circadian-Immune Interactions

The circadian oscillator is able to influence the immune system, however in turn the immune system has the ability to regulate clock gene expression. This ability of the immune system was demonstrated in vivo by upregulation of TNFα which resulted in downregulation of core circadian clock proteins. Moreover, previous studies showed that innate immune system cytokines such as interferon alpha and gamma (IFNα and IFNγ) can influence clock gene expression. The upregulation of IFNγ resulted in reduction of the *PER1* gene expression while alternation in IFNα influenced the expression of *CRY1, PER1,2* genes as well as the protein levels of BMAL1: CLOCK. The results of these studies suggest that cytokines are able to modify the expression of core clock proteins in peripheral tissues, which especially can occur in chronic inflammatory diseases. Furthermore, there is increasing evidence showing that the time of the day variation in the number of circulating leukocytes and the release of pro-inflammatory cytokines might be directly controlled by the core clock proteins, including REV-ERBα and BMAL1 in a 24-hour pattern. This can have a crucial impact on clinical diagnosis of disease as well as drug therapy.

1.6 Regulation of NLRP3 Inflammasome complex by circadian oscillator and implications in pathologies

Apart from the important role of mammalian circadian oscillator in behavioural and physiological processes, findings from several studies reveal a regulatory role of circadian oscillator in inflammatory responses. Indeed, multiple studies have shown that alteration of circadian clocks can lead to an increased risk for metabolic and chronic inflammatory diseases such as colitis, atherosclerosis and rheumatoid arthritis (***Figure 1.9***) (Buttgereit et al., 2015; Fontaine et al., 2008; Yang et al., 2015). The majority of the NLRP3 inflammasome-associated disorders show a similar chronic inflammatory component, which could be a severe infiltration of leukocytes in the vascular wall due to inadequate build-up of DAMPs (cholesterol) which causes atherosclerosis or accumulation of hydroxyapatite in a joint cavity which occurs in rheumatoid arthritis. Recent in vivo studies in peritoneal mouse macrophages demonstrated that nuclear factor REV-ERBα is a negative regulator of the mRNA expression and transcription of the core NLRP3 inflammasome components (Wang et al., 2018). It is now known that transcription of NLRP3 components oscillates in a daily manner with peak mRNA expression during the active phase, corresponding to the low expression of *REV-ERBα* and hence reduced *REV-ERBα* suppression of *BMAL1* transcription. Furthermore, researchers also observed a loss in circadian oscillations in Nlrp3 mRNA when REV-ERBα was knocked down in human and mouse-derived macrophages (Pourcet et al., 2018). The modulation of REV-ERBα activity is responsible for the regulation of NLRP3 inflammasome protein amounts as well as their assembly into NLRP3 complex (priming step). Interestingly, changes in the NLRP3 inflammasome pathway stimulated by impairment of REV-ERBα expression trigger alterations in the secretion of proinflammatory cytokines IL-1β and IL-18 (Gibbs et al., 2012). In addition, REV-ERBα is able to control the activation step of NLRP3 inflammasome. Ablation of the REV-ERBα nuclear factor was shown to result in the induction of NLRP3 inflammasome complex assembly by cleavage of caspase-1 and subsequent maturation and release of IL-1β and IL-18 in human macrophages primed with LPS (Gibbs et al., 2012). In contrast, stimulation of REV-ERBα by natural ligand (heme) or pharmacological agonist SR9009 resulted in a reduction in proinflammatory cytokine release (Yin et al., 2010). It is now known that *REV-ERBα* binds to specific response elements in *IL-1B* and *Nlrp3* gene promoters and silences their expression, therefore it is directly regulating the assembly and activation of NLRP3 inflammasome complex. Interestingly, the findings from an in vivo model of sterile peritonitis demonstrated that plasma levels of IL-1β and IL-18 were higher in *REV-ERBα* deficient rodents during the resting phase when expression of *REV-ERBα* was highest in wild-type, however, there was no differences observed during the active phase when REV-ERBα was almost absent (Pourcet et al., 2018). Moreover, another in vivo model of acute lung injury induced by LPS demonstrated that inhibition of REV-ERBα with an antagonist led to increased injury severity due to an increase of NLRP3-mediated release of IL-1β (Yang et al., 2020; Yu et al., 2019). The increasing evidence

from multiple studies suggests that pharmacological modulation of circadian clock components such as REV-ERBα can be beneficial for the treatment of chronic and acute inflammatory diseases in which the NLRP3 inflammasome complex is deregulated (Welch et al., 2017).

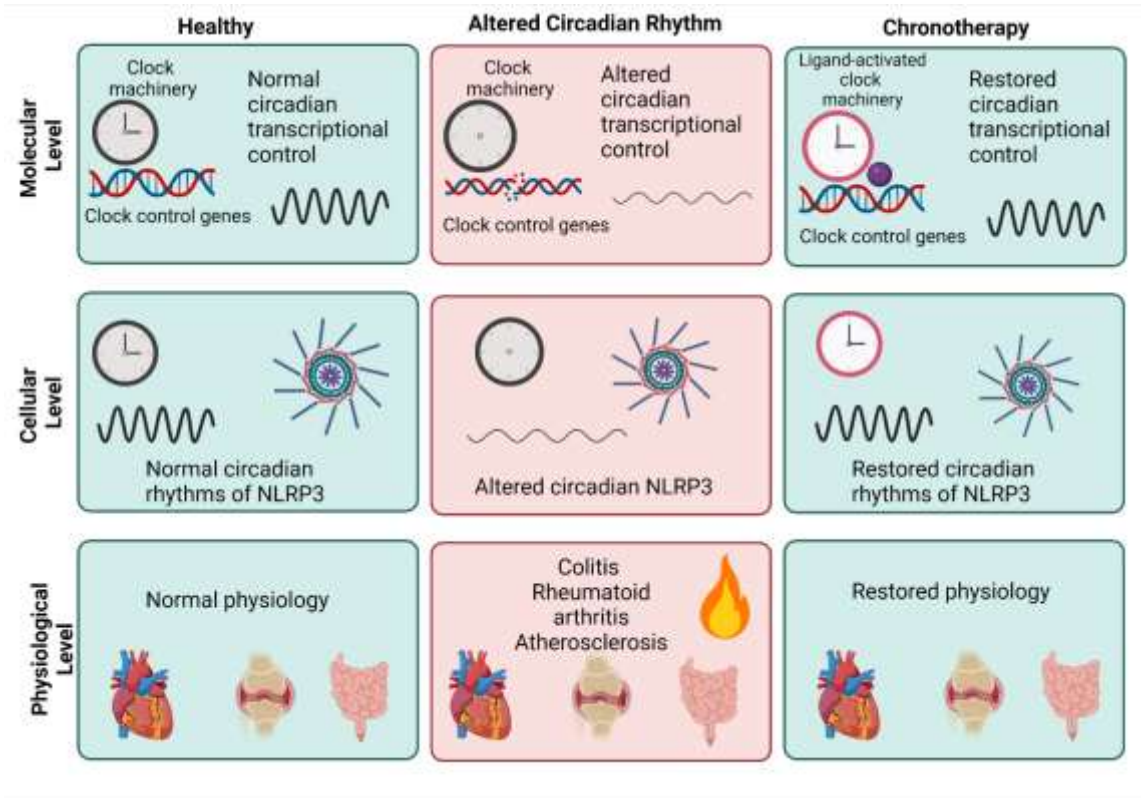

Figure 1.9 NLRP3 inflammasome-associated inflammatory diseases. Inflammatory diseases associated with dysregulation of NLRP3 inflammasome and potential for novel chrono-pharmacological therapies. Figure created by Dmitry Popov using Biorender software based on information in (Pourcet & Duez, 2020).

1.6.1 Interaction of circadian clocks and NLRP3 inflammasome in colitis

Several lines of evidence indicate that circadian clocks play an important role in the regulation of the NLRP3 inflammasome in inflammatory intestinal diseases such as colitis. In mice, it has been demonstrated that circadian clocks are necessary to maintain the epithelial barrier of the gut (Summa et al., 2013). Pagel et al demonstrated that impairments of circadian rhythms by desynchronization of environmental signals or by genetic mutation of the core clock genes such as *PER 1-3* resulted in alteration of epithelial homeostasis, increase of necrosis and therefore more severe colitis (Pagel et al., 2017). Moreover, in vivo studies showed greater sensitivity to inflammatory damage and an increase in severity of colitis in mice who went through a phase shift in the light-dark cycle. This resulted from activation of inflammatory pathways such as NLRP3 inflammasome complex and subsequent secretion of pro-inflammatory cytokines IL-1β and IL-18 (Liu et al., 2017; Nowarski et al., 2015). Bauer et al identified that the NLRP3 inflammasome plays a role of a central mediator of intestinal inflammation in dextran sulfate sodium (DSS) induced colitis. The researchers

demonstrated that PAMPs such as DSS initiates the activation of NLRP3 inflammasome complex which in turn regulates the secretion of pro-inflammatory cytokines and causes inflammation and necrosis in epithelial lining (Bauer et al., 2010). Wang et al demonstrated that one of the core components of circadian clocks (REV-ERBα) regulates the clocks of the cells in the colon by controlling the activation of NF-kB/NLRP3 axis (Wang et al., 2018). The researchers found that DSS-induced colitis is more severe in mouse models of genetic or environmental disruption of the circadian clock. The knockout of *REV-ERBα* in mice was found to display transcriptional activation of NF-kB signalling and increased activation of the NLRP3 inflammasome complex which accounted for a more severe phenotype of the disease. However, pharmacological activation of REV-ERBα significantly decreased the severity of colitis *in vivo*. Interestingly, in in vitro experiments, the REV-ERBα agonist was only active on the priming step, however, was ineffective during the cleavage of pro-caspase 1 into active caspase-1 in LPS-induced macrophages. The potential reason for this could be due to the fact that macrophage cells were not synchronized in this study. The patients or mice with inflammatory diseases such as colitis that show altered circadian rhythms highlight the potential of mutual interactions between circadian and immune systems (Liu et al., 2017). Although we have a better understanding of the effects of the circadian oscillator on inflammation, the time-of-day dependent molecular mechanisms that regulate the activity of NLRP3 inflammasome and secretion of inflammatory cytokines remain elusive.

1.6.2 Interaction of circadian oscillator and NLRP3 inflammasome in atherogenesis

Atherogenesis is a cardiovascular disease caused by a build-up of fats and cholesterol on the walls of arteries. The atherosclerotic lesion formation is triggered by the infiltration and modification of lipoproteins and the influx of macrophages into subepithelial space and subsequent formation of foam cells. The accumulation of inflammatory cells mainly macrophages, T and B cells result in inefficient efferocytotic removal of foam cells and as a result formation of an advanced lesion with a necrotic core that can become a plaque and lead to myocardial infarct or stroke (Hirota et al., 2013; Solt et al., 2012). Previous studies showed that genetic alteration of the circadian clock in lipoproteins contributes to inflammation which promotes atherosclerotic disease (Tedgui & Mallat, 2006). Circadian clock protein BMAL1 is able to modulate the production of lipoproteins and cholesterol. Its inhibition leads to atherosclerosis and hyperlipidaemia in animal models (Steffens et al., 2017). Macrophage cyclic trafficking and polarization are also regulated by BMAL1, and *BMAL1* gene knockout in animal models resulted in induction of monocyte recruitment and increased risk of atherosclerosis (McAlpine & Swirski, 2016). Moreover, knockdown of *REV-ERBα* resulted in a reduction in lipoprotein plasma levels and modulation of the inflammatory profile of immune cells towards an anti-inflammatory phenotype (Huo et al., 2017; Pan et al., 2016).

In atherosclerotic lesions, oxidized low-density lipoproteins (oxLDL) undergo phagocytosis by macrophages which results in intra-lysosomal crystallization. The crystals act as DAMPs and trigger assembly of NLRP3 inflammasome complex, thus provoking the enhanced release of proinflammatory cytokines IL-1β and IL-1α (Raspé et al., 2002). Duewell et al inhibited NLRP3 inflammasome in apolipoprotein E-deficient and LDL receptor-deficient mice and observed a significant reduction in atherogenesis, which suggests that NLRP3 plays a crucial role in the formation of atherosclerotic lesions (Duewell et al., 2010) Furthermore, abnormal cholesterol efflux in myeloid cells leads to accumulation of unesterified cholesterol and promotes activation of NLRP3 inflammasome, cytokine release and formation of atherosclerotic plaques. Altern et al found that IL-1β neutralizing antibody Canakinumab significantly reduced the incidence of NLRP3 inflammasome mediated atherogenesis in vivo (Alten et al., 2008). The anti-IL-1β antibody successfully inhibited the release of proinflammatory cytokines IL-1β and therefore reduced chance of inflammation. In line with this study, Canakinumab Anti-inflammatory Thrombosis Outcome study by Ridker et al demonstrated that inhibition of IL-1β also significantly reduced the risk of atherosclerotic disease as well as decreased systemic inflammation in patients with previous cardiovascular diseases in the absence of the effect of lipoproteins (Ridker et al., 2020). Despite the neutralization of IL-1β by this antibody, the residual inflammatory risk is still present due to the production of proinflammatory cytokines IL-6 and IL-18 which have also been associated with cardiovascular diseases. Therefore, there is a possibility for novel therapies that will be able to simultaneously inhibit the release of all of these proinflammatory cytokines. Currently, there is not enough evidence to determine whether circadian control of NLRP3 inflammasome complex activation is disrupted in macrophage foam cells. From this perspective, there is a need for a better understanding of interactions between cell clock and regulation of NLRP3 inflammasome. Perhaps development of a therapy that will target the circadian clock components, in particular, REV-ERBα can modulate activation of NLRP3 inflammasome and lead to a decrease in levels of IL-1β and IL-18 as well as modulation of MCP-1 expression and IL-6 release (Gibbs et al., 2012).

1.6.3 Involvement of the circadian clock in the pathogenesis of rheumatoid arthritis

Recent studies have determined interesting bi-directional interaction between the circadian clock and immune response in inflammatory diseases such as rheumatoid arthritis (RA). There is multiple evidence that disruption of biological clock has a significant effect on the functioning of the immune system and therefore it negatively impacts the pathogenesis of chronic inflammatory diseases such as RA. The first observation that supported the concept that circadian clock not only affects the symptoms of RA disease but is also involved in RA pathogenesis of RA was made in 2010. The study by Puttonen et al provided a significant link between shift work and an enhanced risk of RA in women (Puttonen et al., 2010). For a long

time, it has been known that there is a relationship between sleep and chronic inflammatory diseases like RA and gout. However, there is still no clear understanding of the molecular mechanisms that are responsible for it. Patients suffering from rheumatoid arthritis often exhibit sleep disorders that are characterized as a nocturnal awakening type. This type of sleep disorder is described by a significant decrease in sleep efficiency and an increase in waking phases. Cakirbay et al reported a decline in the quality of sleep-in patients suffering from RA due to the increase in RA disease activity during the night (Çakirbay et al., 2004).

The main source of proinflammatory cytokines in RA is innate immune cells such as B cells and T cells and adaptive immune cells like macrophages. In vivo and ex vivo studies demonstrated that macrophages derived from spleen, lymph nodes and peritoneal fluid utilize autonomous circadian oscillations. The lymph node and spleen cells secrete IL-6 and TNFα following a circadian rhythm when stimulated with bacterial endotoxin (Keller et al., 2010.). Moreover, the secretion of proinflammatory cytokines and chemokines induced by endotoxin was significantly impacted by expression of circadian clock components REV-ERBα and BMAL1. As was discussed previously, nuclear receptors REV-ERBα and RORα are the two main clock regulators that modulate transcription of BMAL1. The knockout of *REV-ERBα* in vivo demonstrated the loss of circadian rhythms to endotoxin response, specifically the release of IL-6 was inhibited (Yang et al., 2006). In contrast, the overexpression of *REV-ERBα* significantly induced the expression of cytokine CCL2 by binding to its promoter regions in macrophages derived from mice. The induction of CCL2 resulted in an increase in recruitment of monocytes, T cells and dendritic cells and subsequent induction of inflammation response. In addition, another nuclear receptor RORα has an important role in activation of differentiation of T cells into T helper 17 cells Th17 (CD4+) cells. The Th17 cells express proinflammatory cytokines such as IL-17 and IL-17F that drive inflammation response. Therefore, these cells represent a majority of T cell population that infiltrate inflamed synovial tissue in RA. Recent studies determined that RORα has an important role in regulation of inflammation as it can directly activate the main inhibitory protein in the NF-κB pathway, IκBα, therefore suppressing inflammatory responses (Delerive et al., 2001). In contrast, RORα is able to up-regulate inflammatory response by binding to a response element on the promotor of the IL-6 gene, thus enhancing production of IL-6 cytokine. In the study by Kopmels et al, the authors used straggerer (sg) mice that had *RORα* gene deletion (Kopmels et al., 1992). They identified that macrophages derived from sg mice are hyperresponsive to PAMPs produced by LPS and therefore produce an elevated level of proinflammatory cytokines IL-6 and IL-1β. Interestingly, it has been previously demonstrated that the number of T cells specifically Th17, and their activity is stable during the daytime (resting phase), however, there is a significant induction in their activity during late evening and night (the active phase for mice since they are nocturnal) (Revu et al., 2018). This might support the regulation of T cells, IL-6 and IL-1β cytokines by clock proteins RORα and REV-ERBα. The studies involving clock-targeting therapies are still in their infancy and although there are promising preliminary results, considerably more work will be

required before it can be determined whether these therapies may have a clinical efficacy for treating inflammatory human diseases (Ruan et al., 2021).

1.6.4 Involvement of the circadian clock in the pathogenesis of gout?

The regulation of NLRP3 inflammasome complex by core components of circadian clock has shown to be involved in initiation of inflammatory response in several inflammatory diseases as was discussed above. Despite the fact that gout is one of the oldest afflictions in humans and a major public health problem worldwide there is still a large gap in current knowledge of the involvement of circadian rhythms in its pathogenesis given the mounting evidence of circadian involvement in controlling NLRP3 inflammasome activity as well as a higher incidence of gout attacks at a certain time of day (Martinon et al., 2006). Gouty arthritis is among the other chronic inflammatory diseases like rheumatoid arthritis and atherosclerosis in which NLRP3 inflammasome complex is regulated by a circadian oscillator. Therefore, there is a possibility that gout flares that are known to be time-of-day dependent can potentially be regulated by circadian rhythms in immune cells. The in vivo and in vitro studies demonstrated that NLRP3 inflammasome complex plays a crucial role in orchestrating MSU-induced inflammatory response (Dalbeth & Haskard, 2005). There is a clear need for a better understanding of the role of NLRP3 inflammasome in gout and the mechanism of initiation of sudden, time-of-day dependent gout attacks. Perhaps the disruption in circadian rhythms in cells of immune system could be directly or indirectly involved in regulation of NLRP3 inflammasome complex and initiation of gout flares.

1.7 Conclusion

Indeed, circadian clock plays a pivotal role in a majority of biological processes in mammals, and it's now been known that disruption of circadian rhythms can lead to severe chronic inflammatory diseases. Although there is increasing evidence that alteration of core circadian clock protein expression could contribute to NLRP3 activation in other chronic inflammatory conditions, there are still no studies that show whether there is a relationship between NLRP3 inflammasome complex activity and circadian immunity in gout. Gout is one of the oldest, most common, debilitating form of inflammatory arthritis in the world. Therefore, there is a clear need for understanding the mechanism of initiation of sudden, time-of-day dependent gout flares. Understanding *if* and *how* MSU crystals might affect the expression of core circadian oscillator components in immune cells and alter activity of NLRP3 inflammasome complex is therefore important. There are two potential benefits from understanding circadian disruption in gouty arthritis. First, we might be able to improve patient outcomes by using chronotherapy alongside pharmacology approaches to target and regulate NLRP3 inflammasome activity. Second, we might be able to identify whether or not novel drug targets are rhythmically active or expressed in the target tissue. Such a strategy will allow

targeting NLRP3 inflammasome specifically in pathological tissues that display disruption in circadian oscillation patterns as well as maintain homeostasis in healthy tissues.

1.8 Aims and Objectives

Over-arching research question and hypothesis

Could alteration in the biological cell clock activity of macrophages and monocytes contribute to the development of gout flares?

Individuals with gout are predisposed to gout flares during the night-time due to alteration of the macrophage circadian rhythm by MSU crystals.

Specific hypotheses of this study

1. MSU crystal exposure will cause changes in the expression of components of the circadian clock in the THP-1 monocyte/macrophage-like cell line
2. BMAL1 and REV-ERBα regulate NLRP3 inflammasome activity in THP-1 cells
3. The time-of-day exposure to heme and prednisolone influence their ability to regulate NLRP3 inflammasome activation

Aim 1: To determine the effect of exposure of MSU crystals on the expression of core circadian oscillator components in macrophage-like cells and a monocyte cell line

Objectives:

1. Compare the expression of core circadian genes (*CLOCK, BMAL1, CRY1/2, PER1/2/3* and *REV-ERBα*) in THP-1 monocyte/macrophages-like cells the absence/presence of MSU crystals

2. Compare protein level of core circadian clock component REV-ERBα and TLR4 in THP-1 monocyte/macrophages-like cells in the absence/presence of MSU crystals

Aim 2: To determine whether BMAL1 regulates NLRP3 inflammasome activity in THP-1 monocyte/macrophage-like cells

Objectives:

1. Compare the activity of NLRP3 inflammasome complex between *BMAL1*-overexpressed and *BMAL-1* knockdown THP-1 monocytes and macrophage-like cells.

Aim 3: To determine whether REV-ERBα activity regulates the NLRP3 inflammasome in THP-1 monocyte/macrophages-like cells

Objectives:

1. Determine the effect of heme (an endogenous REV-ERBα agonist) and a pharmacological REV-ERBα antagonist on NLRP3 inflammasome activity

Aim 4: To determine whether time of day affects the ability of prednisolone to regulate NLRP3 inflammasome activity in THP-1 monocyte/macrophage-like cells

2.0 Method Development

2.1 Optimisation of THP-1 cell culture

2.1.1 Materials and reagents

Details of materials and reagents used in this study presented in Appendix.

2.1.2 Cells and cell growth conditions

The human acute monocytic leukemia cell line THP-1 were obtained from (American Type Culture Collection ATCC). THP-1 cells were cultured in the Heraeus HERAsafe Laminar Flow hood following aseptic techniques. Cells were suspended in 15ml of RPMI 1640 medium supplemented with 1% penicillin/streptomycin (P/S) and 10% fetal bovine serum (FBS), hereafter which would be referred as growth media (GM). The cells were cultured in a sterile flask with a filter cap (T75) and incubated at 37°C in humidified air with 5% CO2.

2.1.3 Revival of Cryopreserved cells

Cryovial with THP-1 cells were first retrieved from liquid nitrogen storage and then transported to the laboratory in ice. Immediately after arrival, THP-1 cells were placed in a bead bath for thawing. Thawed THP-1 cells were mixed in a 50ml tube with pre-warmed 15ml of GM and then centrifuged at 200G for 5 min in a room temperature 23°C. The supernatant was discarded, and the entire cell pellet was transferred into T75 flask, followed by resuspension with 15ml of pre-warmed GM. THP-1 cells were cultured for at least 2 passages before usage in all assays, however they did not exceed passage 20 to avoid any changes in cell's phenotype.

2.1.4 Cell maintenance

THP-1 cells were passaged every 2-3 days when cells would reach approximately 70-80% confluency in order to maintain log phase growth. GM and PBS were prewarmed in bead bath at 37°C prior to cell re-seeding. Cells in the GM were transferred into the 50ml falcon tube and flask was washed twice with 5ml of PBS to assure the removal of THP-1 cells from the flask. The cells were centrifuged at 200G for 5 min

(name of centrifuge) and supernatant was removed in one motion. THP-1 cell pellet was resuspended with 1ml of GM prior to determining the cell concentration.

To measure the cell concentration, 10µL of 0.4% trypan blue dye (Sigma) was diluted with 10µL of cell suspension in 1:1 ratio. The stained mixture (10ul) was placed onto the CountessTM counting slide and covered with a coverslip to create an even focal surface. The CountessTM Automated Cell Counter (Invitrogen) was used to determine the total number of live cells. The volume of the cell suspension for subculturing was calculated with the following equation:

Equation 2.1

*Total Seeding Media (mL) / (Cell Concentration (cells per mL) / Cell Number Required) * 1000 = Volume of cell suspension to seed (ul) in total seeding media (GM)*

The cells were subcultured into a new T75 flask with fresh GM every 2-3 days at a concentration of 1x10^5 cells/mL to achieve approximately 1x10^6 cells per flask.

If the cell concentration could not be determined by the CountessTM Automated Cell Counter, then it was determined manually by using the Neubauer counting chamber (hemocytometer). The cells were mixed with trypan blue stain in 1:1 ration as described previously, loaded on a hemocytometer, and counted under the light microscope. The viable cells were not stained with trypan blue whereas dead cells appeared blue in the light microscope. The average number of viable cells were determined by counting cells in two squares and dividing it by 2. The cell concentration was calculated with the following equation:

Equation 2.2

*Cell Average * 1x10^4 * Dilution Factor = Cell Concentration (cells/mL)*

As example:

Cell Average = 60

Dilution factor = 2

60 * 1x10^4 * 2 = 1.2 x 10^6 cells/mL

The volume of the cell suspension for subculturing was calculated as described above and cells were subcultured as previously described.

2.1.5 Cell differentiation

To stimulate differentiation of THP-1 monocytes into macrophages-like cells phorbol 12-myristate 13-acetate (PMA) was used. Working 10uM PMA solution was made by diluting 10mM stock PMA with PBS in 1:1000 ratio. In 96-well plates and 24-well plates the THP-1 cells were seeded at 2x10^5cells/mL. The required volume of 10uM PMA was calculated by using ***Equation 3*** and diluted with appropriate volume of GM depending on size and number of wells required, 96-well plate (100uL/well), 24-well plate (500uL/well). The THP-1 cells were centrifuged, and supernatant was removed. 100uL of PMA diluted in GM was added into each well and cells were incubated for 3 days. An increase of macrophage markers (CD14, TLR4, CD36) in differentiated THP-1 macrophages-like cells was measured by real time RT-PCR.

Equation 3

$$C_1V_1 = C_2V_2$$

2.1.6 MSU treatment

Monosodium urate crystals (MSU) were used in this study to simulate the effect of endogenous molecules that activate NLRP3 inflammasome in joints and cause gout attacks. MSU crystals had been manufactured by the protocol stated in (Denko et al., 1976)) and readily available to use in stock concentration of 0.004g/ml. The crystals had been tested and were endotoxin free. Working solution was made by calculating required volume of MSU from stock to achieve the final concentration of 500ug/ml per well (***Equation 3***). Stock solution was made by mixing 0.004g/ml of stock MSU powder with 1ml of GM in separate Eppendorf tube. The required volume of MSU was aliquoted from stock solution and diluted with GM to required final volume (number of wells*uL/well*10%). Hence it is not possible to determine a physiologically relevant MSU crystal concentration, the concentration of MSU crystals used in this study was consistent with the previous in vitro study (Zheng et al., 2015).

2.1.7 Drug Treatments

To determine whether time of day affects the ability of prednisolone and heme to regulate NLRP3 inflammasome activity in THP-1 monocyte/macrophage-like cells, the drugs such as prednisolone and

heme as well as their vehicles DMSO and NaOH respectively, were used in Caspase-1 assay. The drugs and vehicles stock concentrations were prepared following consultation of the literature to match concentrations observed in circulation following prednisone treatment (for prednisolone) or normal healthy adults (heme). These concentrations were also similar to those used in similar studies. The concentration of prednisolone was obtained from the clinical study of asthma (Ramsahai et al., 2020) and concentration of heme used in this study was consistent with the following studies (Figueiredo et al., 2007; Song et al., 2020). Prednisolone and heme were used at 100ug/L and 30uM respectively by diluting the solvent-based stock 1:1000 with media. DMSO and NaOH (0.1M) were used as negative control and also diluted at 1:1000 with media.

To determine whether REV-ERBα activity regulates the NLRP3 inflammasome in treated THP-1 monocyte/macrophages-like cells (+/- MSU, +/- PMA), the pharmacological REV-ERBα antagonist (SR8278) and heme (an endogenous REV-ERBα agonist) as well as their vehicles DMSO and NaOH respectively, were used in Caspase-1 assay. The concentration of SR8278 (1uM) used in this study was obtained from the previous study which investigated the effect of SR8278 in HEK293 cells (Kojetin et al., 2011). The researchers determined that the peak of SR8278 inhibitory effect is achieved at 1uM with IC50= 0.35uM. SR8278 was used at 1uM by diluting the solvent-based stock 1:1000 with media. DMSO and NaOH were used as negative control and diluted at 1:1000 with media.

2.2 Development of a method for THP-1 cell transfection

2.2.1 Chemical Transfection method

The University of Auckland biosafety approval for this experiment was granted by the number APP202708, approved user BSC2918. One of the main aims of the study was to determine the effect of altered *BMAL1* expression on NLRP3 inflammasome activation in THP-1 cells and differentiated THP-1 macrophages-like cells. In order to achieve this, a protocol to effectively transfect undifferentiated and differentiated THP-1 cells needed to be established. Firstly, a chemical transfection protocol was trialled using lipofectamine reagents in which the *BMAL1* gene was knocked down by short-interfering RNA (siRNA) and ectopically overexpressed using plasmid transfection. The knockdown and ectopically expressed differentiated THP-1 cells were not directly compared to untreated THP-1 cells due to the nature of plasmid transfection which can induce cell stress and cell death. To eliminate these potentially confounding factors of transfection, the *BMAL1* knockdown THP-1 cells were compared to cells treated with control siRNA targeting enhanced green fluorescent protein (EGFP). Cells ectopically overexpressing *BMAL1* were compared to cells transfected with a control plasmid encoding Green Fluorescent Protein (GFP).

To determine the proportion of cells successfully transfected with siRNA, cells were transfected with siRNA encoding laminin A. Knockdown of laminin A leads to cell death therefore by determining the number of surviving cells relative to the number of cells originally seeded, the percentage of cells which have taken up the siRNA could be determined. To determine the proportion of cells successfully transfected with plasmid, direct count of GFP-positive cells under a fluorescent microscope was undertaken.

Knockdown with siRNA

THP-1 cells were seeded at a concentration of 2x10^5 cells/mL in 96-well plates with a total of 100ul per well. The cells were seeded 24h prior to transfection resulting in ~70-80% cell confluence at time of transfection. One hour prior to cell transfection, the GM was replaced with serum-free medium. The volume of serum-free medium was decreased to half of the initial volume of GM. For this experiment the following conditions were included as controls: untreated THP-1 cells, THP-1 treated with transfection reagent alone in the absence of siRNA, THP-1 treated with siRNA in the absence of transfection reagent and THP-1 treated with siRNA alone.

The knockdown transfection was performed using LipofectamineTM RNAiMAX Transfection Reagent (LifeTechnologies). The cells were seeded in triplicate for each condition. Three different siRNA concentrations (1pmol, 1.5pmol, 2pmol) were used to determine the optimum siRNA concentration for cell transfection in keeping with the manufacturer's recommendations for transfections with lipofectamine RNAiMAX. The siRNAs in concentration of 200ng/uL were diluted in sterilised TE buffer (Tris-EDTA buffer) pH 8 (1:3 ratio). The siRNA solution was further diluted in Opti-MEM reduced serum medium (1:27.7 ratio) and kept on ice. LipofectamineTM RNAiMAX Reagent was diluted in Opti-MEM (1:50.6 ratio). Diluted siRNA was added to LipofectamineTM RNAiMAX Reagent (1:1 ratio), mixed thoroughly, incubated at room temperature for 5 min and 10uL of complex was added to each well.

The cells were incubated for 18 hours at 37°C, then media in all wells was replaced with 100uL of GM and cells were left to recover in an incubator for another 30 hours at 37°C. The cells were analysed under a fluorescent microscope after 48 hours from the moment of transfection.

Ectopic overexpression with plasmid

Cells were seeded as described for knockdown with siRNA. Ectopic overexpression was performed using Lipofectamine™ 3000 Transfection Reagent (ThermoFisher Scientific). To transfect each well in 96-well plate 0.15ul of LipofectamineTM 3000 Reagent was diluted with 4.85uL of Opti-MEM Reduced serum medium to a total of 5uL as per the manufacturer's recommendation. To prepare master mix of DNA 0.2uL/well of P3000 was mixed with 100ng/well of plasmid in a separate Eppendorf tube. The concentration of BMAL1 plasmid was 282.2ng/uL, therefore 0.35uL was used per well. The concentration of GFP plasmid was 239.8ng/uL, therefore 0.42uL was used per well. It was made up to 5uL with Opti-MEM. The master mix was mixed with diluted LipofectamineTM 3000 Reagent in 1:1 ratio, incubated for 10 min at room temperature and 10uL of complex was added to each well. Triplicates wells were used for each condition.

Treated cells were incubated for 18 hours at 37°C, then media in all wells was replaced with 100uL of GM and cells were left to recover in an incubator for another 30 hours at 37°C.

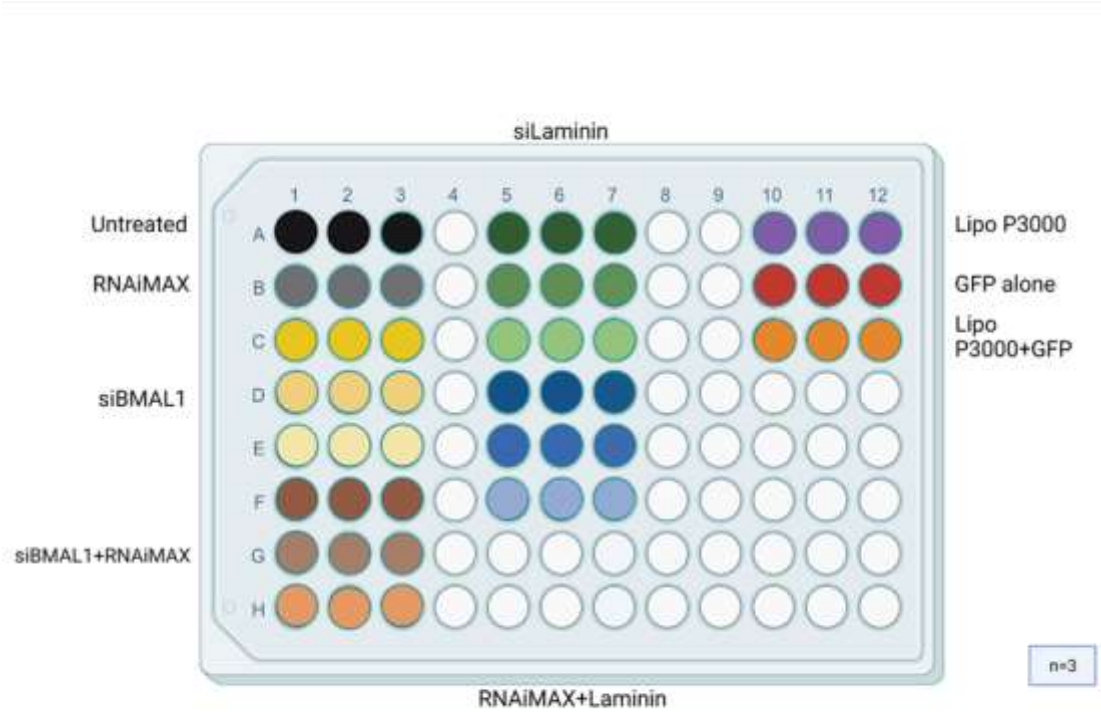

Figure 2.1 Plate layout of the THP-1 cell transfections. Cells were seeded in a 96-well plate. RNAiMAX is vehicle control. siBMAL1 is the control for knockdown. siBMAL1+RNAiMAX is the *BMAL1* knockdown treatment. siLaminin is the control for cell toxicity. RNAiMAX+Laminin is the control for cell toxicity. Lipo3000 is vehicle control, GFP alone is the control for overexpression and Lipo3000+GFP is *BMAL1* overexpression treatment. Cells were seeded in 96-well plate. 'n' represents the number of technical replicates. Figure created using Biorender software.

Knockdown with siRNA method analysis

The knockdown transfection of THP-1 cells with siRNA didn't show the adequate results. The percentage of alive cells treated with RNAiMAX+Laminin at three different concentrations (1pmol, 1.5pmol, 2pmol) is almost the same as the percentage of alive cells treated with RNAiMAX or untreated cells.

Table 2.1. Laminin cell count results. The percentage of alive cells is shown.

Untreated cells	RNAiMAX	siLaminin (1pmol)	siLaminin (1.5pmol)	siLaminin (2pmol)	RNAiMAX+Laminin (1pmol)	RNAiMAX+Laminin (1.5pmol)	RNAiMAX+Laminin (2pmol)
48%	10%	47%	42%	7%	23%	27%	19%
29%	37%	14%	50%	12%	11%	34%	25%
48%	28%	39%	25%	12%	14%	13%	27%

Plasmid Method Analysis

To check the efficacy of cell transfection using plasmid, the cells were analysed using fluorescent microscope (Nikon Eclipse Ni-E Upright Microscope System) after 48h from transfection. The images of each well were taken to determine whether a plasmid was taken or not by THP-1 cell. At least two images were taken for each well with 10x and 20x magnification at 10 seconds exposure using the NIS-Elements Advanced Research Microscope Imaging Software. To determine total cell number, Hoechst dye was used as a counterstain.

The following images demonstrate the efficacy of plasmid transfection:

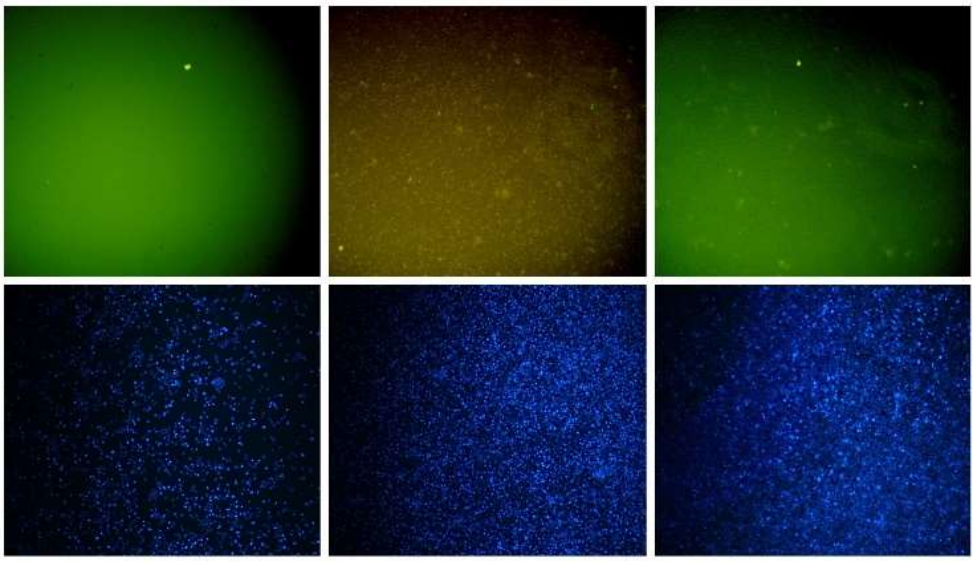

The successfully transfected cells were presented as green dots due GFP-tag, the rest of the cells were not transfected. The efficacy of plasmid transfection of THP-1 cells was very low (<1%), therefore the decision

was made to perform next trial using a virus transfection method. This decision on using viral-mediated gene delivery was based on consultation with other researchers who used THP-1 cells and had no success in transfecting the cells using the same plasmid method (lipofectamine) (Lee et al., 2004).

2.2.2 Virus Transfection

Pilot testing using adenovirus

The University of Auckland biosafety approval for this experiment was granted by the number APP202708, approved user BSC2918. To determine the transduction efficiency and to optimize viral infection condition in THP-1 cell line, the recombinant adenovirus that expressed enhanced GFP under the control of a CMV promoter was used, Ad-CMV-GFP. The AdGFP adenovirus was used as a potential non-targeting control for overexpression of *BMAL1* gene and Ad-CMV-shRNA (Scramble)-GFP was used as a potential non-targeting control for knockdown of *BMAL1*. The THP-1 cells were seeded into 96-well plate at 2x10^5 cells/well. To determine optimum concentration of virus, cells were plated in triplicates for 3 conditions (Untreated, shGFP and adGFP) with a different volume of virus/well (4uL/well, 12uL/well, 20uL/well). Each volume of virus/well meant to change the Multiplicity of Infection (MOI) to 100, 300, 500 respectively. The MOIs to be trialled were determined based on previous study (Cao et al., 2018). From the literature search it was determined that high MOIs are required as THP-1 cells express low levels of adenovirus receptor and transfection reagent assisted adenoviral delivery does not work in THP-1 cells. Opti-MEM was pre-warmed in a bead bath at 37°C, and adenoviruses removed from -80C storage and thawed on ice. Working stocks of adenoviral vectors shGFP and adGFP were made at a concentration of 500,000pfu/uL by diluting with Opti-MEM in a separate Eppendorf tube for each viral vector. Viral vector was added to corresponding wells and cells were incubated for 24h at 37°C at 5% CO2 for transfection analysis using fluorescent microscope. The cells were centrifuged and washed with PBS to remove virus and replace old medium with new GM and incubated for additional 48h to check the efficiency of virus transduction. The optimal transduction efficiency was observed between 100 and 300 MOI, therefore 8uL virus/well (200MOI) was decided to be used for the future experiments.

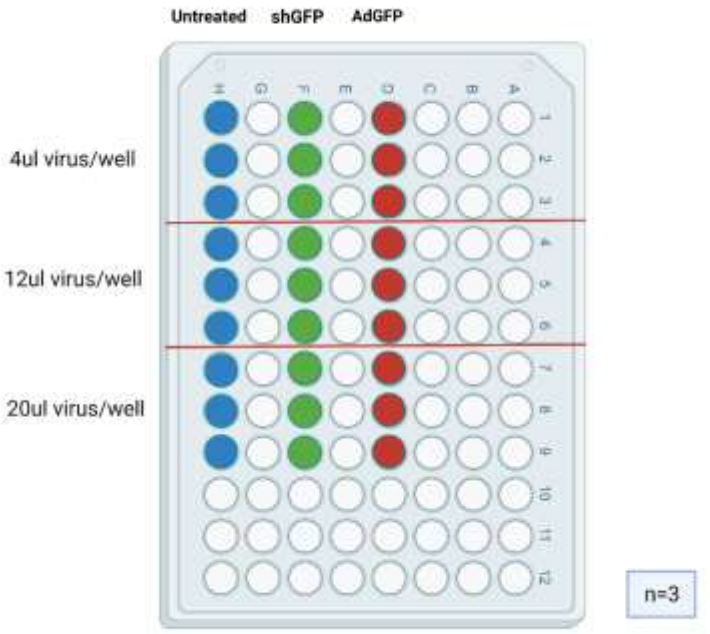

Figure 2.2. Plate layout for pilot testing of adenoviruses. Cells were seeded in 96-well plate. 'n' represents the number of technical replicates. Figure created using Biorender software.

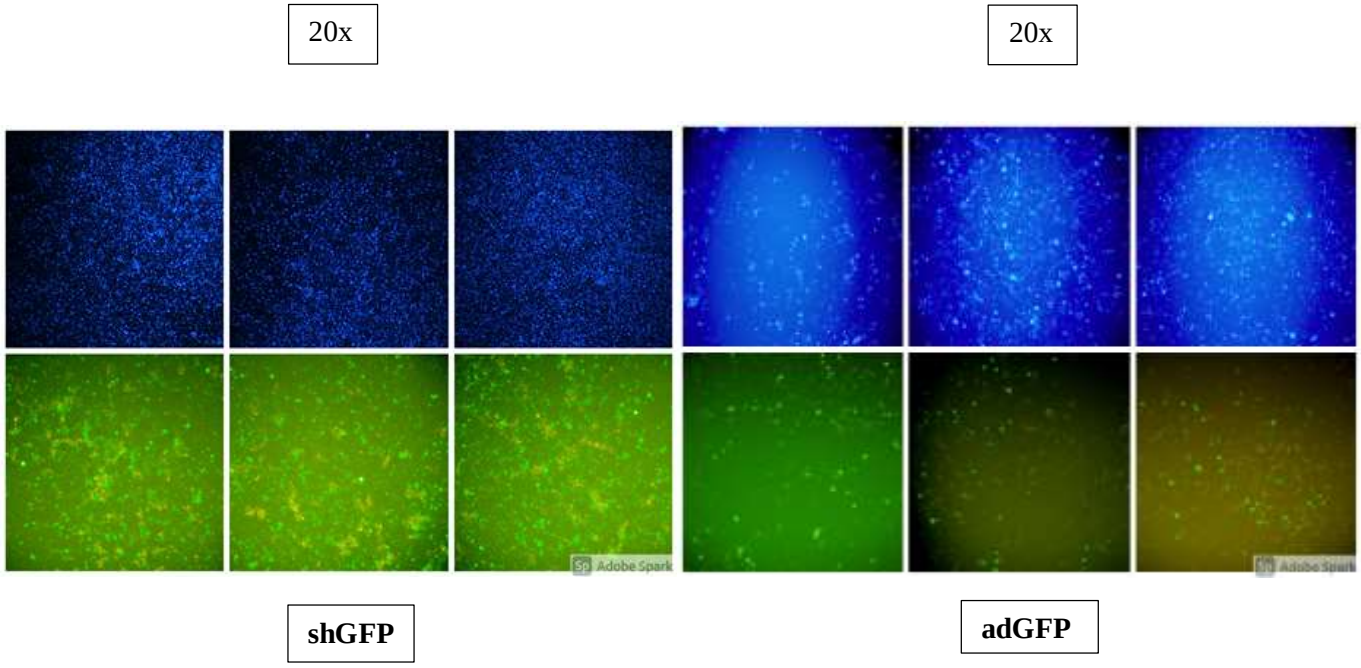

The efficacy of adenovirus transfection of THP-1 cells was high (>60%), therefore the decision was made to proceed with this transfection method.

2.3 Analysis of Gene Expression

One of the main aims of the study was to determine the effect of MSU exposure on expression of circadian clock components in THP-1 cells and macrophages-like cells. This required measurement of RNA expression at multiple timepoints across a 24h period. A relatively high-throughput method of cDNA synthesis was required due to the large number of samples that would be generated.

2.3.1 Cell lysis and preparation of cDNA using Cells-to-cDNA II Kit

A direct cells-to-cDNA method was utilized to examine transduction efficiency and the effects of treatments. This method was already established in the lab and successfully worked for other cell types to enable direct production of cDNA from cells grown in 96-well plates.

Cells in three 96-well plates (24h,48h,72h) were centrifuged at 240g for 5 min to remove supernatant (100uL) and washed with ice-cold PBS (100uL/well) using multichannel pipette. The cells were centrifuged again at 240g for 5min to remove PBS and 30uL of ice-cold cell lysis buffer II was added to each well pipetting up and down to lyse the cells. Cell lysate was transferred into 96-well PCR plate and quickly heated at 75°C for 15min in a thermocycler (PTC-100Ⓡ Thermal Cycler) to minimize RNA degradation. The plate was removed from thermocycler and placed on ice. Subsequently, 1uL/well of DNase and 3uL/well of DNase buffer were mixed in Eppendorf tube and added to the cell lysate. The plate was heated at 37°C for 15min then 75°C for 5min to degrade genomic DNA and deactivate DNase. The plate was kept on ice and 8uL of the DNase-treated lysates were moved into a new 96-well PCR plate. The left-over lysate was labelled and stored at -20°C. Diluted 1uL/well of random primers and 3uL/well of dNTPs were mixed in separate Eppendorf tube and 4uL of mix was added into each well containing 8uL of the DNase-treated lysate. The plate was heated at 70°C for 5min in a thermocycler. For the required number of samples, a sufficient volume of the following mix was prepared in an Eppendorf tube:

Table 2.2 cDNA mix for Reverse transcription reaction. The components were obtained from MMLV- Reverse Transcriptase Kit.

Component	Volume per well (µL)
0.1M DTT	2
MMLV Reverse Transcriptase (200U/uL)	0.5
First Strand RT Buffer 5X	4
RNase-free water	2
Total	8.5

PCR preparation for cells to cDNA II method

The mix from ***Table 1*** was added into each well and plate was heated to 37°C for 50min then 75°C for 15min and chilled at 4°C. The cDNA samples were diluted with 30uL of DEPC water per well and stored at -20°C until required for PCR. Real time PCR was performed for the housekeeper genes 18S and Beta-actin as described in 2.3.3 using 2uL of the synthesized cDNA per reaction. Each reaction was done in duplicates, plus water blanks were added as a negative control. 8uL of reaction mixture was added into corresponding wells *(**Table 5**)*.

Table 2.3 Composition of reaction mixture for RT-qPCR using Cells-to-cDNA II method.

Component	Volume per reaction (µL)
Primer (18S, BMAL1, ACTB, TLR-2, CD14, CD36)	1
DEPC water	2
SYBR® Select Master Mix Primer	5
cDNA	2
Total volume	10

2.3.2 Cell lysis and preparation of cDNA using TRIzol® Reagent

The Ct values of housekeeper genes such as 18S and Beta-actin (ACTB) were abnormally high. The range of Ct values for 18S was between 25 and 30 (expected Ct values 8-12) and the range of Ct value

for ACTB was between 30 and 36 (expected Ct values 20-25). Therefore, these results could not be used be compared to BMAL1 gene expression. To eliminate experimental error, the cells to cDNA II method was performed twice and in both times Ct values for 18S and ACTB were not in adequate range.

To improve the quality and quantity of RNA extraction, the TRIzol® Reagent and Quick-RNA Miniprep kit (ZYMO Research) were employed.

RNA Purification

The cells were centrifuged at 260g for 5min, and all the supernatant was removed. TRIzol reagent (200uL) was added into each well, the cells were pipetted up and down for homogenization and incubated for 5 min at room temperature. The plate was wrapped using a film and placed in -80°C freezer for 10min to complete the cell lysis process. After 10 min in -80°C the plate was thawed on ice and an equal volume of ethanol (95%) was added to the samples lysed in TRIzol reagent and mix thoroughly. The mixture was then transferred into ZYMO-spin column which was placed in a collection tube and complex was centrifuged at 15,000g for 30 sec. The column was transferred into a new collection tube and the flow-through was discarded. 400uL of RNA Wash Buffer was added into each column and centrifuged at 15,000g for 30 sec. To improve the quality of RNA extraction, DNA was removed using DNase. DNase (1500U) from the kit was eluted in 275uL of DNase/RNase free water and stored at -20°C. In a separate Eppendorf tube 5ul/column of DNase was mixed with 75uL/column of Digest Buffer. 80uL of mixture was added to each column and incubated at room temperature for 15min. 400uL of Direct-zol RNA Prewash was added to the column and centrifuged at 15,000 for 30sec, this step was repeated twice. 700uL of RNA Wash Buffer was added to the column and centrifuged for 2min to remove impurities. Subsequently the column was carefully transferred into RNase Free tube for RNA elution. To elute RNA, 15uL-25uL of DNase/RNase Free water was added into the column and centrifuged for 30sec. Eluted RNA was either immediately used to synthesise cDNA or stored frozen at -80°C.

Nanodrop Measurements of RNA

To measure RNA concentration a Nanodrop Lite Spectrometer was used. The DNase/RNase-free water (1uL) was used as a blank to calibrate the readings. The RNA concentration from each sample was determined by measuring the light absorbance at wavelengths of 260-280nm. The purity of RNA is indicated by the A260/A280 ratio which is approximately 2.0. If the values were between the range 1.7-2.0 it would indicate that sample has minimum contaminants such as phenol, TRIzol and DNA. The RNA concentration of each sample was measured in ng/ul. The RNA concentrations were standardised to the

lowest RNA value only if the RNA yield was sufficient. Standardization of sample was done by diluting it with DNase/RNase free water to make all RNA concentrations equal.

Pilot Testing

Pilot testing of this method was conducted to determine the RNA yield. During the THP-1 cell line subculturing, required cell suspension was calculated ***(Equation 1)***. The cells were placed in 4 separate Eppendorf tubes and diluted with GM to make up 1mL/tube in total. The Eppendorf tubes were centrifuged at 260g for 5min, and supernatant was removed. Cells were lysed using TRIzol Reagent. RNA was extracted using different amount of RNase Free Water 15uL and 25uL to determine if there is a difference in RNA concentration. The results showed that increasing cell number did not result in increased RNA yield ***(Table 2.4).*** Therefore, the decision was made to procced with 2x10^4 cells/mL eluted in 15uL of RNase free water as it produced just enough RNA yield (12.7ng/uL) for RT-qPCR.

Table 2.4 Pilot testing of TRIzol reagent and RNA Purification method.

Number of cells/mL	Volume of RNase free water (uL)	RNA concentration (ng/uL)
2x10^4	15	12.7
2x10^4	25	9.8
5x10^4	15	8.2
5x10^4	25	6.8

Synthesis of cDNA from RNA

To synthesis cDNA from RNA, 11uL of standardised RNA samples were placed in a 96-well PCR plate and treated with Master Mix A and Master Mix B. Master Mix A was prepared in separate Eppendorf tube by mixing 1uL/well of dNTP (10mM) with 1uL/well of Random Primers (50ng/uL) and adding 2uL/well to RNA samples. The plate was heated in thermocycler at 65°C for 5min to anneal primers and then kept on ice prior to addition of Master Mix B. Master Mix B was prepared in separate Eppendorf tube using the reagents described in ***Table 2.5***. 7uL of Master Mix B was added to each well and placed in thermocycler at 25°C for 5min, 50°C for 60min, and 70°C for 15min for reverse transcription. The synthesised cDNA was either used immediately for RT-qPCR reactions or stored frozen at -20C. The cDNA samples were not diluted with DEPC water prior to RT-qPCR.

Table 2.5 Master Mix B for cDNA reverse transcription.

Component	Volume per well (uL)
Superscript III Enzyme	1
RNase OUT	1
0.1M DTT	1
First Strand Buffer 5X	4
Total volume	7

2.3.3 Real-time Quantitative Polymerase Chain Reaction (RT-qPCR)

The housekeeper ribosomal 18S primer (Life Technologies) was used as a reference gene.
For each individual primer the reaction mixture was made in the separate Eppendorf tubes. The primers were chosen depending on the type of experiment.

18S Forward sequence: GTAACCCGTTGAACCCCATT
18S Reverse sequence: CCATCCAATCGGTAGTAGCG

Table 2.6 SYBR Green Primers used for RT-qPCR.

Gene of interest	Abbreviation	Assay Name	Catalogue Number
BMAL1	ARNTL [Human]	Hs_ARNTL_1 Quantitect primer assay	QT00011844
PER1	PER1 [Human]	Hs_PER1_1_SG Quantitect primer assay	QT00069265
PER2	PER2 [Human]	Hs_PER2_1_SG Quantitect primer assay	QT00011207
PER3	PER3 [Human]	Hs_PER3_1_SG Quantitect primer assay	QT00097713
CRY1	CRY1 [Human]	Hs_CRY1_SG Quantitect primer assay	QT00025067
CRY2	CRY2 [Human]	Hs_CRY2_SG Quantitect primer assay	QT00094920
REV-ERBα	NR1D1 [Human]	Hs_NR1D1_1_SG Quantitect primer assay	QT00000413
TLR4	TLR4 [Human]	Hs_TLR4_SG Quantitect primer assay	QT00047937
CD14	CD14 [Human]	Hs_CD14_SG Quantitect primer assay	QT00046382
CD36	CD36 [Human]	Hs_CD36_SG Quantitect primer assay	QT00039648
CLOCK	CLOCK [Human]	Hs_CLOCK_1_SG Quantitect primer assay	QT00054481

PCR preparation for TRIzol reagent and RNA purification method

The synthesized cDNA from each sample (4uL) was added into the 384-well PCR plate. Each reaction was done in duplicates, plus water blanks were added as a negative control. 6uL of reaction mixture was added into corresponding wells to create a final reaction volume of 10ul ***(Table 2.7)***.

Table 2.7 Composition of reaction mixture for RT-qPCR using TRIzol reagent and RNA purification method.

Component	**Volume per reaction (µL)**
Primer (18S, BMAL1, ACTB, TLR4, CD14, CD36, CRY1/2, PER1/2/3, REV-ERBα)	1
DEPC water	0
SYBR® Select Master Mix Primer	5
cDNA	4
Total volume	10

The plate was sealed using transparent PCR adhesive cover and centrifuged at 1000rpm for 30sec to make sure all the components were mixed. The QuantStudio^{TM} 12K Flex Real-Time PCR machine was used to perform RT-qPCR. The PCR cycle for SYBR green was the following:

Hold Stage:

50°C, 2 minutes

Denaturation Stage:

95°C for 2 minutes

PCR Stage (40 cycles):

95°C, 15 seconds

60°C, 1 minute

Melt Curve Stage:

95°C, 15 seconds

60°C, 1 minute

95°C, 15 seconds

To determine the threshold cycle (C_T) values the QuantStudio 12K Flex Software was used. Those (C_T) values were exported on a Microsoft Excel spreadsheet and analysed. The standard deviation of the

duplicates was <0.1, therefore the average measurements of the replicates could be determined. First, the average C_T value of each sample was determined from the duplicates by using Excel formula "=AVERAGE". Next, for every gene of interest C_T value were normalized to its corresponding 18S C_T value (***Equation 4***). Delta C_T value of each sample was converted into log value by using formula: = 2^ (Δ C_T). The gene expression was expressed as a fold change by dividing log value of each sample by control value (untreated cells) to give a 2^ Δ Δ C_T value. The overexpression and down regulation of gene of interest was presented as >1 and <1 fold change, respectively.

Equation 4

$$\Delta C_T \; of \; each \; sample = \; C_T \; (BMAL1) - \; C_T \; (18S)$$

2.3.4 Data Analysis

The experiment was performed once with 6 technical replicates (n=6) for each time point for statistical purposes. The expression between controls and treatments were statistically analysed by two-way ANOVA with Tukey and Sidak multiple comparison testing using Prism GraphPad 9. The time course data for majority of the genes of interest had to be log 2 transformed to pass Spearman's test and Normality of Residuals tests. The Friedman's test was used to analyse the genes which failed to pass all the normality tests as well as Spearman's test in transformed form. Results are shown as mean ± SEM. A p-value of <0.05 was considered statistically significant.

Transfection of THP-1 cells using adenoviruses

To determine the effect of altered BMAL1 expression on NLRP3 inflammasome activation in THP-1 cells and differentiated THP-1 macrophages-like cells virus transduction method was used. This experiment was conducted in three 96-well plates, a plate per time point (24h, 48h, 72h). The THP-1 cells were seeded in 96-well plate and treated with PMA (PMA treatment protocol). After 3 days, THP-1 cells were seeded at 2x10^5cells/well and after 8 hours both macrophages-like cells and THP-1 cells were treated with different adenoviruses for BMAL1 gene knockdown and overexpression ***(Figure 2.3).*** The cells were incubated at 37°C for 24h, 48h, 72h. After each time point the corresponding plate was removed from an incubator, centrifuged at 240g for 5 min, supernatant was removed, and cells were washed with 100uL of PBS x 1. Subsequently, cells were lysed with TRIzol Reagent and RNA was isolated following the method described in 2.3.2. cDNA was synthesised from RNA and RT-qPCR was conducted.

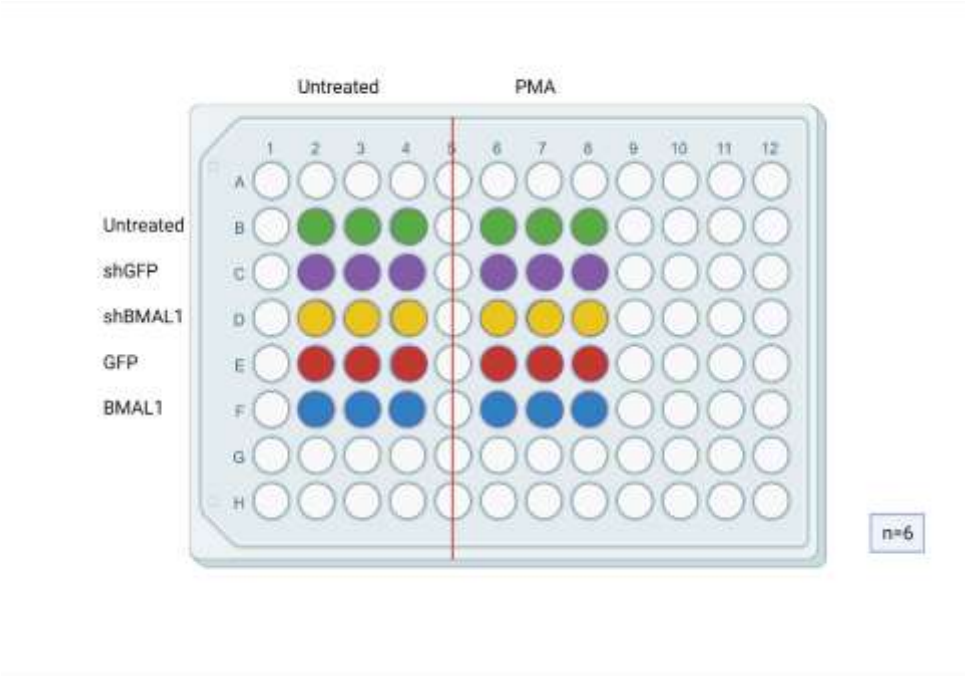

Figure 2.3. Plate layout of the adenovirus transfection applied to THP-1 and macrophages-like cells. Cells were seeded in 96-well plate. 'n' represents the number of technical replicates. Figure created using Biorender software.

The efficacy of adenovirus transfection of THP-1 cells was determined based on two time points 48h and 72h as the 24h time point couldn't be used for RT-qPCR analysis due to contamination. shGFP was used as a control for *BMAL1* knockdown (shBMAL1). BMAL1 adenovirus was used for *BMAL1* overexpression. The data were normalized to 18S, and fold change was determined for shBMAL1 expression relative to shGFP. The results showed a significant reduction in *BMAL1* expression, therefore adenovirus was used as a method of transfection in the next experiments.

2.4 24-hour overnight experiment

96-well plate

To determine whether treatment of THP-1 (+/-MSU, +/- PMA) effect the expression of core circadian oscillator components a 24h time-course experiment was conducted with cell lysates collected at 4-hourly intervals over 24h period. In preparation for this 24-hour experiment, seven 96-well plates were used with one plate for each of the 4-hour time points ***(Figure 2.4).*** Six plates had cells seeded in 4 different conditions: Untreated, PMA treated, MSU treated and PMA+MSU treated. One plate (0 time point) had cells seeded in 2 conditions: Untreated and PMA treated and was used for baseline data. The cells were seeded with 6 wells per condition at 2x10^5cells/well, volume of cell suspension was calculated using

Equation 3. The THP-1 cells were seeded first only for PMA and PMA+MSU conditions following PMA treatment protocol as described previously. After 3 days, the rest of the cells were seeded for the two other conditions to make sure the cell numbers are similar. The time period of 3 days was necessary as the PMA treated cells don't proliferate whereas non-PMA treated cells will be overly confluent in this time. Monocytes and differentiated macrophages-like cells were serum starved for ~18 h by replacing GM with 100uL FBS Free serum media and then fed with GM (to synchronise cell clock) in the presence or absence of MSU crystals (MSU Treatment protocol). Cells in replicate wells were collected for RNA analysis prior to feeding and/or MSU crystal exposure (0h timepoint plate) for baseline data and at 4 hourly intervals for a period of 24 h after feeding/MSU crystal exposure. The 24h experiment required the collection of cell lysates after hours, therefore RNA Later was used to preserve cells as hazardous substances like TRIzol Reagent could not be handled after hours. To preserve the cells for future cell lysis and RNA Purification, supernatant was replaced with 100uL of RNA Later and plates were stored at -20°C. The cells were lysed using TRIzol Reagent, RNA was purified (RNA Purification protocol) and cDNA was synthesised. The expression of only three core circadian genes (*BMAL1, CRY2, REV-ERBα*) was measured by RT-qPCR due to the low concentration of RNA. Therefore, the next overnight experiment was performed in 24-well plates to achieve higher RNA concentration and measure the full range of core circadian genes.

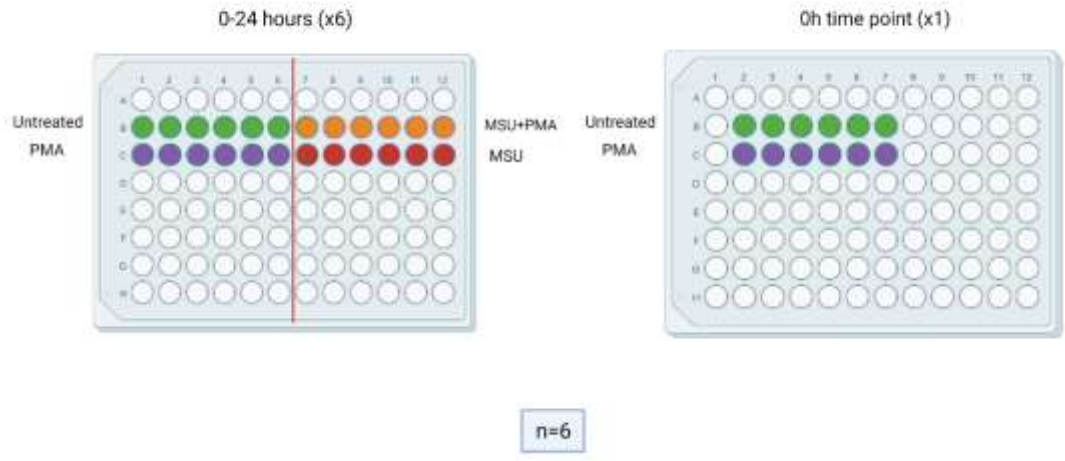

Figure 2.4 Plate layout for 24-hour experiment. Cells were seeded in 96-well plate with 6 technical replicates per treatment. A separate 96-well plate was used per time point to enable cells to be harvested at each timepoint without disturbing cells for subsequent timepoints. Figure created using Biorender software.

24-well plate

The same protocol was used for cell seeding and cell treatment as for 96-well plate but in the scale of 24-well plate ***(Figure 2.5).*** The cells were not preserved with RNA later but instead were lysed using 300uL TRIzol Reagent and frozen at -80°C for future RNA Purification and cDNA synthesis. The expression of the full range of core circadian genes (*BMAL1, CLOCK, CRY1/2, PER1/2/3*) and auxiliary clock gene which is implicated in the control of inflammation (*REV-ERBα*) as well as genes involved in mediation of MSU crystal inflammation (CD14, CD36 and TLR4) were measured by real time PCR.

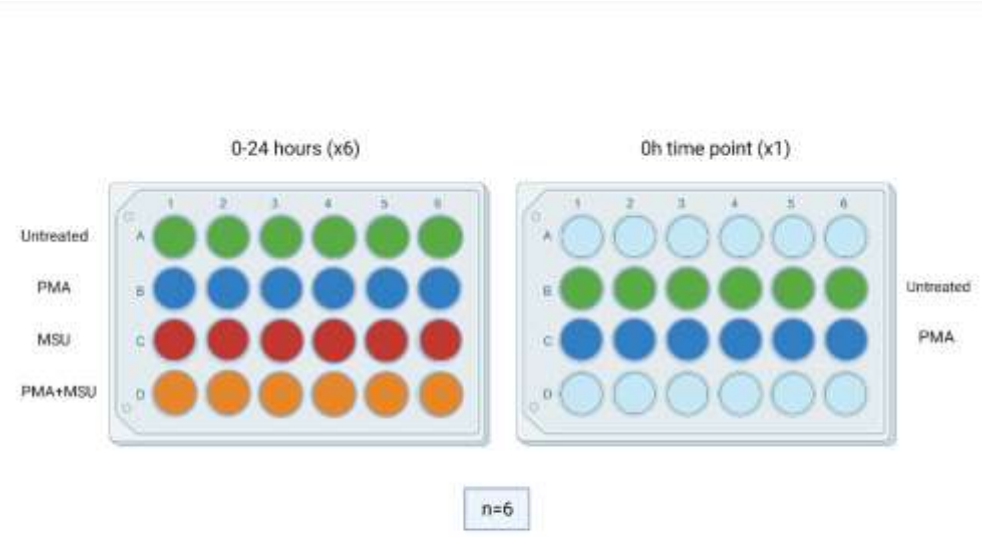

Figure 2.5 Plate layout for 24-hour experiment. Cells were seeded in 24-well plate with 6 technical replicate per condition. A separate 96-well plate was used per time point to enable cells to be harvested at each timepoint without disturbing cells for subsequent timepoints. Figure created using Biorender software.

2.5 Caspase-Glo-1 Inflammasome Assay

To determine the effect of altered BMAL1 levels on NLRP3 inflammasome, Caspase-Glo-1 Inflammasome assay was conducted. It is a bioluminescent method to selectively measure the activity of the essential component of the NLRP3 inflammasome, caspase 1. The selective caspase-1 substrate (Z-WEHD) enabled detection of catalytically active caspase-1 in treated cells or culture media alone and quantitative measurement of NLRP3 activity. The assay included the use of two proteosome inhibitors MG-132 and Ac-YVAD-CHO. MG-132 was used to eliminate non-specific proteosome substrate cleavage to enable sensitive detection of caspase-1. Ac-YVAD-CHO was used as caspase-1 specific inhibitor to confirm

specific activity in parallel samples and distinguish caspase-1 activity from other caspases. The Caspase-Glo 1 buffer and Z-WEHD substrate were equilibrated to room temperature prior to use. The Z-WEHD substrate was in a powder form, therefore it had to be reconstituted by transferring the contents of Caspase-Glo 1 buffer into the amber bottle with Z-WEHD. The reagent was thoroughly mixed by swirling and inverting the bottle. The proteosome MG-132 Inhibitor and Ac-YVAD-CHO Inhibitor were thaw at room temperature prior to use. The Caspase-Glo-1 Reagent was prepared by adding 60 uL of MG-132 Inhibitor to 10mL of reconstituted Z-WEND Substrate and swirling the contents until the reagent thoroughly mixed. Subsequently, The Caspase Glo 1 YVAD-CHO Reagent was made by transferring half of the Caspase-Glo 1 Reagent to a separate tube and adding Ac-YVAD-CHO Inhibitor at a ratio 1:1000 (2uL of Ac-YVAD-CHO Inhibitor added to 2mL of Caspase-Glo 1Reagent). The mixture was thoroughly mixed by inverting the tube multiple times. The 96-well plate containing cells in different conditions were removed from the incubator and equilibrated at room temperature for 5min. 100uL of Caspase-Glo 1 Reagent was added to half of the wells containing 100uL of treated cells, negative-control or blank (GM without cells). The other half of the wells were treated with 100uL of Caspase Glo 1 YVAD-CHO Reagent, 200uL in total/well. The 96-well plate was incubated at room temperature for 1 hour to stabilize the luminescent signal. The activity of caspase-1 in cells or culture media was detected by measuring a stable luminescent signal using a Tecan Spark plate reader at 30min, 60min and 90min after incubation.

2.5.1 Pilot Testing of Caspase-Glo-1 Inflammasome Assay (Attempt #1)

To determine the optimal conditions for cell number and their treatment period the Caspase-Glo 1 assay was performed with the following conditions: Untreated (THP-1 cells), MSU treated, PMA treated (macrophages-like cells), MSU+PMA treated, blank (GM only, no cells) ***(Figure 2.6).*** In addition, negative control (MSU+GM, no cells) was included to determine whether the crystals themselves interfered with the assay. The THP-1 cells were seeded on 96-well plate (2x10^5 cells/mL) in 100uL of GM and treated with PMA 3 days prior to Caspase-Glo 1 assay. THP-1 and macrophages-like cells were treated with MSU crystals 24 hours prior to Caspase-Glo 1 assay to promote inflammation and release of caspase-1. At the day of the experiment Caspase-Glo 1 assay was conducted and caspase-1 activity was measured according to the method described previously.

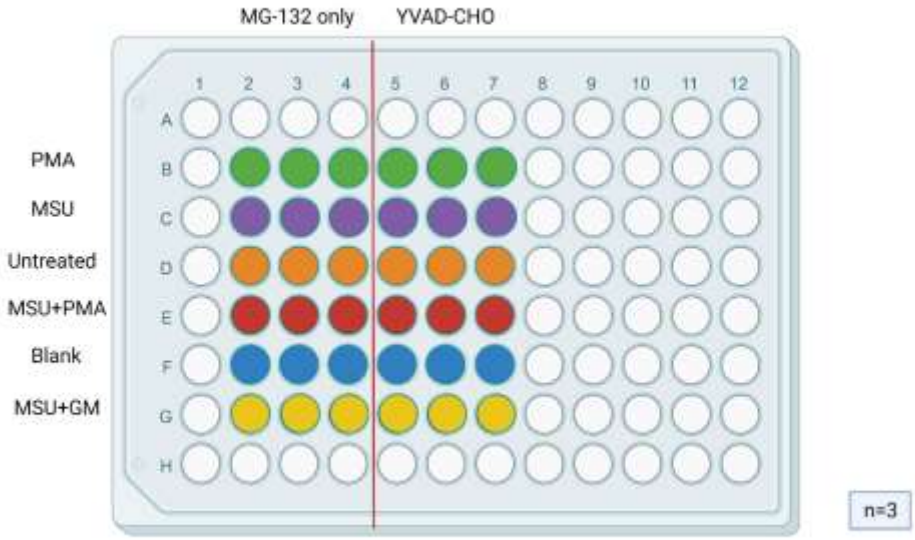

Figure 2.6 Plate layout of Caspase-Glo-1 Assay Attempt #1. Cells were seeded in 96-well plate with 3 technical replicates per condition. Figure created using Biorender software.

Analysis of #1 attempt Caspase Glo-1 assay

The results of the first attempt were not satisfactory as we did not observe difference in caspase-1 activity between cells treated with specific caspase-1 inhibitor YVAD-CHO and cells treated with non-specific inhibitor MG-132. Therefore, a few changes in the protocol were made following consultation of the literature to see what protocols had been used in similar studies (Jhang et al., 2015). First, the THP-1 cells were seeded in 96-well plate for only PMA and PMA+MSU conditions, the rest of the THP-1 cells were seeded 6-8 hours prior to addition of MSU crystals and conducting an assay. This was done to make sure the number of cells per well is similar in both PMA treated and THP-1 untreated conditions. As from the first attempt there was a clear difference in cell number evident by viewing cells under a microscope between PMA treated and untreated cells. Second, Z-WEHD Substrate was added in triplicates into the wells with no cells as an additional condition to provide a reading of the assay background. Third, as per manufacturer's instructions only growth medium was used to try and detect caspase-1 activity in 4 conditions (untreated, MSU, PMA, PMA+MSU). Fourth, the total assay volume of 100uL/well in 96-well plate was used to determine whether it would be sufficient for detection of caspase-1 activity. Fifth, for MSU and PMA+MSU conditions, the cells were treated with MSU crystals 4 hours prior to an assay, instead of 24 hours as it was stated in previous studies (Jhang et al., 2015). Lastly, the assay was performed at 3 different time points (30min, 60min, 90min) and based on the findings the optimal caspase-1 activity was detected at 60 and 90

minutes reading as the stable luminescent signal was observed. Therefore, 60min and 90min time points were used for the future assays.

30min

	MG-132 only			YVAD-CHO		
PMA	32033	41562	42423	66910	49275	47357
MSU	35528	39219	46389	52939	54506	43421
Untreated	10789	11686	12117	10306	8945	7532
MSU+PMA	6064	6721	7048	7151	6947	6437
Blank	2201	2204	1913	2589	1616	1261
MSU+GM	1680	1654	1687	1677	1474	1259

60min

	MG-132 only			YVAD-CHO		
PMA	2813	3468	3603	5410	4104	4002
MSU	3343	3542	4559	4996	4648	4089
Untreated	1719	1691	1786	1792	1593	1498
MSU+PMA	1175	1370	1355	1532	1501	1596
Blank	525	488	430	463	291	280
MSU+GM	294	301	352	309	290	264

90min

	MG-132 only			YVAD-CHO		
PMA	2398	2950	2782	4184	3175	3132
MSU	3002	3022	3615	3639	3448	2996
Untreated	1671	1565	1597	1657	1521	1386
MSU+PMA	1124	1397	1381	1352	1591	1662
Blank	551	509	434	406	331	274
MSU+GM	340	281	347	338	250	257

2.5.2 Caspase-Glo-1 Inflammasome Assay (Attempt #2)

For this experiment two 96-well plates were used ***(Figure 2.7).*** Plate **A)** was the main plate with cells treated with different conditions. Plate **B)** was a trial plate with only GM derived from cells treated with different conditions. The cells for PMA and PMA+MSU condition were seeded first at 2x10^5cells/mL in 50uL culture medium per well in both 96-well plates and incubated for 3 days. After 3 days, the cells for untreated and MSU treated conditions were seeded at the same concentration in 50uL of GM. All the cells were seeded in triplicates for each condition. The cells for PMA and PMA+MSU conditions were centrifuged, old media was removed, and cells were treated with 50uL of MSU crystals and incubated for 4 hours prior to an assay. After 4 hours, plate B) was centrifuged and 50uL of only growth media was moved into new

wells. The Caspase-Glo-1 Inflammasome assay was performed on both 96-well plates (A, B) as described above.

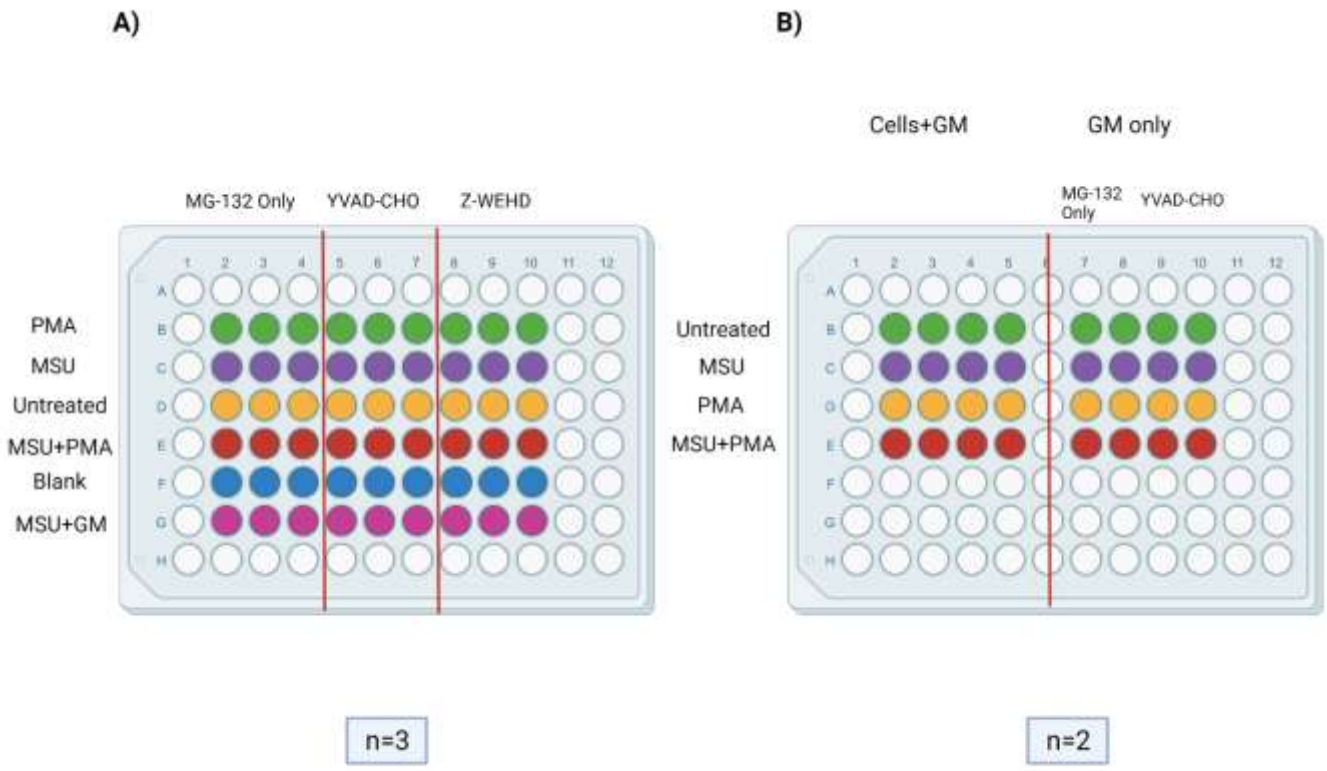

Figure 2.7 Plate layout of Caspase-Glo-1 Assay performed in (A) treated cells and (B) media only. Cells were seeded in 96-well plate with 3 technical replicates per condition. Figure created using Biorender software.

A) Treated cells

60min

	NO inhibitor			Inhibitor			Substrate only		
PMA	1953	2339	1892	2371	3499	2866	48487	20832	51391
MSU	4515	2829	3999	3502	3645	4362	272591	228766	319159
Untreated	8000	2155	6524	2314	2240	2390	116263	109397	354538
MSU+PMA	2218	1441	1808	2512	2157	3150	57202	54542	83006
Blank	183	199	225	217	276	349	721	722	725
MSU+med	194	172	204	197	215	222	524	566	605

90min

	NO inhibitor			Inhibitor			Substrate Only		
PMA	1966	2258	1818	2292	3214	2590	46371	19958	49179
MSU	3730	2307	3418	2909	2927	3547	261638	218290	333211
Untreated	7022	2104	5895	2113	2095	2067	110569	102064	372737
MSU+PMA	2154	1369	1833	2424	2048	3032	56809	54528	81930
Blank	218	205	222	273	273	327	701	736	712
MSU+med	199	256	201	233	253	237	514	507	599

B) Only GM (no cells)

60min

	NO inhibitor		Inhibitor	
Untreated	240	362	342	320
MSU	605	532	492	442
PMA	246	187	221	249
PMA+MSU	577	375	539	451

90min

	NO inhibitor		Inhibitor	
Untreated	238	391	364	340
MSU	626	545	517	431
PMA	243	222	224	227
PMA+MSU	549	400	608	526

2.5.3 Final optimized protocol for Caspase-Glo-1 Inflammasome Assay

The results of the second attempt were better than the first attempt, however there a few changes had been made to increase quality of the results. First, to clearly determine the difference in caspase-1 activity between cells that were treated with specific caspase-1 inhibitor YVAD-CHO and cells treated with non-specific inhibitor MG-132, the assessment of cell number was conducted. Second, the 96-well plate that had only GM that was transferred from the treated cells demonstrated clearer results for caspase-1 activity in comparison to 96-well plate that had treated cells and GM.

The cells were seeded in 96-well plate and treated with PMA and MSU as it was described in attempt #2. Subsequently, 50uL of GM was transferred into another white 96-well plate and Caspase-Glo-1 Assay was performed as described previously. Caspase-1 activity was measured at 60 and 90 minutes after incubation. The assessment of cell number was conducted using the original 96-well plate with treated cells ***(Figure 2.8).***

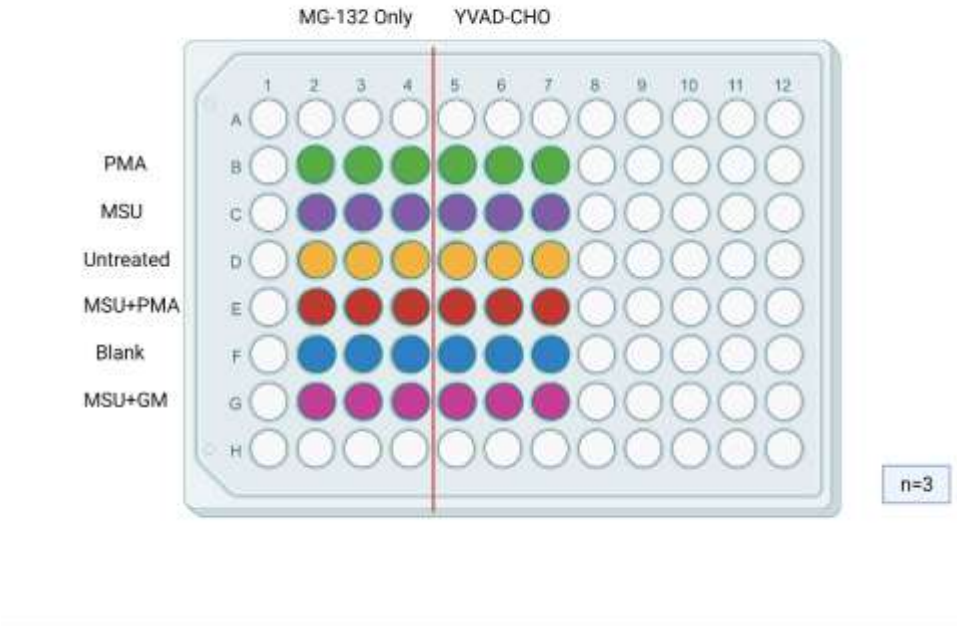

Figure 2.8 Plate layout of Caspase-Glo-1 Assay final attempt. Cells were seeded in 96-well plate with 3 technical replicates per treatment. Figure created using Biorender software.

Assessment of cell number

Cell numbers were measured in 96-well plates after conducting Caspase-Glo-1 Inflammasome Assay to allow variation in cell number between different conditions to be accounted. The Cyquant GR dye (ThermoFisher Scientific) was used to measure the fluorescence which is made upon binding of dye to cellular DNA. Cyquant GR dye stock solution in DMSO was diluted with 400-fold into DNA/RNA free molecular water and 20-fold into the cell-lysis buffer. Frozen 96-well plates with cells were thawed at room temperature and incubated in Cyquant GR dye (200 ul/well) at 23°C for 5 min. Fluorescence was detected using fluorescent plate reader with excitation 485±10nm and emission 528±20nm. Cell number was determined by reference to standard curves for THP-1 cells and PMA-treated THP-1 macrophage-like cells.

2.5.4 Caspase-Glo-1 Inflammasome Assay with Virus transfection

To determine whether the reduction in BMAL1 expression levels in THP-1 monocyte/macrophage-like cells will result in deregulation of the inflammatory cascade, the cells were transfected with adenovirus and Caspase-1 assay was performed. The cells were seeded at 2x10^5 cells/well in 6 replicates for each condition (Untreated, PMA, MSU, PMA+MSU). The cells for PMA and PMA+MSU condition were

seeded first in 100uL/well culture medium and incubated for 72 hours. After 72 hours, cells were seeded for the rest of the conditions and after 8h treated with different adenoviruses 10ul/well for BMAL1 gene knockdown and overexpression ***(Figure 2.9)*** and left in the incubator for 24h. After 24h, the media with virus was replaced with fresh GM and incubated for further 24h. Next morning MSU crystals (0.004g/ml) were added into the wells (MSU and MSU+PMA conditions) and incubated for 4h. After 4h, 50ul of media were transferred into a white 96-well plate and Caspase-1 assay was performed.

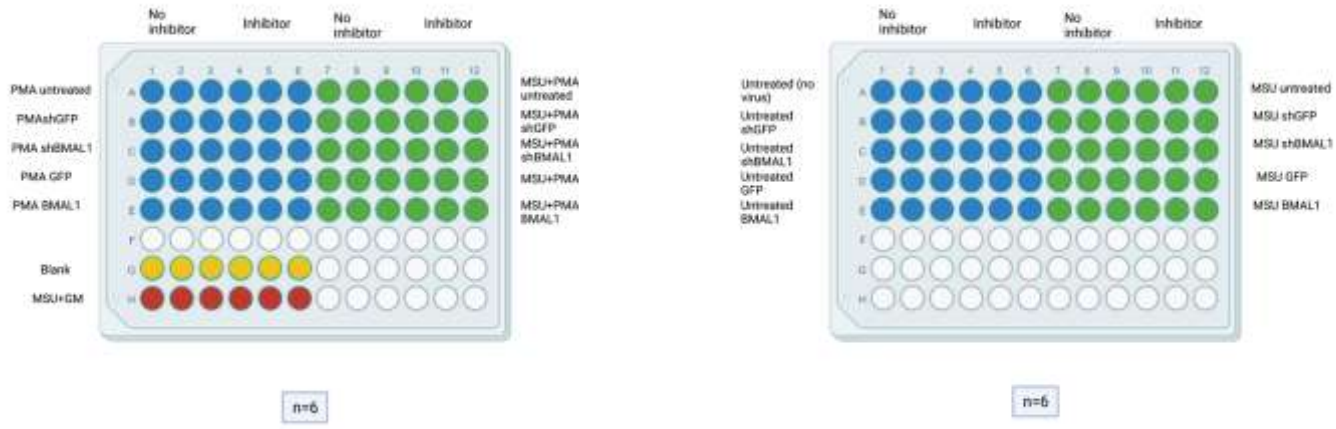

Figure 2.9 Plate layout of Caspase-Glo-1 Assay with virus transfection. Cells were seeded in 96-well plate with 6 technical replicates per condition. Figure created using Biorender software.

2.5.5 Caspase-Glo-1 Inflammasome Assay with Prednisolone and Heme

To determine the effect of heme and prednisolone (the active metabolite of prednisone) treatment of THP-1 (+/- MSU, +/- PMA) on caspase-1 activity and whether or not the effect is depending on time of the day, Caspase-Glo-1 assay was performed. The cells were seeded at 2x10^5cells/mL in triplicates for each condition (Untreated, PMA, MSU, PMA+MSU) and each condition had 4 sub-conditions (Heme, Heme vehicle (NaOH), Prednisolone, Prednisolone vehicle (DMSO)) ***(Figure 2.10).*** The drugs and vehicles stock concentrations were prepared prior to the day of experiment as described in **2.1.7 Drug treatments**. The cells for PMA and PMA+MSU condition were seeded first in 100uL/well culture medium in both 96-well plates (0-12h and 12-24h) and incubated for 3 days. After 3 days, GM was replaced with serum free media for PMA treated cells, cells for untreated and MSU treated conditions were seeded at the same concentration in 100uL of serum free media. Both plates were incubated for 18h. After 18h of serum starvation serum free media was replaced with GM for 12-24h plate and incubated for 12h. At 0h time point the serum free media

in 0-12h plate was replaced with 90ul of media containing drugs/vehicles and incubated at 37°C for 8 hours. The double concentrated stock for drugs, vehicles and MSU crystals were made. After 8h, 5ul/well of the double concentrated drugs, vehicles and MSU crystals were added to corresponding wells to make the total volume of 100ul/well. After 12 hours, 0-12h plate was centrifuged and 50ul/well of GM was transferred to white 96 well plates to detect caspase-1 activity. Simultaneously after 12 hours, the cells in the 12-24h plate were treated with drugs and vehicles the same procedure was performed for 12-24h plate. At the end both 96 well plates with treated cells were used for assessment of cell number.

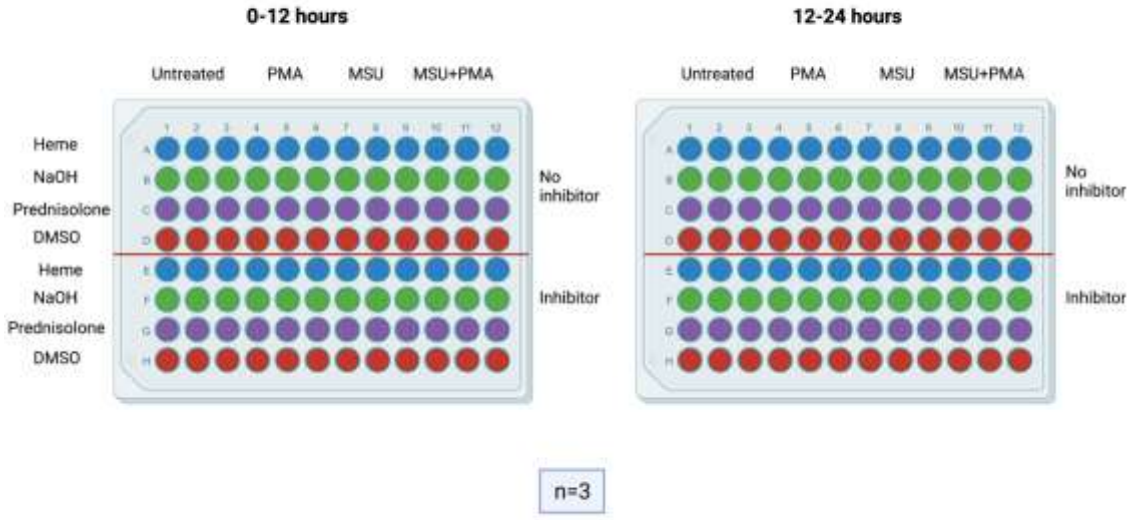

Figure 2.10 Plate layout of Caspase-Glo-1 Assay with Drug Treatments. Cells were seeded in 96-well plate with 3 technical replicates per condition. Figure created using Biorender software.

2.5.6 Caspase-Glo-1 Inflammasome Assay with REV-ERBα antagonist and Heme

To determine whether REV-ERBα activity regulates the NLRP3 inflammasome in treated THP-1 monocyte/macrophages-like cells (+/- MSU, +/- PMA) and whether or not the effect is depending on time of the day, Caspase-Glo-1 assay was performed. This experiment was conducted using SR-8278 (pharmacological REV-ERBα antagonist) and heme (an endogenous REV-ERBα agonist) to determine the effect on NLRP3 inflammasome activity. The cells were seeded in triplicates for each condition (Untreated, PMA, MSU, PMA+MSU) and each condition had 4 sub-conditions (Heme + REV-ERBα antagonist, Heme + DMSO, Heme vehicle (NaOH + DMSO), REV-ERBα + NaOH) ***(Figure 2.11)***. The drugs and vehicles

stock concentrations were prepared prior to the day of experiment as described in **2.1.7 Drug treatments**. The cells for PMA and PMA+MSU condition were seeded first at 2x10^5cells/mL in 100uL culture medium per well in both 96-well plates (0-12h and 12-24h) and incubated for 3 days. After 3 days, GM was replaced with serum free media for PMA treated cells, cells for untreated and MSU treated conditions were seeded at the same concentration in 100uL of serum free media. Both plates were incubated for 18h. After 18h of serum starvation serum free media was replaced with GM for 12-24h plate and incubated for 12h. At 0h time point the serum free media in 0-12h plate was replaced with 90ul of media containing drugs/vehicles and incubated at 37°C for 8 hours. The double concentrated stock for drugs, vehicles and MSU crystals were made. After 8h, 5ul/well of the double concentrated drugs, vehicles and MSU crystals were added to corresponding wells to make the total volume of 100ul/well. After 12 hours, 0-12h plate was centrifuged and 50ul/well of GM was transferred to white 96 well plates to detect caspase-1 activity. Simultaneously after 12 hours, the cells in the 12-24h plate were treated with drugs and vehicles the same procedure was performed for 12-24h plate. At the end both 96 well plates with treated cells were used for assessment of cell number.

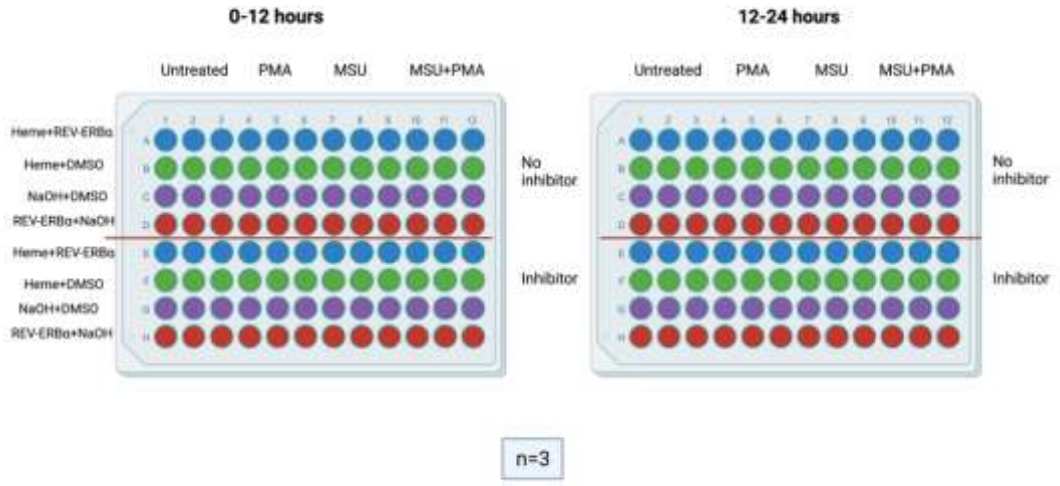

Figure 2.11 Plate layout of Caspase-Glo-1 Assay with SR-8278 and Heme. Cells were seeded in 96-well plate with 3 technical replicates per condition. Figure created using Biorender software.

2.5.7 Caspase-1 data analysis

The experiment with prednisolone and heme treatment was performed 3 times with 3 technical replicates (n=3) for each condition for statistical purposes. The experiment with SR-8278 and heme was performed once with 3 technical replicates (n=3) for each condition. The luminescence readings from each caspase-1 assay were normalized to cell number and calculated as a fold change relative to the controls. All the results were analysed using one-way ANOVA with Turkey multiple comparison test using Prism GraphPad 9. Results are shown as mean ± SEM. A p-value of <0.05 was considered statistically significant.

2.6 Western Blot

The effect of exposure of MSU crystals on the expression of core circadian oscillator component (REV-ERBa), transcriptional activator of NLRP3 (NF-κβ) and transmembrane protein (TLR4) in THP-1 monocyte/macrophages-like cells was further assessed at the protein level. To determine whether time of the day alternations in REV-ERBa, NF-κβ and TLR4 protein expression were apparent, time course studies were conducted. The level of protein expression was quantified by Western Blot.

2.6.1 Preparation of protein lysates

A 24h time-course experiment was conducted with cell lysates collected at 6-hourly intervals over 24h period. Due to the logistics of performing 24-hour experiments, replicates were performed in the same 24h period. Although these were plated and treated independently it is noted that these are not true "biological replicates". In preparation for this 24-hour experiment, eighteen 6-well plates were used with 4 plates for each of the 6-hour time points. Sixteen plates had cells seeded in 4 different conditions: Untreated, PMA treated, MSU treated and PMA+MSU treated. Two plates (0h time point) had cells seeded in 2 conditions: Untreated and PMA treated and was used for baseline data. The cells were seeded at 4x10^5cells/well, volume of cell suspension was calculated using ***Equation 3.*** The THP-1 cells were seeded first only for PMA and PMA+MSU conditions following PMA treatment protocol as described previously. After 3 days, the rest of the cells were seeded to account for the difference in cell number. THP-1 monocytes/ macrophages-like cells were serum starved for ~18 h by replacing GM with 1.5ml of FBS Free serum media and then re-fed with GM (to synchronise cell clock) in the presence or absence of MSU crystals. Cells in replicate wells were collected for protein analysis prior to feeding and/or MSU crystal exposure (0h timepoint plate) for baseline data and at 6 hourly intervals for a period of 24 h after feeding/MSU crystal exposure. The cells were lysed with 100ul of cold RIPA lysis buffer with added protease inhibitors (sodium

fluoride, sodium orthovanadate and PMSF; 1mM each) and incubated with shaking on ice for 10min. The wells were scrapped using cell scrapers, all the content were transferred into 1.5ml Eppendorf tubes and stored at -80°C.

All the samples were thawed on ice and the cell suspension was passed through an insulin needle 5 times. The cell lysates were purified by centrifugating at 12,000 rpm for 20 minutes at 4°C. The supernatant was gently aspirated and transferred into new cold Eppendorf tubes.

2.6.2 Protein Quantification

To quantify the concentrations of protein in the samples, the Pierce 660 Protein Assay was performed using 10uL of cell lysate from each sample was transferred to 96-well plate and 150uL of the Pierce 660 Reagent was added into each well. The plate was mixed by shaking for 1 minute and incubated at room temperature for 5 minutes in the darkness. Synergy 2 Multi-Mode Microplate Reader was used to quantify protein concentrations by measuring light absorbance at 660nm.

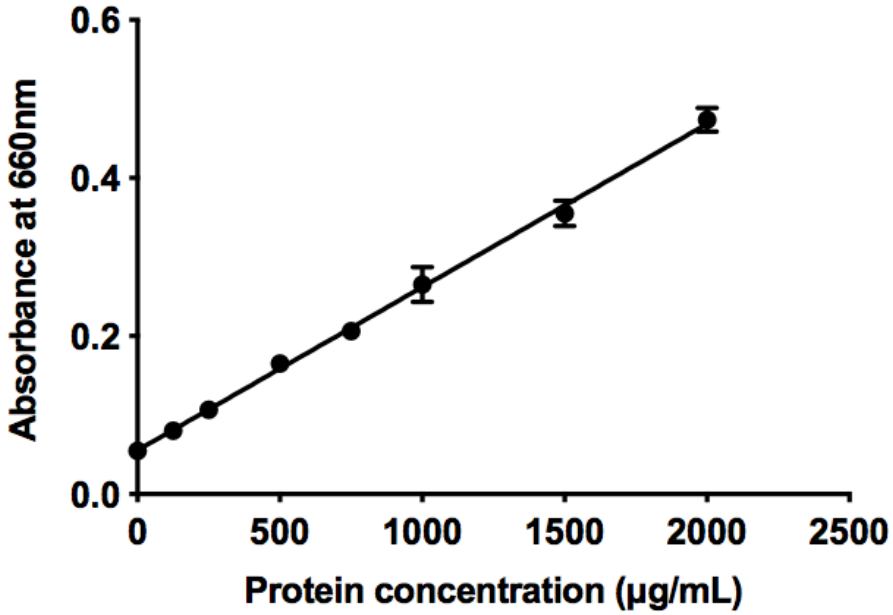

Figure 2.12 Standard curve for Pierce 660 Protein Assay. The linear calibration curve of protein concentration (µg/mL) relative to the absorbance at 660nm. R^2 value = 0.9986, slope = 0.0002065, and y-intercept = 0.05538.

Protein concentrations (ug/mL) of each sample was calculated using standard curve ***(Figure 2.12)***. The target concentration for the remaining samples was the lowest concentration obtained. ***Equation 5*** was used to calculate volume of RIPA lysis buffer required to dilute the samples.

Equation 5.

$$\boldsymbol{Volume\ of\ RIPA\ Buffer\ required\ to\ dilute\ the\ sample} = \frac{(\boldsymbol{concentration\ of\ sample\ of\ interest} \times \mathbf{100})}{\boldsymbol{lowest\ concentration}} - \mathbf{100}$$

Protein concentration of lysates was equalized by diluting more concentrated samples with RIPA lysis buffer. 100uL of each lysate sample was mixed with 50uL of 4xLaemmli sample buffer with B-mercaptoethanol (in 9:1 ratio). The samples were heated to 95°C for 5 minutes before storing at -20°C.

2.6.3 SDS-PAGE

Ready to use Criterion TGX^{TM} Precast Midi Protein Gels (4-15%, 26-well) were placed inside the electrophoresis chambers. The reservoir was filled with SDS Running buffer. Prior to loading the samples, the gels were run for 5min at 170V to clear any residue/bubbles. 7uL of Precision Plus Protein Dual Colour protein ladder was loaded in the first and last well of each gel at a volume of 7ul. The lysate samples were loaded in the wells at a volume of 15uL. The gel was run at 170V for 45 minutes or until the blue loading dye had run off to the bottom of the gel.

The Immun-Blot PVDF blotting membranes were cut to match the size of the gels. The membranes were soaked in 100% Methanol for 30 seconds and then soaked in cold transfer buffer until the gels were ready for transfer. The filter paper and fibre pads were soaked in the transfer buffer until saturation, prior to protein transfer.

2.6.4 Western Blotting

The transfer sandwich was prepared in the following order: cathode (-) platform, pre-soaked fibre pad, 2x pre-soaked filter paper, gel, PVDF membrane, 2x pre-soaked filter paper, pre-soaked fibre pad, and anode (+) platform. The cassettes were firmly closed and placed in the transfer tank with ice cold transfer buffer. The transfer was run at 100V for 60 minutes.

While transfer step was conducted, 5% skim milk solution was made in TBS Tween (4g per 100ml). Upon completion of the transfer step, the blotting membranes were placed in 100% methanol for 30 seconds and

then placed on the side to dry. Dry membranes were cut accordingly to molecular weight of individual protein. The blotting membranes were then blocked in 5% skim milk solution for 1 hour with shaking. After 1 hour the membranes were washed 3 times for 30 seconds in TBS Tween. The blotting membranes were incubated with a total of 15ml of the primary antibody of interest diluted 1:1000 (NF-kB), 1:1000 (REV-ERBα), 1:100 (TLR4) and 1:10000 (B-actin) with TBS-Tween. The membranes were incubated overnight at 4°C on a plate shaker.

The following day, the membranes were washed 5 times for 5 minutes using the fresh TBS-Tween for each wash. Secondary antibody mix was prepared by diluting both anti-mouse (B-actin) and goat anti-rabbit HRP (TLR4, NF-kB, REV-ERBα) secondary antibodies 1:10000 in TBS-Tween. The blotting membranes were incubated with a total of 15ml of secondary antibody for 1 hour at room temperature with shaking. Upon completion, the membranes were washed 3 times for 5 minutes with TBS-Tween. Clarity Western ECL solution was made (3ml of each detection solution per membrane-kit) and pipetted to cover the surface of the membranes. The membranes covered in detection reagent mix were incubated for 5 minutes in the darkness and then placed inside a strip of transparent plastic sheets and smoothed out with blot roller to remove the air bubbles and excess ECL. The BioRad ChemiDoc Touch Imaging System was used to visualize the membranes. Colometric images were taken for each blot to image the ladder, following by chemiluminescence images to image proteins for each antibody of interest.

Table 2.8 The list of antibodies used for Western blotting.

Primary Antibody	Source	Supplier & Catalogue No.	Primary Antibody Dilution	Secondary Antibody Dilution	Molecular Weight (kDa)
NF-kB	Rabbit	Life Technologies, PA1186	1:1000 with TBS-Tween	1:10000 with TBS-Tween	~65
pNF-kB	Rabbit	Life Technologies, MA515160	1:1000 with TBS-Tween	1:10000 with TBS-Tween	~65
TLR4	Rabbit	Life Technologies, 482300	1:100 with TBS-Tween	1:10000 with TBS-Tween	~95
REV-ERBα	Rabbit	Abcam inc, ab174309	1:1000 with TBS-Tween	1:10000 with TBS-Tween	~67
B-actin	Mouse	Santa Cruz Biotechnology, sc-69879	1:10000 with TBS-Tween	1:10000 with TBS-Tween	~42
GAPDH	Rabbit	Sigma G9545-100UL	1:10000 with TBS-Tween	1:10000 with TBS-Tween	~40

2.6.5 Data Analysis

Digital images for each replicate were developed from the BioRad ChemiDoc^{TM} Imaging System using colometric and chemiluminescence detection methods. The images of the blots were exported to the Bio-Rad Image Lab Software for further quantification of signal intensity and band densitometry. Background volume was subtracted from the calculations. The resulting adjusted density of the band of each target protein were divided by the adjusted density of the respective β-actin band density. An extra housekeeper GAPDH was used to assure that there is no effect of β-actin on target proteins. All the data points for each

time point were then optimized and calculated as a fold change relative to the 0h untreated. Results are shown as mean ± SEM. Effects of time and treatment for each target protein were transformed into Log2(Y) form to pass Spearman's test and Normality of residuals test and subsequently analysed using two-way ANOVA with Tukey and Sidak testing. A p value of < 0.05 was considered statistically significant.

3.0 Results

3.1 THP-1 monocyte differentiation into macrophages-like cell

3.1.1 Validation at mRNA level

To confirm PMA treatment led to induction of a more macrophage-like phenotype in THP-1 cells, expression of macrophage differentiation markers (TLR4, CD36, CD14) was measured at the mRNA level by real-time PCR.

The expression of *TLR4* was not significantly different in PMA- differentiated macrophages-like cells compared to monocytes ($p>0.05$). However, there was a significantly ($p<0.01$) higher expression of *CD14* levels in differentiated macrophages-like cells in comparison to THP-1 monocytes. Similarly, *CD36* expression was also significantly higher ($p<0.05$) in PMA-differentiated macrophages-like cells compared to PMA untreated monocytes.

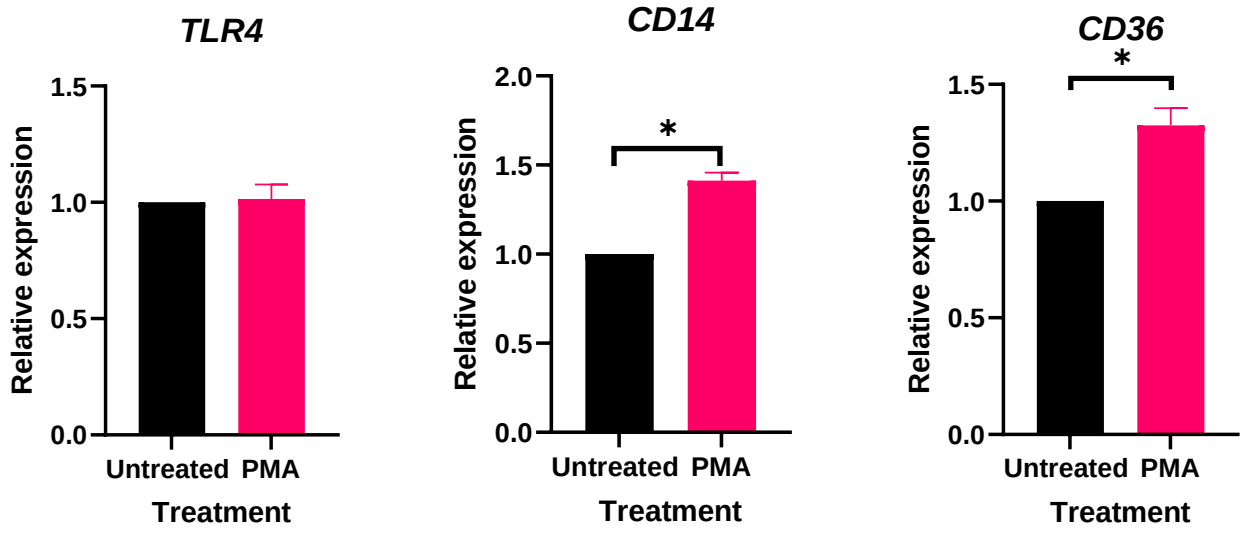

Figure 3.1 Expression of *TLR4, CD14* and *CD36* in THP-1 monocyte and macrophages-like cells. Data shown as the mean ± SEM of a single experiment. All data were normalized to 18S and expressed relative to untreated cells. * $p<0.05$,

3.2 The effect of exposure of MSU crystals on the expression of core circadian oscillator components in THP-1 monocytes and macrophages-like cells

Hyperuricemia and accumulation of MSU crystals in the joint is hallmark of gout. Gout flares characterized by activation of the NLRP3 inflammasome by MSU crystals and are known to be initiated during the night. Although, it is now known that NLRP3 inflammasome activity and trafficking of immune cells controlled by circadian oscillator, there is no information on how exactly MSU mediated inflammation linked to the circadian clock machinery. Therefore, to determine the effect of exposure of MSU crystals on the expression of core circadian genes in THP-1 monocytes and macrophages-like cells, real-time PCR was performed, and mRNA expression of each gene was analysed.

3.2.1 MSU crystals altered the expression of core circadian genes in THP-1 monocytes

The total expression of each core circadian gene appears to vary over the 24-hour time course in the synchronised population of THP-1 monocytes in the absence/presence of MSU crystals. The was a significant effect of time on the expression of *BMAL1*, *REV-ERBα*, *CRY1* and *PER1* but not *PER2* or *CRY2*. Data for *PER3* and *CLOCK* were non-parametric and hence the effects of time on expression of these genes could not be determined. MSU crystal treatment had no significant effect on expression of any of the clock genes measured (main effect treatment $p>0.05$ for all), however a significant interaction between time and treatment was observed for *REV-ERBα*, however, not in other clock genes indicating MSU crystals treatment resulted in a time-dependent reduction in *REV-ERBα* expression.

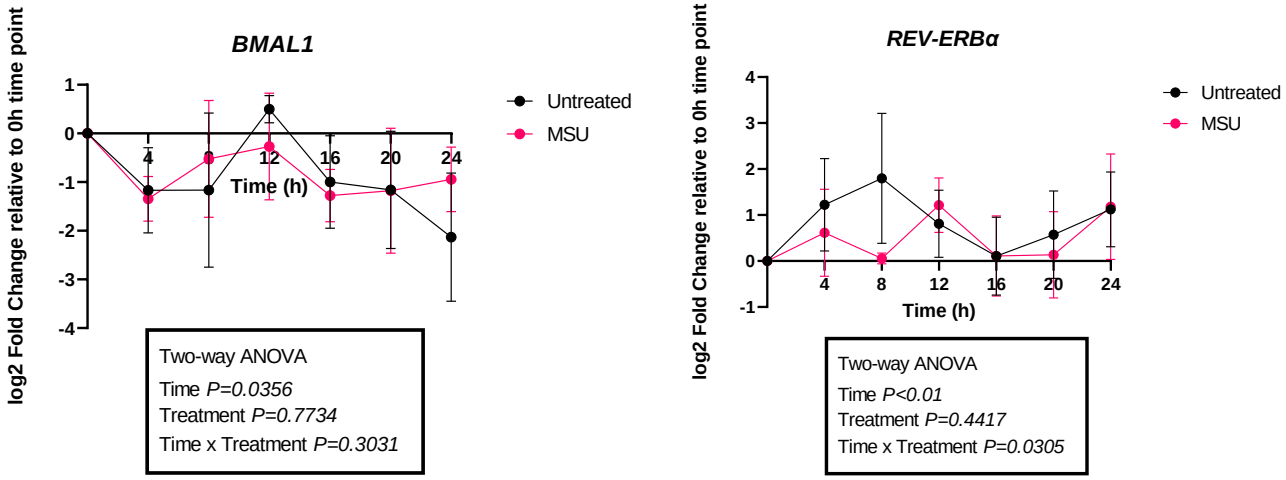

Figure 3.2 Log2 fold changes in *BMAL1* and *REV-ERBa* expression in THP-1 monocyte cells across 24-hour time course. *BMAL1* and *REV-ERBa* mRNA levels at each time point are expressed relative to

the 0h time point in untreated cells. Fold change is expressed in Log2 transformed form. Data shown is the mean ± SEM (n=6).

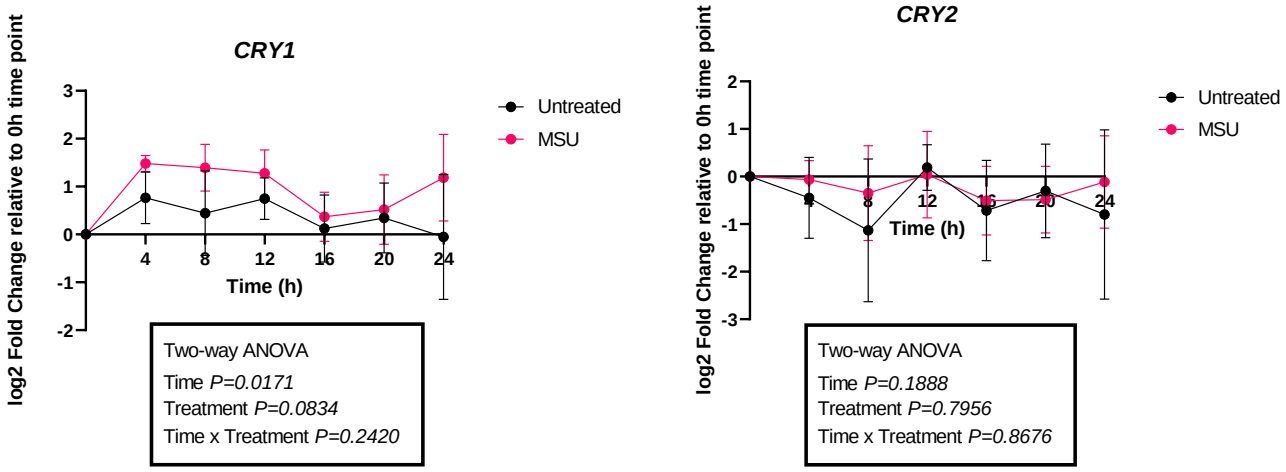

Figure 3.3 Log2 fold changes in *CRY1* and *CRY2* expression in THP-1 monocyte cells across 24-hour time course. *CRY1* and *CRY2* mRNA levels at each time point are expressed relative to the 0h time point in untreated cells. Fold change is expressed in Log2 transformed form. Data shown is the mean ± SEM (n=6).

PER3 and CLOCK expression was analysed using the non-parametric Friedman's Test as data did not pass the Normality tests and Spearman's Homoscedasticity test. This test assesses the overall effect of MSU treatment only and not the effects of time or time-treatment interactions. MSU crystal treatment had no significant effect on expression of either gene.

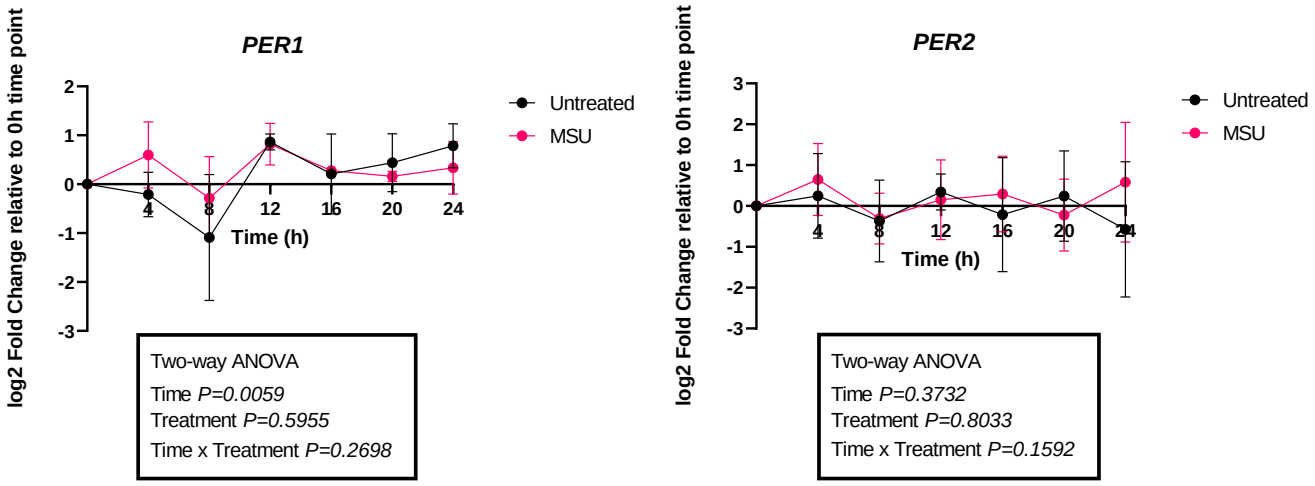

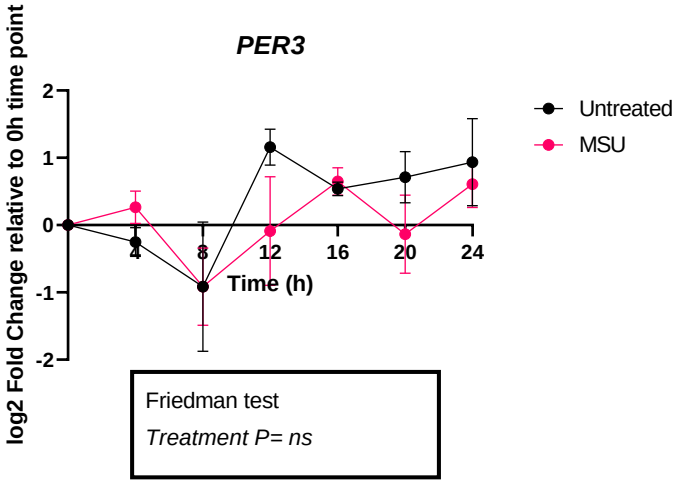

Figure 3.4 Log2 fold changes in *PER1, PER2* and *PER3* expression in THP-1 monocyte cells across 24-hour time course. *PER1, PER2* and *PER3* mRNA levels at each time point are expressed relative to the 0h time point in untreated cells. Fold change is expressed in Log2 transformed form. Data shown is the mean ± SEM (n=6).

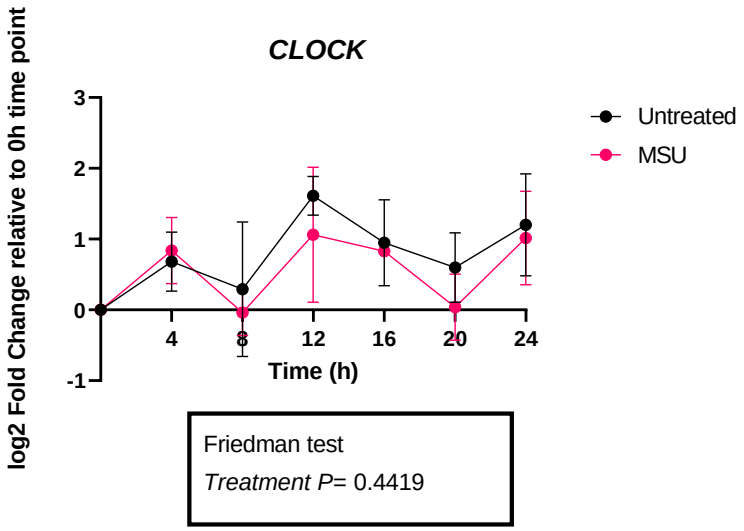

Figure 3.5 Log2 fold changes in *CLOCK* expression in THP-1 monocyte cells across 24-hour time course. *CLOCK* mRNA levels at each time point are expressed relative to the 0h time point in untreated cells. Fold change is expressed in Log2 transformed form. Data shown is the mean ± SEM (n=6).

3.2.2 MSU crystals changes the expression of core circadian genes in THP-1 macrophages-like cells

The overall expression of each core circadian gene varied over the 24-hour time course in the synchronised population of THP-1 macrophages-like cells in the absence/presence of MSU crystals. Our results showed a significant effect of time on the expression of *BMAL1, REV-ERBα, CRY1* and *PER1* but not *CRY2* or *PER2* in macrophages-like cells. Data for *PER3* and *CLOCK* mRNA expression were non-parametric and hence

the effects of time on expression of these genes could not be determined. The MSU treatment showed a significant main effect on expression of *CRY1* gene and a significant interaction between time and treatment was observed for *REV-ERBα* and *CRY1*, indicating that MSU crystal treatment resulted in a time-dependent increase in *CRY1* expression and reduction in *REV-ERBα* fluctuation during 24h period.

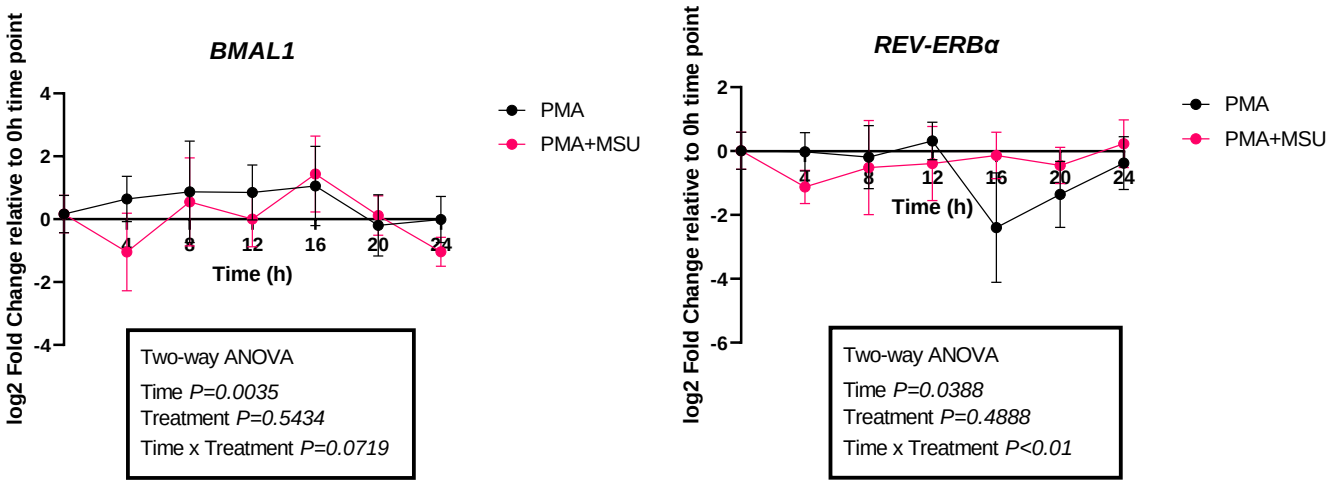

Figure 3.6 Log2 fold changes in *BMAL1* and *REV-ERBα* expression in THP-1 macrophages-like cells across 24-hour time course. *BMAL1* and *REV-ERBα* mRNA levels at each time point are expressed relative to the 0h time point in untreated cells. Fold change is expressed in Log2 transformed form. Data shown is the mean ± SEM (n=6).

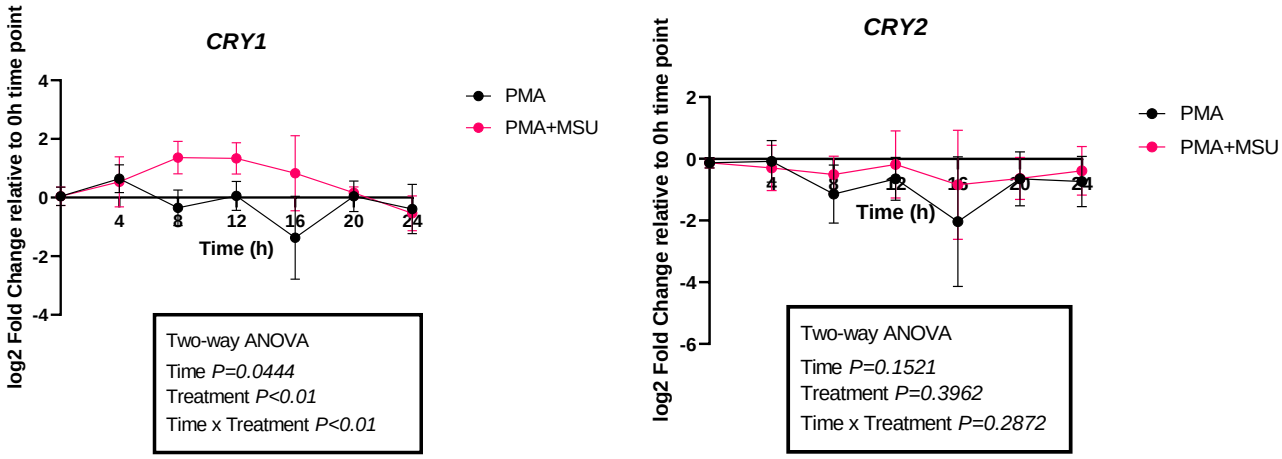

Figure 3.7 Log2 fold changes in *CRY1* and *CRY2* expression in THP-1 macrophages-like cells across 24-hour time course. *CRY1* and *CRY2* mRNA levels at each time point are expressed relative to the 0h time point in untreated cells. Fold change is expressed in Log2 transformed form. Data shown is the mean ± SEM (n=6).

Again, the expression of PER3 and CLOCK genes was analysed using the non-parametric Friedman's Test as data did not pass the Normality tests and Spearman's Homoscedasticity test. The treatment with MSU crystals did not show a significant effect on expression of either gene.

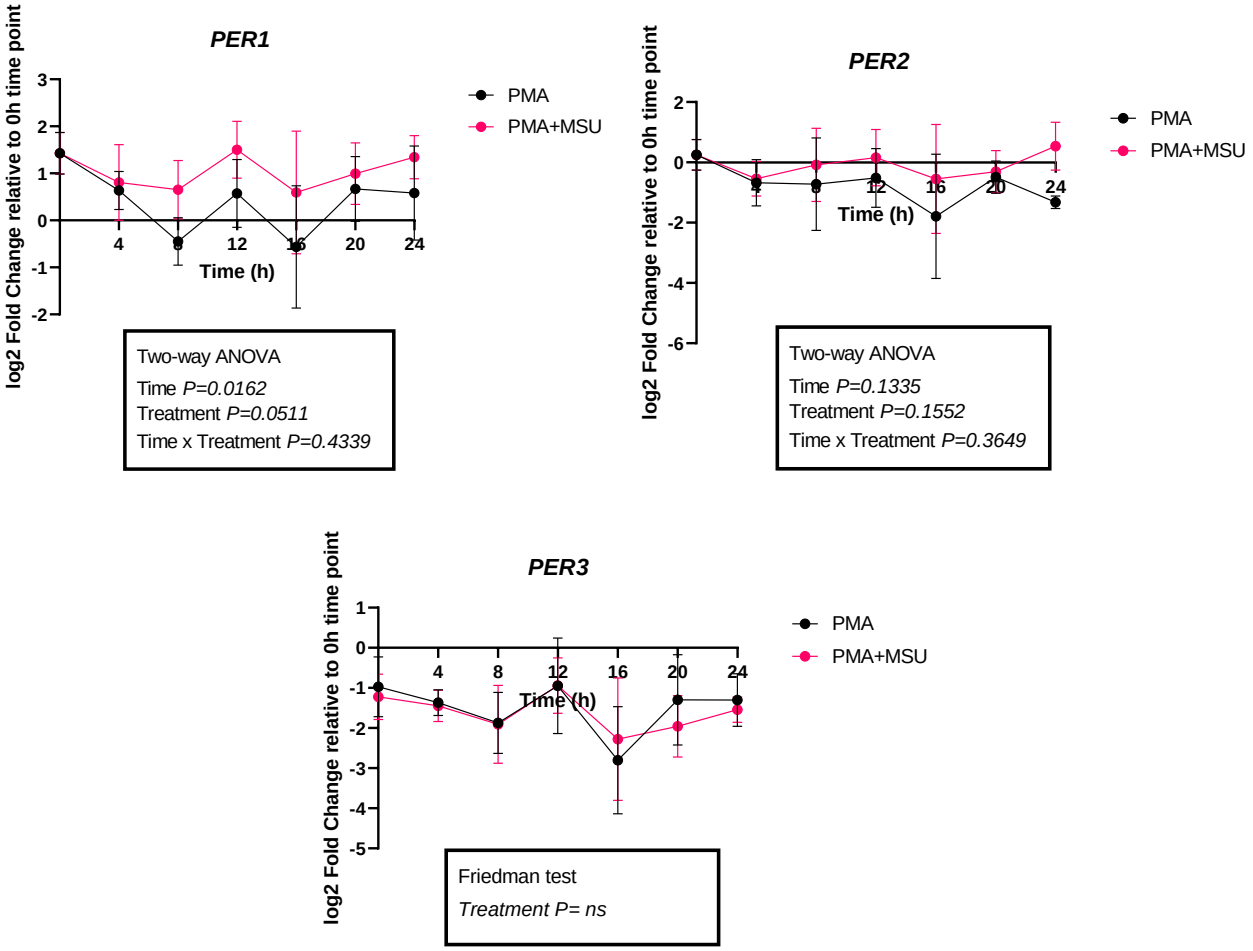

Figure 3.8 Log2 fold changes in *PER1, PER2* and *PER3* expression in THP-1 macrophages-like cells across 24-hour time course. *PER1*, *PER2* and *PER3* mRNA levels at each time point are expressed relative to the 0h time point in untreated cells. Fold change is expressed in Log2 transformed form. Data shown is the mean ± SEM (n=6).

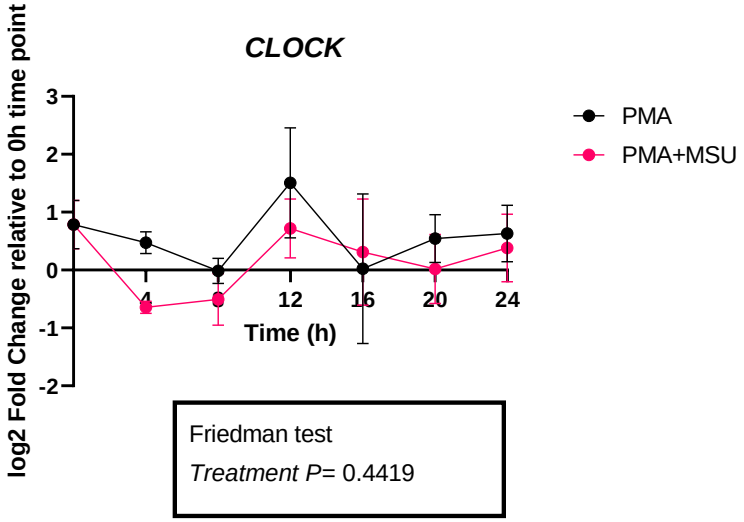

Figure 3.9 Log2 fold changes in *CLOCK* expression in THP-1 macrophages-like cells across 24-hour time course. *CLOCK* mRNA levels at each time point are expressed relative to the 0h time point in untreated cells. Fold change is expressed in Log2 transformed form. Data shown is the mean ± SEM (n=6).

3.2.3 Differences in expression of core clock genes between THP-1 monocytes and macrophage-like cells during 24h period

The expression of individual circadian gene varied over 24-hour time period in both THP-1 monocyte and macrophage-like cells. The effect of time on the expression of *REV-ERBα, CRY1* and *PER1* was significant but not for the expression of *BMAL1, CRY2* or *PER2*. The analysis of data for *PER3* and *CLOCK* mRNA expression were non-parametric and therefore the effects of time on expression of these genes could not be determined. There was a significant effect of PMA treatment on expression of *BMAL1, REV-ERBα,* and *PER3* genes. In particular, *REV-ERBα* and *PER3* were mainly upregulated in monocytes and downregulated in macrophage-like cells during 24h period. However, *BMAL1* expression was mainly upregulated in macrophage-like cells and downregulated in monocytes. A significant interaction between time and treatment was also observed for *REV-ERBα* and *PER1*.

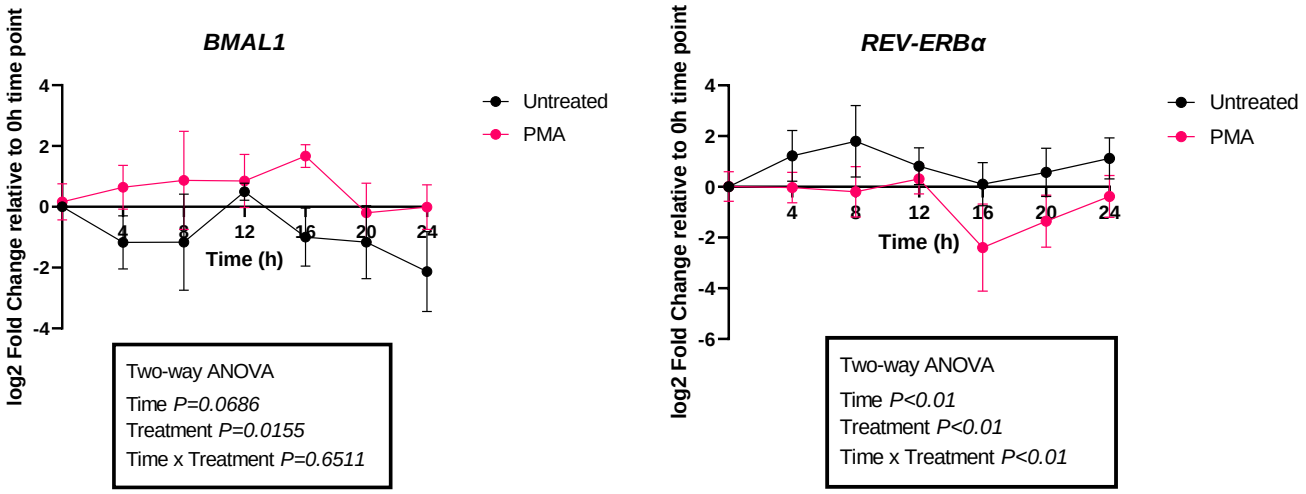

Figure 3.10 Log2 fold changes in *BMAL1* and *REV-ERBa* expression in THP-1 monocyte/macrophages-like cells across 24-hour time course. *BMAL1* and *REV-ERBa* mRNA levels at each time point are expressed relative to the 0h time point in untreated cells. Fold change is expressed in Log2 transformed form. Data shown is the mean ± SEM (n=6).

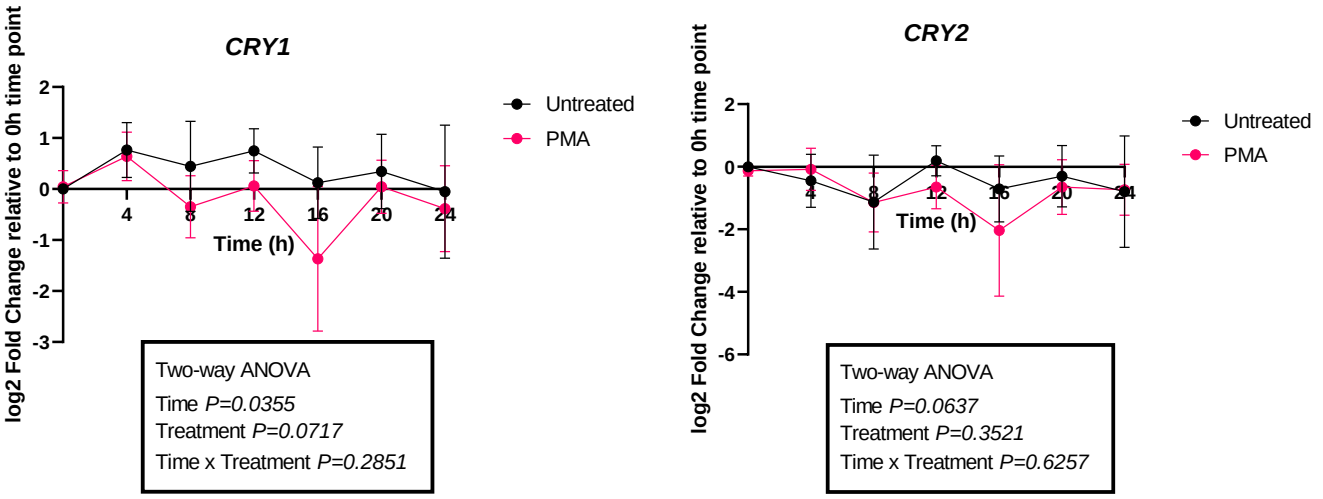

Figure 3.11 Log2 fold changes in *CRY1* and *CRY2* expression in THP-1 monocyte/macrophages-like cells across 24-hour time course. *CRY1* and *CRY2* mRNA levels at each time point are expressed relative to the 0h time point in untreated cells. Fold change is expressed in Log2 transformed form. Data shown is the mean ± SEM (n=6).

The non-parametric Friedman's Test was used to analyse expression of *PER3* and *CLOCK* genes as the data did not pass the Normality tests and Spearman's Homoscedasticity test. A significant effect on expression of *PER3* was detected between PMA treated and untreated cells, in particular there was mainly downregulation of *PER3* in PMA-treated cells during 24h time course.

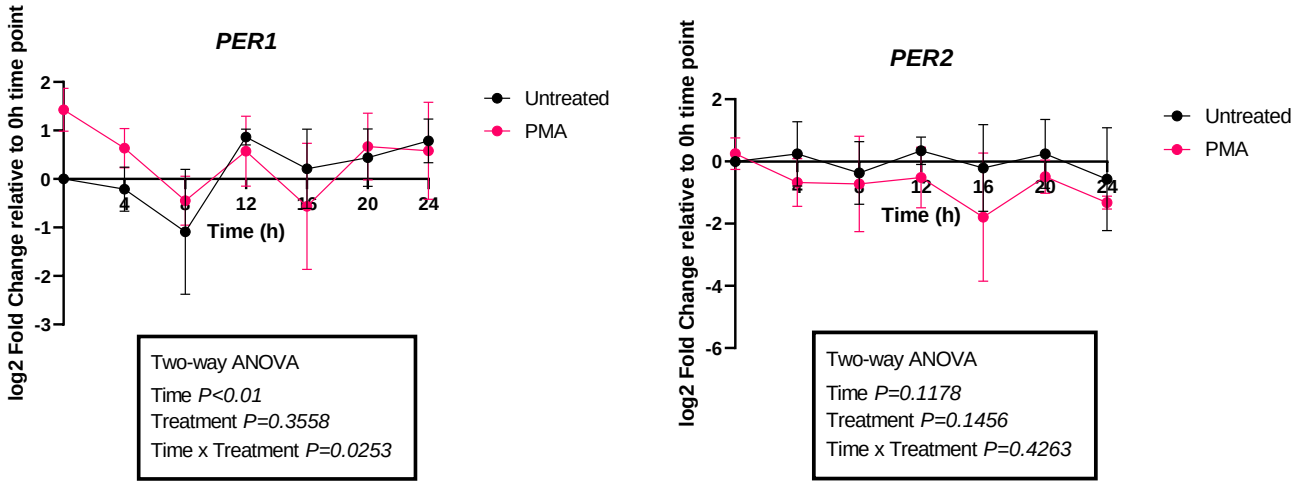

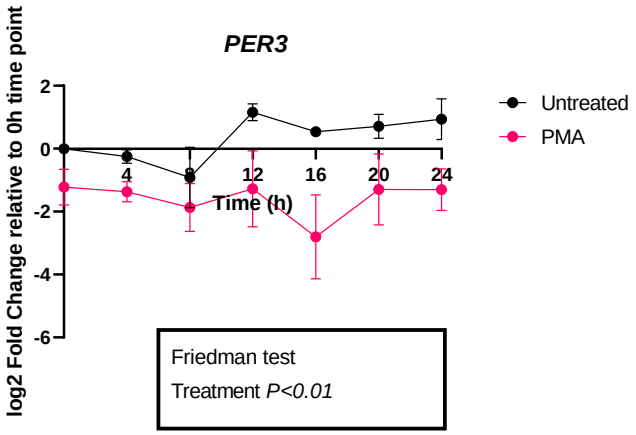

Figure 3.12 Log2 fold changes in *PER1, PER2* and *PER3* expression in THP-1 monocyte/macrophages-like cells across 24-hour time course. *PER1*, *PER2* and *PER3* mRNA levels at each time point are expressed relative to the 0h time point in untreated cells. Fold change is expressed in Log2 transformed form. Data shown is the mean ± SEM (n=6).

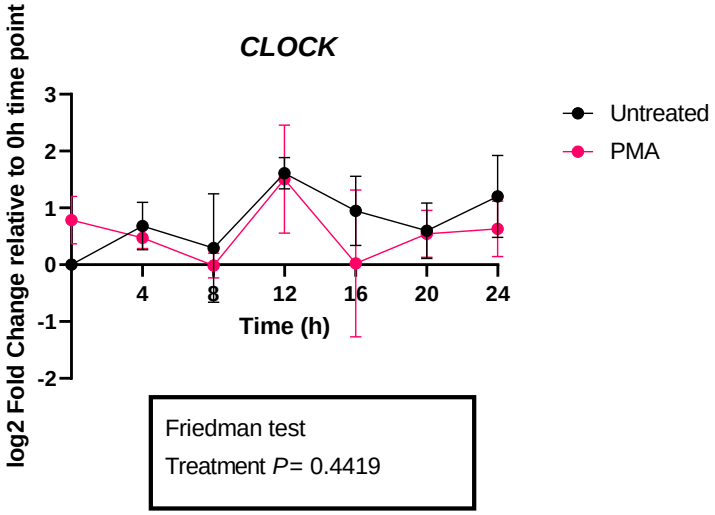

Figure 3.13 Log2 fold changes in *CLOCK* expression in THP-1 monocyte/macrophages-like cells across 24-hour time course. *CLOCK* mRNA levels at each time point are expressed relative to the 0h time point in untreated cells. Fold change is expressed in Log2 transformed form. Data shown is the mean ± SEM (n=6).

Summary of Findings:

Table 3.1 The effect of MSU crystals on the expression of core circadian oscillator components THP-1 monocytes

Circadian gene	Effect of Time	Effect of MSU Treatment	Interaction
BMAL1	$p < 0.05$	ns	ns
REV-ERBα	$p < 0.01$	ns	$p < 0.05$
CRY1	$p < 0.05$	ns	ns
CRY2	ns	ns	ns
PER1	$p < 0.01$	ns	ns
PER2	ns	ns	ns

THP-1 macrophages-like cells

Circadian gene	Effect of Time	Effect of MSU Treatment	Interaction
BMAL1	$p < 0.01$	ns	ns
REV-ERBa	$p < 0.05$	ns	$p < 0.01$
CRY1	$p < 0.05$	$p < 0.01$	$p < 0.01$
CRY2	ns	ns	ns
PER1	$p < 0.05$	ns	ns
PER2	ns	ns	ns

3.3 The effect of MSU crystals on NLRP3 inflammasome activity in THP-1 monocyte/macrophages-like cells

The previous studies on inflammatory diseases showed that NLRP3 inflammasome complex activation and subsequent release of pro-inflammatory cytokines is mediated via binding and recognition of DAMPs such as MSU crystals. MSU crystals believed to stimulate the assembly and activation of the NLRP3

inflammasome. Therefore, Caspase-Glo 1 Inflammasome Assay was performed to investigate the effect of MSU crystals on NLRP3 activity in THP-1 monocytes and macrophages-like cells.

The NLRP3 inflammasome activity is represented as a fold change in caspase-1 activity. Both THP-1 monocytes and macrophages-like cells treated with MSU crystals demonstrated a significant increase in NLRP3 inflammasome activity respectively compared to non-MSU treated cells (1.4-fold ($p<0.001$) and 1.8-fold ($p<0.0001$) respectively).

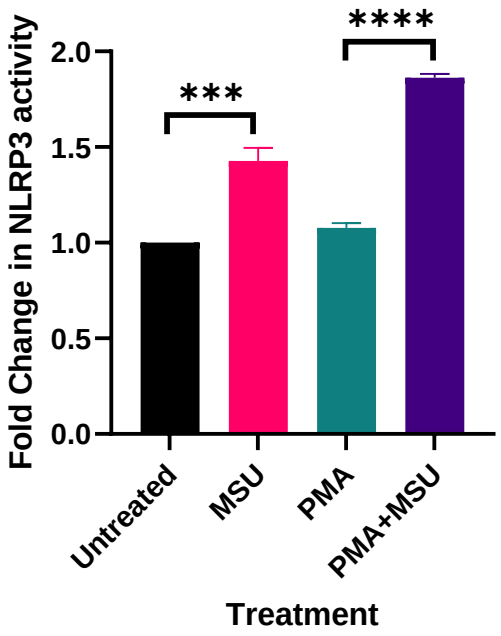

Figure 3.14 Fold changes in NLRP3 inflammasome activity in THP-1 monocytes/macrophages-like cells in the absence/presence of MSU crystals. NLRP3 inflammasome activity is equivalent to caspase-1 activity and expressed relative to untreated cells. The bars indicate the mean fold change ± SEM of a single experiment (n=3). (*** $p < 0.001$), (**** $p < 0.0001$)

3.4 The effect of REV-ERBα on NLRP3 inflammasome activity

As REV-ERBα has previously been shown to regulate the NLRP3 inflammasome, SR-8278 (REV-ERBα antagonist) was used to determine whether REV-ERBα activity regulates the NLRP3 inflammasome in THP-1 monocyte/macrophage-like cells. Heme treatment was used as it is an endogenous agonist of REV-ERBα. The effect of drugs was measured at two separate time points 0-12h and 12-24h to capture two different points in the circadian cycle. The THP-1 monocytes and macrophage-like cells were pre-treated with drugs (SR-8278 and Heme) at 0h for 0-12h timepoint and at 12h for 12-24h timepoint as described in (**Section 2.5.5).** The cells were exposed to MSU crystals only 4h prior to Caspase-1 Inflammasome assay therefore the effect of MSU crystals that occurred was measured at 8-12h and 20-24h for 0-12h and 12-24h

timepoints respectively. The effect of drugs has been normalized to the cell number. The drugs used for this experiment did not cause a change in number of cells.

MSU untreated monocytes:

In the absence of MSU crystals, SR-8278 alone did not show a significant effect ($p>0.05$) on NLRP3 activity in monocytes at either timepoint. Similarly, in the absence of MSU crystals heme alone did not show a significant effect ($p>0.05$) on activity of NLRP3 at either timepoint.

NLRP3 activity was also unchanged after co-treatment with heme+SR-8278 compared to monocytes treated with heme alone. Furthermore, there was no significant effect on NLRP3 activity in monocytes co-treated with heme+SR-8278 in the absence of MSU crystals compared to monocytes treated with only SR-8278 at either timepoint.

MSU treated monocytes:

In contrast, in the presence of MSU crystals, NLRP3 activity was significantly lower ($p<0.01$) in heme treated cells at both timepoints. Moreover, in the presence of MSU crystals, SR-8278 significantly reduced the activity of NLRP3 inflammasome ($p<0.0001$) at 0-12h timepoint but had no effect at the 12-24h timepoint.

There was no significant difference in NLRP3 activity between monocytes treated with heme alone and those co-treated with heme+SR-8278 at the 0-12h timepoint indicating that the effects of heme were not dependent on REV-ERBα activity. At the 12-24h timepoint, NLRP3 activity was significantly lower ($p<0.01$) in monocytes co-treated with heme+SR-8278 compared to in monocytes treated with heme alone indicating that the REV-ERBα antagonist potentiated rather than inhibited the repressive effects of heme on NLRP3 activation. The combined treatment of monocytes with heme+SR-8278 in the presence of MSU crystals showed a significant reduction ($p<0.0001$) in NLRP3 activity compared to monocytes treated with only SR-8278 at 12-24h timepoint but had no effect at 0-12h.

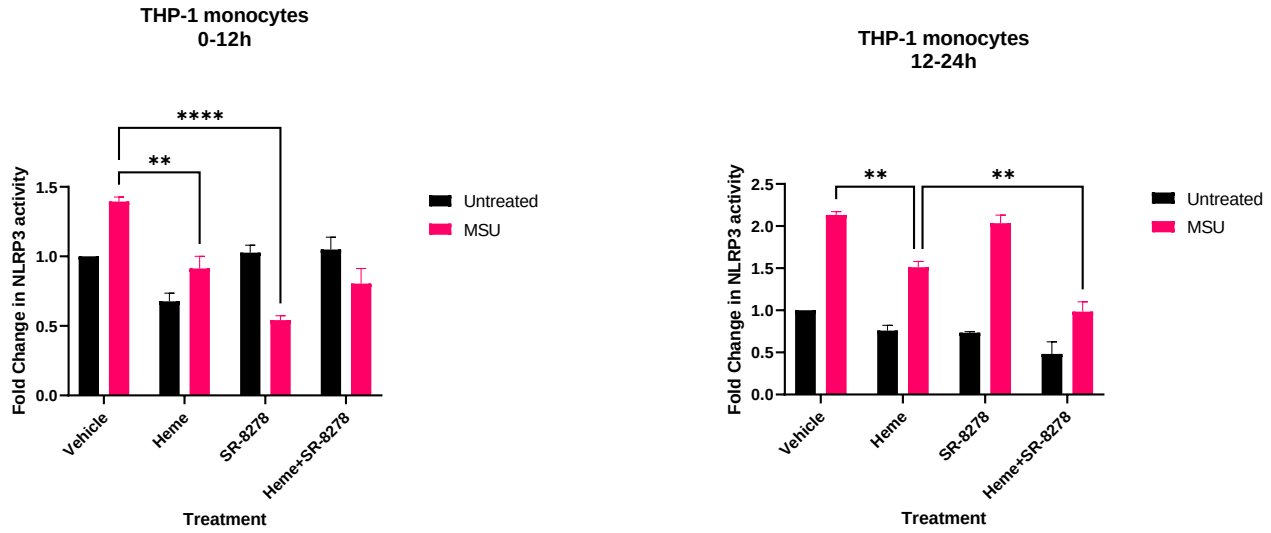

Figure 3.15 Fold changes in NLRP3 inflammasome activity in THP-1 monocyte cells treated +/- SR-8278 antagonist and +/- Heme in the absence/presence of MSU crystals. NLRP3 inflammasome activity expressed is equivalent to caspase-1 activity. The bars indicate the mean fold change ± SEM of a single experiment (n=3). All data were optimized to cell number. (* $p < 0.05$), (** $p < 0.01$), (*** $p < 0.001$), (**** $p < 0.0001$)

MSU untreated macrophage-like cells:

In the absence of MSU crystals, SR-8278 alone did not show a significant effect ($p>0.05$) on NLRP3 activity in macrophage-like cells at either timepoint. Conversely, heme alone demonstrated a significant induction ($p<0.05$) and ($p<0.01$) on expression of NLRP3 activity at 0-12h and 12-24h timepoint respectively.

NLRP3 activity was unchanged after co-treatment with heme+SR-8278 compared to macrophage-like cells treated with heme alone, suggesting the effects of heme were not mediated by REV-ERBα. There was a significant increase ($p<0.05$) and ($p<0.0001$) in NLRP3 activation in macrophage-like cells co-treated with heme+SR-8278 compared to macrophage-like cells treated with only SR-8278 at 0-12h and 12-24h timepoints respectively.

MSU treated macrophage-like cells:

By contrast, in the presence of MSU crystals, NLRP3 activity was significantly reduced ($p<0.01$) in heme treated cells at both timepoints. The treatment with SR-8278 significantly decreased ($p<0.01$) activation of NLRP3 inflammasome at 0-12h timepoint but significantly increased its activity ($p<0.001$) at 12-24h timepoint.

The significant induction ($p<0.0001$) and ($p<0.01$) in NLRP3 activity was observed in macrophage-like cells co-treated with heme+SR-8278 compared to cells treated with heme alone at 0-12h and 12-24h timepoints respectively. These results indicating that the effect of heme was dependent on REV-ERBα activity. However, there was a significant reduction ($p<0.001$) in NLRP3 activity in macrophage-like cells co-treated with heme+SR-8278 compared to cells treated with SR-8278 alone at 12-24h timepoint but a significant increase in its activity ($p<0.0001$) at 0-12h timepoint.

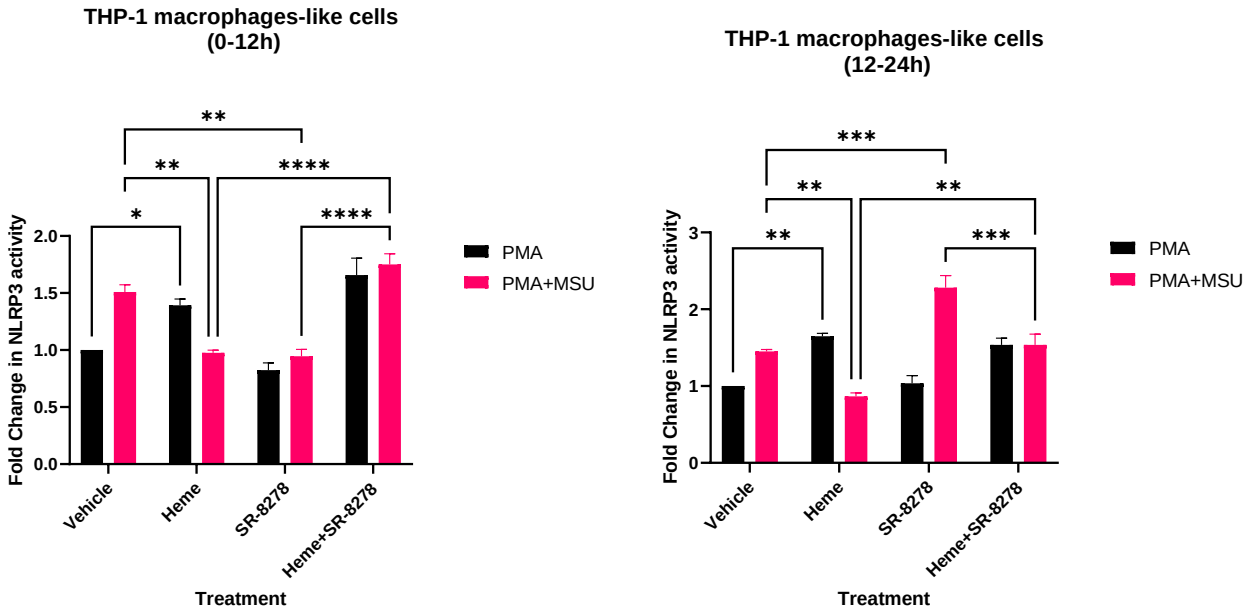

Figure 3.16 Fold changes in NLRP3 inflammasome activity in THP-1 monocyte cells treated +/- SR-8278 and +/- Heme in the absence/presence of MSU crystals. NLRP3 inflammasome activity expressed is equivalent to caspase-1 activity. The bars indicate the mean fold change ± SEM of a single experiment (n=3). All data were optimized to cell number. (* $p < 0.05$), (** $p < 0.01$), (*** $p < 0.001$), (**** $p < 0.0001$)

3.5 Validation of Gene Transfection

3.5.1 Validation of *BMAL1* knockdown at mRNA level

Adenoviral-mediated transduction of shBMAL1 was confirmed at the RNA level using real-time PCR 48h and 72h post-transfection. The cells transfected with shGFP were used as a control for *BMAL1*-knockdown cells (shBMAL1). *BMAL1* expression was significant lower ($p<0.05$) in observed monocytes treated with shBMAL1 than shGFP controls confirming the success of knockdown. The expression of *BMAL1* was approximately 35% lower relative to the shGFP control at both timepoints. Approximately 60% of all cells took up the virus.

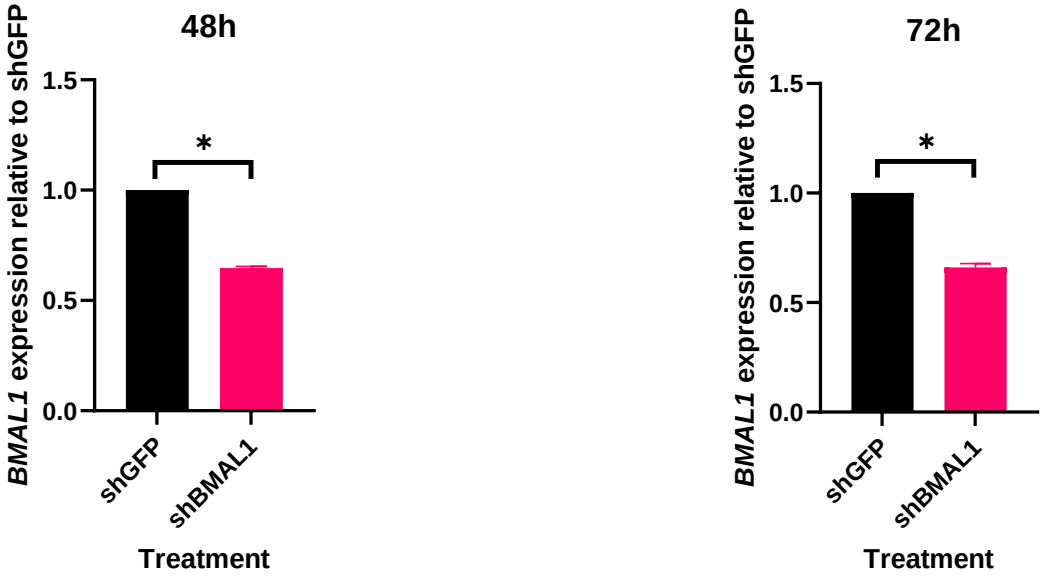

Figure 3.17 Expression of *BMAL1* in THP-1 monocyte cells relative to shGFP (control) following transient knockdown of *BMAL1* with adenovirus. Data shown as the mean ± SEM of a single experiment (n=3). All data were normalized to the housekeeper gene 18S. (* $p < 0.05$).

3.5.2 Validation of *BMAL1* overexpression at mRNA level

Ectopic-overexpression of *BMAL1* was confirmed by the statistically significant increase in *BMAL1* mRNA levels in THP-1 monocytes ($p<0.05$) transfected with the BMAL1 adenovirus and compared to GFP-transfected controls. The expression of *BMAL1* was approximately 41% higher relative to the GFP control. Approximately 60% of all cells took up the virus.

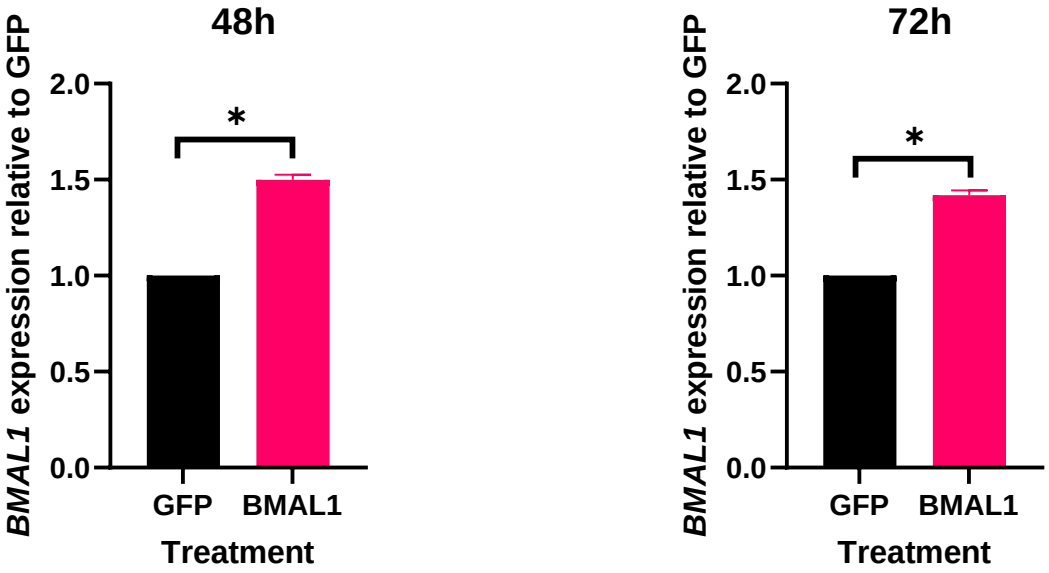

Figure 3.18 Expression of *BMAL1* in THP-1 monocyte cells relative to GFP (control) following transient ectopic overexpression of *BMAL1* with adenovirus. Data shown as the mean ± SEM of a single experiment (n=3). All data were normalized to the housekeeper gene 18S. (* $p < 0.05$).

3.6 The effect of *BMAL1* of NLRP3 Inflammasome activity

BMAL1 is known to act as transcription factor that stimulates the expression and suppression of a variety of immune genes including components of the NLRP3 inflammasome. Recent studies showed that alteration in *BMAL1* gene expression leads to altered NF-kB signalling and subsequently NLRP3 inflammasome, however it is still not well understood. Therefore, to uncover whether alteration of *BMAL1* expression in THP-1 monocyte/macrophages-like cells will result in deregulation of the NLRP3 inflammatory cascade, Caspase-Glo 1 Inflammasome Assay was performed.

3.6.1 NLRP3 inflammasome activity in *BMAL1*-overexpressed THP-1 monocytes/macrophages-like cells

Similar to as was observed in non-adenoviral transduced cells ***(Figure 4.2),*** MSU crystals resulted in a significant increase in NLRP3 activity ($p<0.0001$) in GFP controls in both monocytes and macrophage-like cells. BMAL1-overexpression in non-MSU treated monocytes and macrophage-like cells resulted in a significant increase in NLRP3 activity relative to GFP control (1.5-fold and 1.6-fold respectively). However, NLRP3 inflammasome activity was significantly lower in BMAL1-overexpressing THP-1 monocytes and macrophage-like cells treated with MSU crystals compared to MSU crystal treated GFP controls.

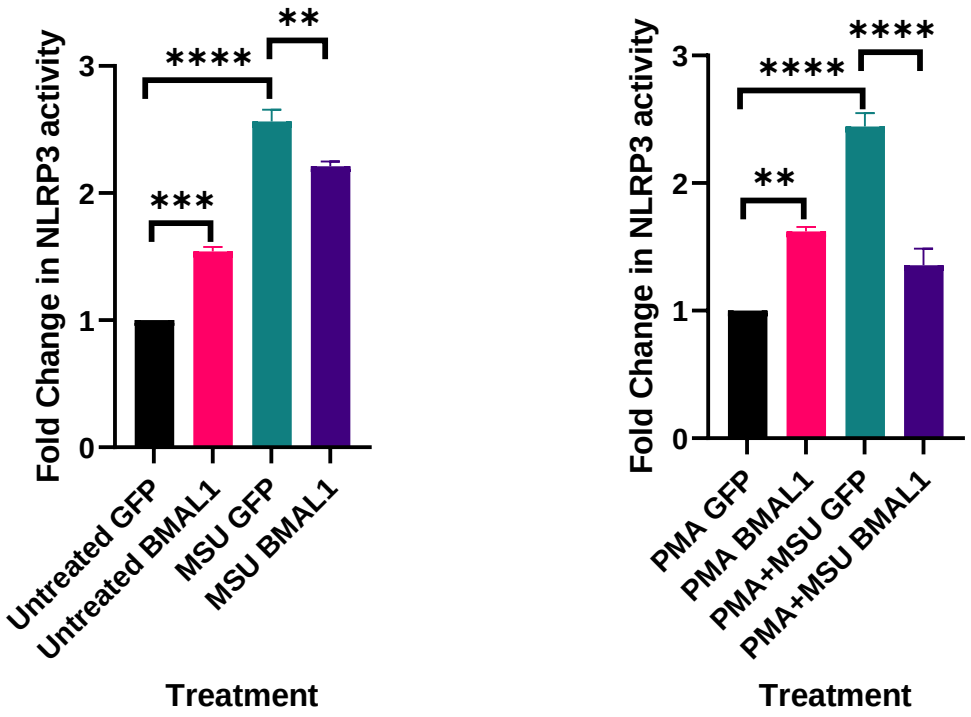

Figure 3.19 Activity of NLRP3 inflammasome in *BMAL1*- overexpressed THP-1 monocytes and macrophages-like cells in the absence/presence of MSU crystals. The BMAL1 expression is relative to GFP (control). Data shown as the mean ± SEM of a single experiment (n=3). (** $p < 0.01$), (*** $p < 0.001$), (**** $p < 0.0001$)

3.6.2 NLRP3 inflammasome activity in *BMAL1*-knockdown THP-1 monocytes/macrophages-like cells

Again, NLRP3 activity was significantly higher in MSU crystal treated shGFP control cells compared to untreated shGFP cells in both THP-1 monocytes and macrophage-like cells. In the absence of MSU crystal treatment, BMAL1-knockdown in both cell types was associated with a significant reduction in NLRP3 activity compared to non-MSU crystal treated shGFP controls. However, the opposite was observed in MSU-treated THP-1 monocytes and macrophage-like cells with NLRP3 activity significantly higher in MSU-treated shBMAL1 cells compared to MSU-treated shGFP cells.

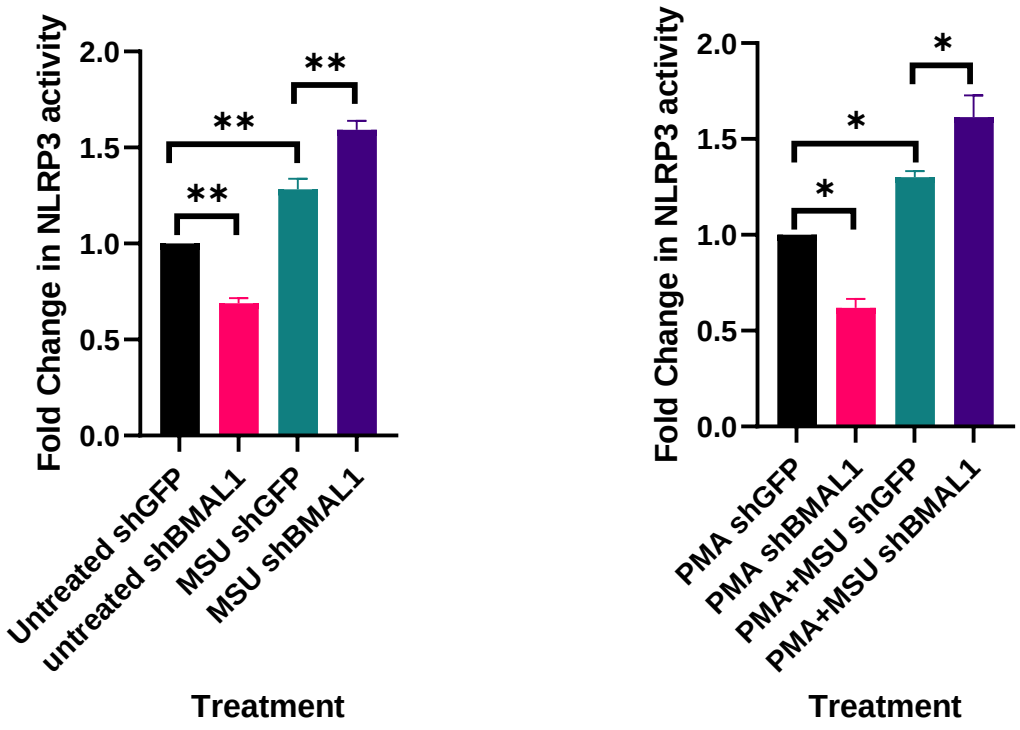

Figure 3.20 Activity of NLRP3 inflammasome in *BMAL1*-knockdown THP-1 monocytes and macrophages-like cells in the absence/presence of MSU crystals. The shBMAL1 expression is relative to shGFP (control). Data shown as the mean ± SEM of a single experiment (n=3). (* $p < 0.05$), (** $p < 0.01$),

3.7 The effect of Prednisolone on regulation of NLRP3 inflammasome activity in THP-1 monocytes/macrophages-like cells

Prednisolone (PDN) is the active metabolite of a synthetic glucocorticoid which is used in a variety of inflammatory disorders including gout. The effect of Prednisolone was measured at two separate time points 0-12h and 12-24h. The THP-1 monocytes and macrophages-like cells were pre-treated with Prednisolone at 0h for 0-12h timepoint and at 12h for 12-24h timepoint as described in (**Section 2.5.5).** The cells were exposed to MSU crystals only 4h prior to Caspase-1 Inflammasome assay therefore the effect of MSU crystals that occurred was measured at 8-12h and 20-24h for 0-12h and 12-24h timepoints respectively.

First, the effect of MSU crystals was clearly observed in monocytes at both timepoints as the NLRP3 activity significantly increased by 1.4-fold and 1.3-fold at 0-12h and 12-24h respectively. During 0-12h

timepoint Prednisolone showed a significant decrease ($p<0.0001$) by 1.8-fold in NLRP3 activity in monocytes treated with MSU crystals compared to vehicle control treated with MSU crystals. Furthermore, there was a significant reduction ($p<0.001$) by 1.2-fold in NLRP3 activity in monocytes treated with Prednisolone in the absence of MSU crystals compared to vehicle control. Conversely, at 12-24h timepoint NLRP3 activity was significantly increased by 2.3-fold ($p<0.0001$) in monocytes treated with PDN and MSU crystals compared to controls exposed to MSU crystals. Moreover, Prednisolone alone (no MSU) significantly increased ($p<0.001$) by 1.4-fold NLRP3 activity compared to vehicle control.

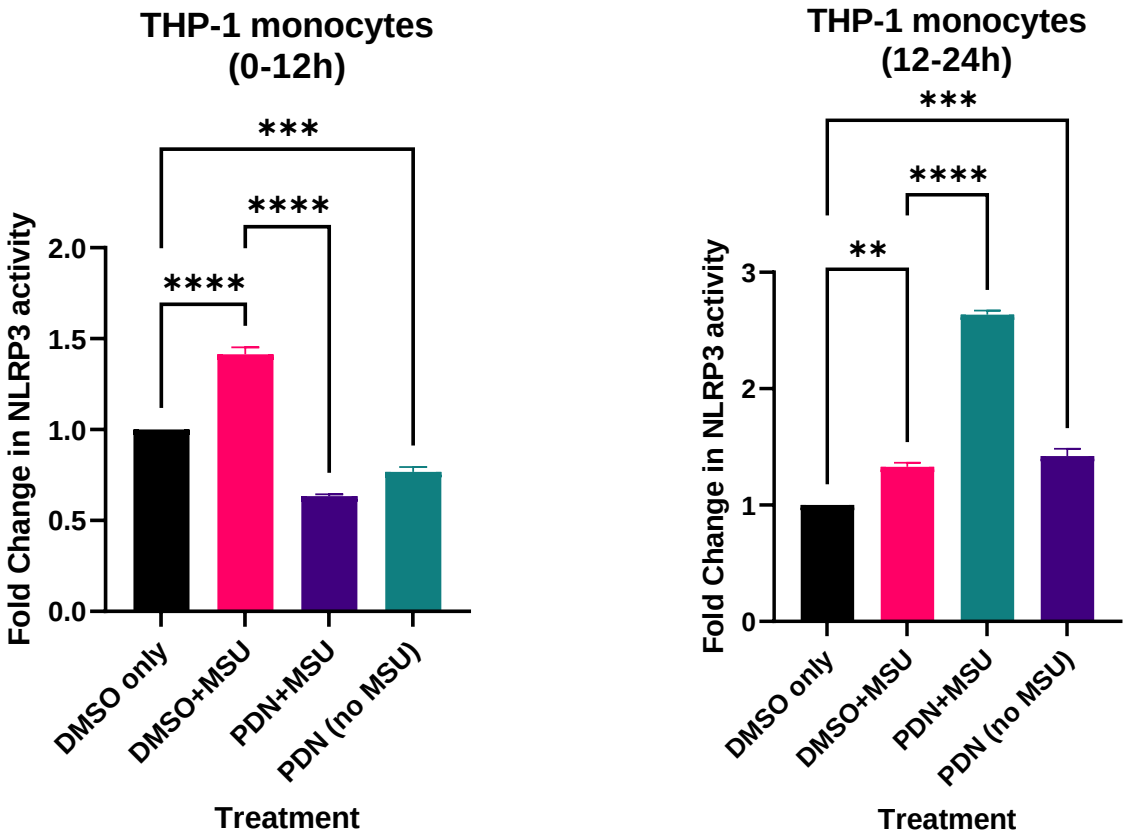

Figure 3.21 Fold changes in NLRP3 inflammasome activity in THP-1 monocytes in the absence/presence of MSU crystals and with/without Prednisolone. NLRP3 inflammasome activity expressed is equivalent to caspase-1 activity. The bars indicate the mean fold change ± SEM of a three separate experiments (n=3). All data were optimized to cell number. (** $p < 0.01$), (**** $p < 0.0001$)

In macrophages-like cells Prednisolone treatment demonstrated similar effect on NLRP3 inflammasome activity as in monocytes. Again, the effect of MSU crystals on NLRP3 activity was first validated by significant increase ($p<0.01$) in NLRP3 activity in macrophages-like cells exposed to MSU crystals compared to MSU-untreated vehicle control. During both 0-12h and 12-24h timepoints the cells pre-treated with Prednisolone and exposed to MSU crystals showed a significant reduction by 1.4-fold and 2-fold respectively in NLRP3 activity compared to MSU treated cells without PDN pre-treatment. The

macrophages-like cells not exposed to MSU crystals demonstrated significant decrease by 1.4-fold in NLRP3 activity compared to vehicle control during 0-12h timepoint. However, there was a significant increase by 1.4-fold in NLRP3 inflammasome detected at 12-24h timepoint in cells treated with Prednisolone without MSU exposure compared to vehicle control.

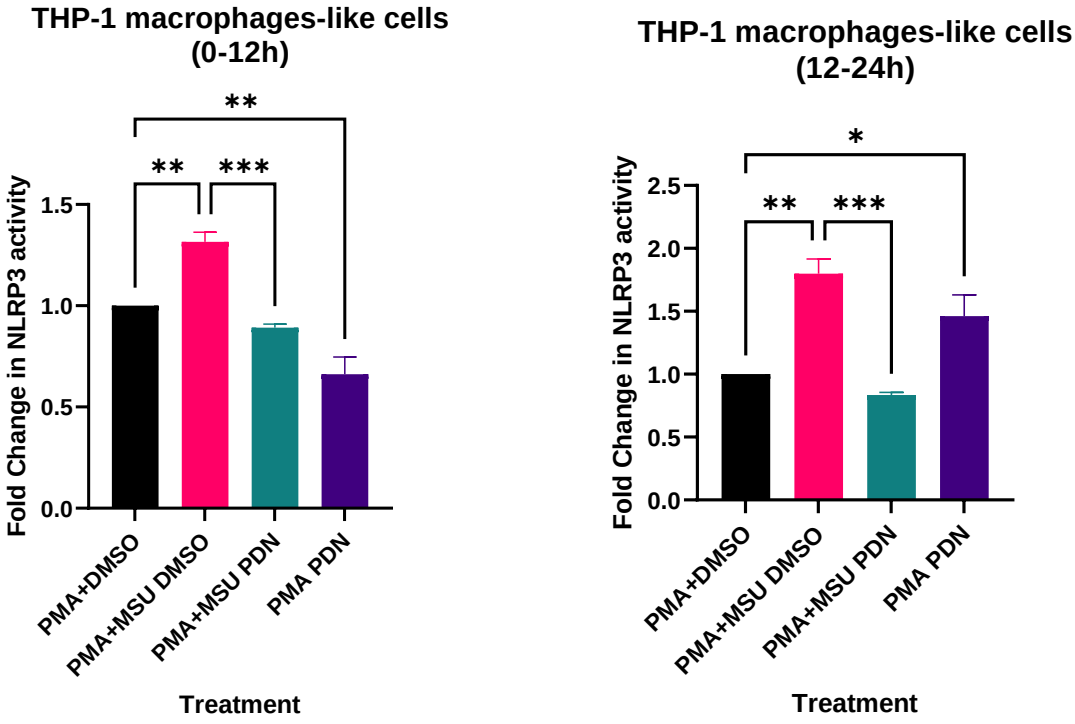

Figure 3.22 Fold changes in NLRP3 inflammasome activity in THP-1 monocytes in the absence/presence of MSU crystals and with/without Prednisolone. NLRP3 inflammasome activity expressed is equivalent to caspase-1 activity. The bars indicate the mean fold change ± SEM of a three separate experiments (n=3). All data were optimized to cell number. (** $p < 0.01$), (**** $p < 0.0001$)

3.8 Relative protein level expression of REV-ERBα compared to TLR4 in THP-1 monocyte/macrophage-like cells in the absence/presence of MSU crystals

Previous studies have shown that REV-ERBα has a role in inhibition of pro-inflammatory signals in macrophages by repressing the TLR4 gene (Fontaine et al., 2008). Therefore, to determine whether or not there is a difference between REV-ERBα and TLR4 protein levels in THP-1 cells +- MSU crystals, western blot was performed.

3.8.1 Optimization of loading control (B-actin vs GAPDH)

B-actin was used as an original loading control, however we observed a clear trend of B-actin levels being consistently higher in PMA treated cells. Therefore, to make sure that B-actin levels are not affected by PMA treatment we used the second housekeeper protein GAPDH. The expression of B-actin protein was very similar to expression of GAPDH across 24-hour time course. The same trend was detected in both housekeepers which confirmed that there is a difference in the amount of protein loaded on the gel between PMA treated and non-treated samples.

Western blot is a semi-quantitative technique, therefore due to a large difference in protein loading between PMA-treated samples and non-PMA treated, those samples were analysed separately from each other.

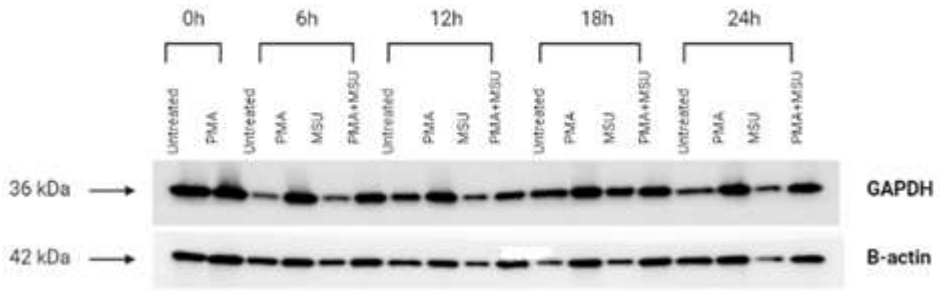

Figure 3.23 Representative blot of B-actin and GAPDH expression in THP-1 monocyte/macrophage-like cells across 24-hour time course. Sizes of proteins were determined relative to Precision Plus Protein Dual Color Ladder.

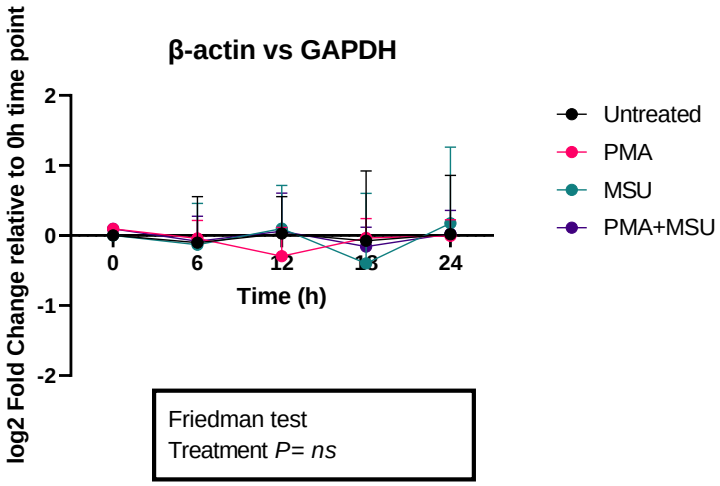

Figure 3.24 Log2 fold changes in protein expression from Western blot in THP-1 monocyte/macrophage-like cells in the presence/absence of MSU crystals. GAPDH normalized to B-actin loading control and expressed as a ratio B-actin vs GAPDH. Expression at each time point is relative to the 0h time point in MSU untreated cells. Fold change is expressed in Log2 transformed form. Data shown is the mean ± SEM (n=6).

3.8.2 The pattern of oscillation in REV-ERBα vs TLR4 protein expression in THP-1 monocyte/macrophage-like cells in the absence/presence of MSU crystals

Time had a significant effect on REV-ERBα expression ($p<0.0001$) in both monocytes and macrophage-like cells. In both monocytes and macrophage-like cells, the peak in REV-ERBα protein levels was observed at 12h timepoint. In monocytes, there was a significant effect ($p<0.05$) of MSU crystals treatment on expression of REV-ERBα protein in MSU treated cells compared to untreated cells. However, this was not observed in macrophage-like cells. No significant interaction between time and treatment was observed following MSU treatment in either cell type.

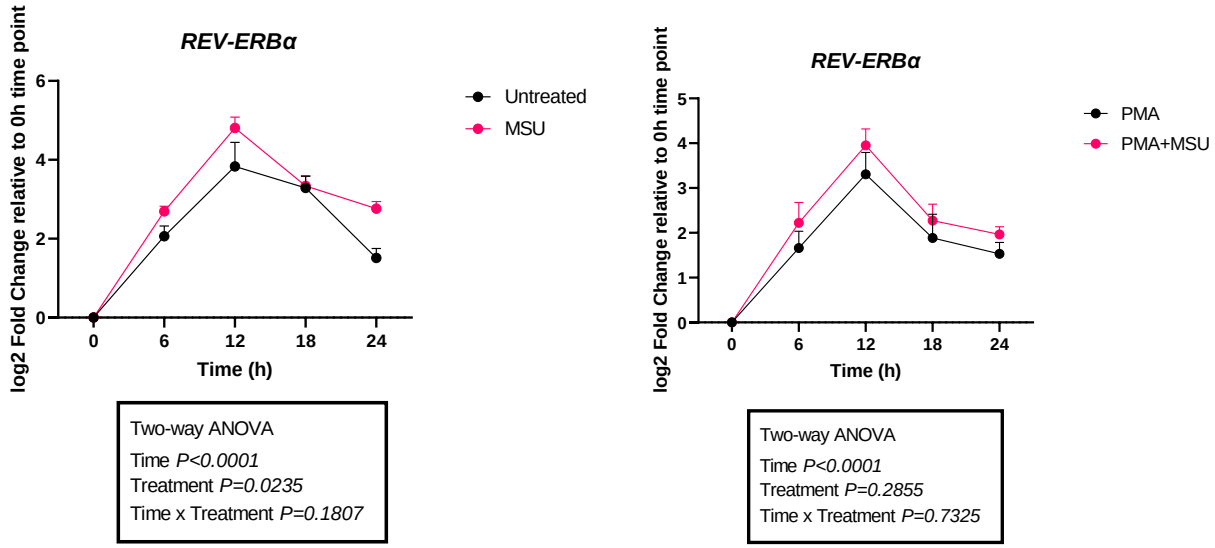

Figure 3.25 Log2 fold changes in REV-ERBα expression in THP-1 monocyte/macrophage-like cells across 24-hour time course. REV-ERBα protein levels at each time point are expressed relative to the 0h time point in MSU untreated cells. Fold change is expressed in Log2 transformed form. Data shown is the mean ± SEM (n=6).

3.8.3 TLR4 protein expression in THP-1 monocyte/macrophage-like cells in the absence/presence of MSU crystals

In both cell types, time showed a significant effect on TLR4 expression. There was no significant main effect of MSU crystal treatment on TLR4 protein levels in either cell type. However, there was a significant ($p<0.05$) interaction between time and MSU treatment in TLR4 protein levels in macrophage-like cells. TLR4 protein levels peaked at the 12h timepoint in non MSU-treated cells but no peak was evident in MSU-treated cells.

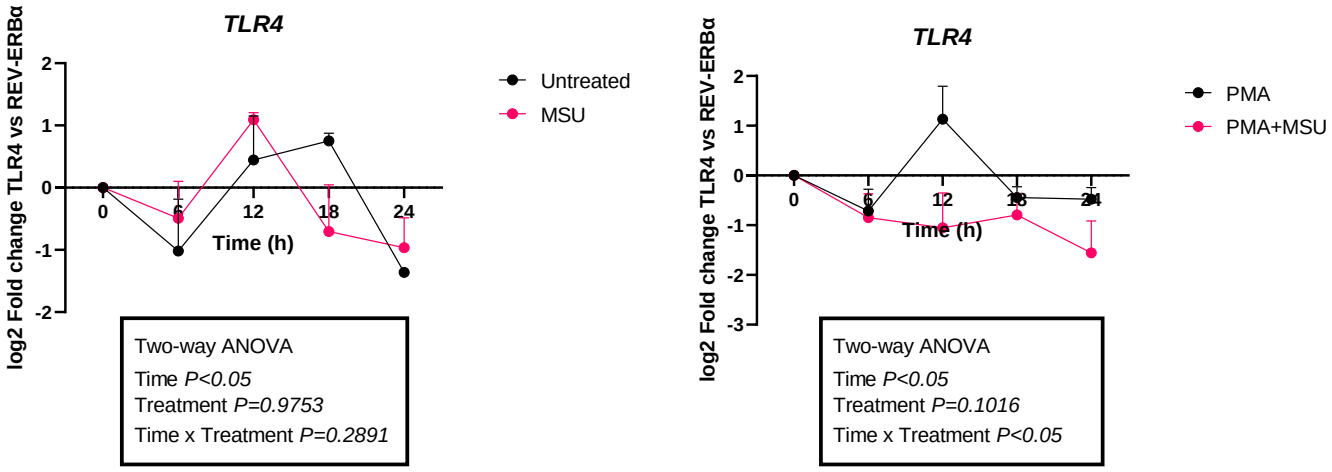

Figure 3.26 Log2 fold changes in TLR4 expression in THP-1 monocyte/macrophage-like cells across 24-hour time course. TLR4 protein levels at each time point are expressed relative to the 0h time point in MSU untreated cells. Fold change is expressed in Log2 transformed form. Data shown is the mean ± SEM (n=6).

3.8.4 REV-ERBα altered protein expression of TLR4 in THP-1 monocyte/macrophage-like cells in the absence/presence of MSU crystals

Both REV-ERBα and TLR4 were detected on the same blot in order to also allow comparison of the relative timing of their peak expression. In monocytes, MSU treatment had no significant effect of the relative levels of TLR4 vs REV-ERBα. However, in macrophages-like cells, treatment with MSU crystals resulted in significant ($p<0.05$) time-dependent reduction of the ratio of TLR4 to REV-ERBα. As can be seen from ***(Figure 3.27)*** this difference was driven by a reduction in TLR4 protein levels in MSU treated macrophage-like cells rather than an increase in REV-ERBα.

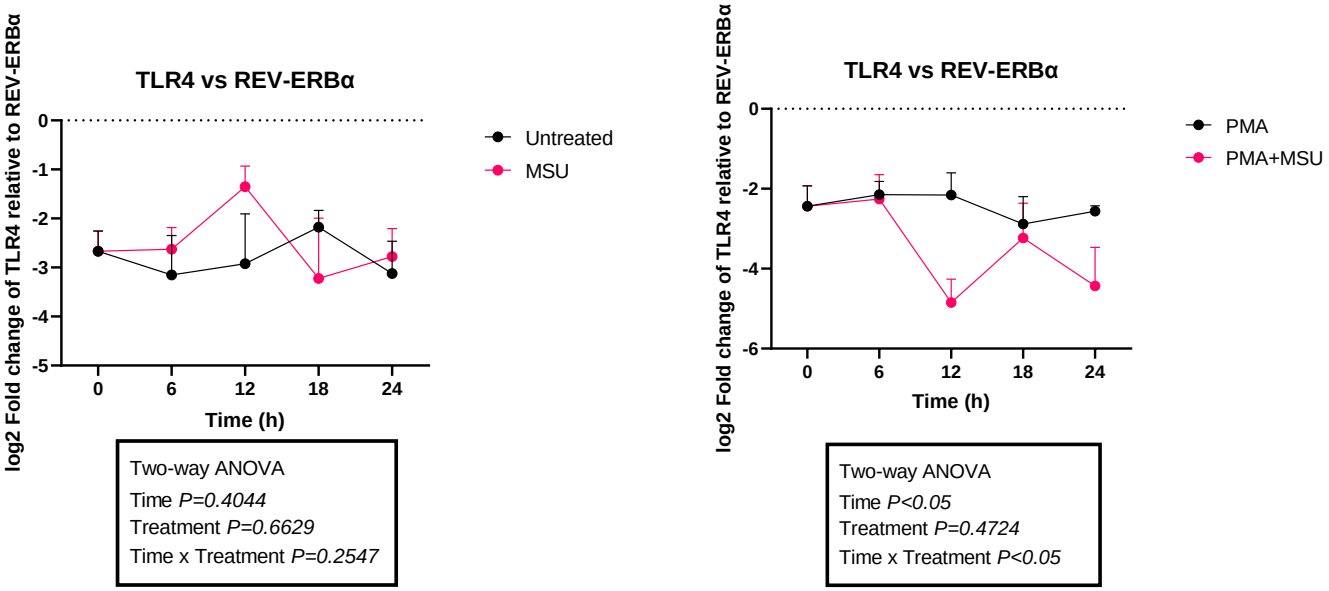

Figure 3.27 Log2 fold changes in TLR4 expression relative to REV-ERBa in THP-1 monocyte/macrophages-like cells across 24-hour time course. The protein levels of TLR4 and REV-ERBa are expressed as a ratio between TLR4 and REV-ERBa relative to the 0h timepoint in MSU untreated cells. Fold change is expressed in Log2 transformed form. Data shown is the mean ± SEM (n=6).

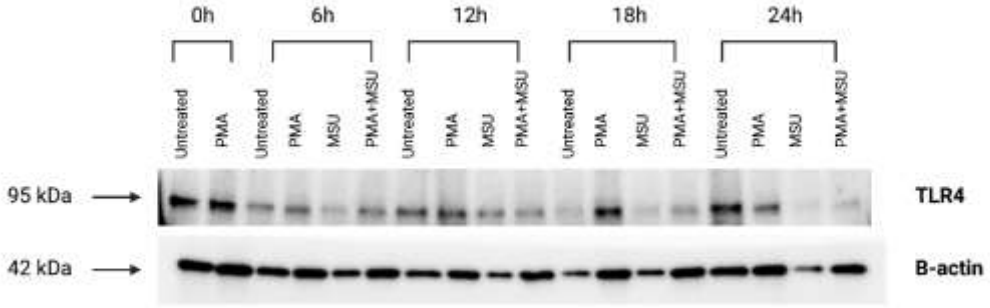

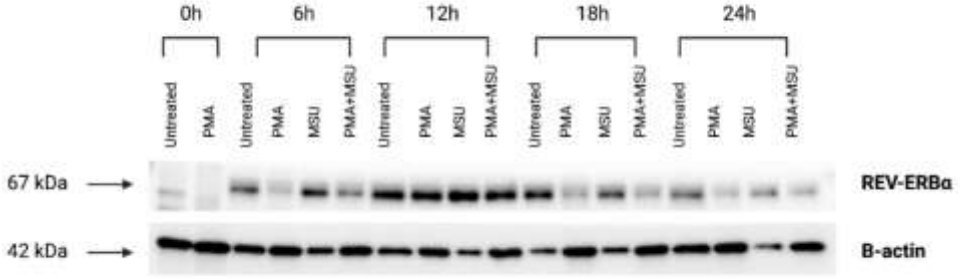

Figure 3.28 Western blots of TLR4 and REV-ERBa expression in THP-1 monocyte/macrophage-like cells across 24-hour time course. All 4 blots are from a single experiment. Sizes of proteins were determined relative to Precision Plus Protein Dual Color Ladder.

Summary of Findings:

Table 3.2 The effect of BMAL1 on MSU-induced NLRP3 inflammasome

***BMAL1*-overexpression**

Cell type	NLRP3 activity
THP-1 monocytes	Reduced ($p < 0.001$)
THP-1 macrophage-like cells	Reduced ($p < 0.0001$)

***BMAL1*-knockdown**

Cell type	NLRP3 activity
THP-1 monocytes	Induced ($p < 0.01$)
THP-1 macrophage-like cells	Induced ($p < 0.05$)

Table 3.3 The effect of Prednisolone on activity of NLRP3 inflammasome

THP-1 monocytes

Treatment	MSU exposure	Timepoint	NLRP3 activity	Significance
Prednisolone vs Vehicle	No	0-12h	Reduced	$p<0.001$
Prednisolone vs Vehicle	No	12-24h	Induced	$p<0.001$
Prednisolone vs Vehicle	Yes	0-12h	Reduced	$p<0.0001$
Prednisolone vs Vehicle	Yes	12-24h	Induced	$p<0.0001$

THP-1 macrophage-like cells

Treatment	MSU exposure	Timepoint	NLRP3 activity	Significance
Prednisolone vs Vehicle	No	0-12h	Reduced	p<0.01
Prednisolone vs Vehicle	No	12-24h	Induced	p<0.05
Prednisolone vs Vehicle	Yes	0-12h	Reduced	p<0.001
Prednisolone vs Vehicle	Yes	12-24h	Reduced	p<0.001

Table 3.4 The effect of MSU crystals on the protein expression of REV-ERBα in THP-1 monocyte/macrophage-like cells

Cell type	Effect of Time	Effect of Treatment	Interaction
THP-1 monocytes	$p < 0.0001$	$p < 0.05$	ns
THP-1 macrophage-like cells	$p < 0.0001$	ns	ns

Table 3.5 The effect of MSU crystals on the protein expression of TLR4 in THP-1 monocyte/macrophage-like cells

Cell type	Effect of Time	Effect of Treatment	Interaction
THP-1 monocytes	$p < 0.05$	ns	ns
THP-1 macrophage-like cells	$p < 0.05$	ns	$p < 0.05$

Table 3.6 The effect of MSU crystals on protein expression of TLR4 relative to REV-ERBα in THP-1 monocyte/macrophage-like cells

Cell type	Effect of Time	Effect of Treatment	Interaction
THP-1 monocytes	ns	ns	ns
THP-1 macrophage-like cells	$p < 0.05$	ns	$p < 0.05$

4 Discussion

4.1 Introduction

Gouty arthritis is an inflammatory condition which is frequently initiated during early hours in the morning or late at night. It is characterized by activation of the NLRP3 inflammasome which is triggered by monosodium urate crystals in the joint cavity and subsequent release of several pro-inflammatory cytokines as well as neutrophil recruitment. It is now known that the trafficking of innate immune cells such as monocytes and macrophages as well as the activity of NLRP3 inflammasome is under control of circadian oscillator. The combination of those facts stated above became the motivation for the current study as our goal was to try and look into whether or not the timing of gout flares could help to explain their origin. We hypothesised that individuals with gout are predisposed to gout flares during the night-time due to alteration of the monocyte/macrophage circadian rhythm by MSU crystals. In this study we investigated the interplay between the circadian clocks in THP-1 monocytes/macrophage-like cells that are exposed to MSU crystals, and the acute inflammatory response driven by NLRP3 inflammasome.

4.2 MSU crystal treatment resulted in altered expression of components of the molecular circadian clock in both THP-1 monocytes and macrophage-like cells

To our knowledge, the current study is the first to investigate the effect of monosodium urate crystals on the expression levels of core circadian components involved in maintaining circadian rhythms in monocytes and macrophage-like cells. To test the former, we first determined whether THP-1 monocytes and macrophage-like cells possess functional autonomous molecular clocks. Our results demonstrated that THP-1 monocytes and macrophage-like cells express canonical circadian genes and that the expression of individual gene varied over a period of 24 hours consistent with the expected circadian oscillation in clock gene expression. In particular we found a significant effect of time on the expression of *BMAL1, REV-ERBa, CRY1* and *PER1* in both monocytes and macrophage-like cells. We did not observe significant effect of time on expression of *CRY2, PER2* genes however this is likely to be due to a lack of statistical power as these genes had been shown to express circadian rhythms in human monocytes (Haimovich et al., 2010). These results support the evidence from the literature and indicate that innate immune cells such as monocytes and macrophages indeed have a functional molecular clock mechanisms which are able to operate autonomously (Keller et al., 2009). Interestingly, for the first time, the results from our study showed that MSU crystal treatment altered the expression of *CRY1* in macrophages-like cells and but not in monocytes ***(Figure 3.3 & Figure 3.7)***. *CRY1* is an important core clock component associated with

regulating of proinflammation through the control of TLR/NF-kB pathway (Yang et al., 2015). The results from previous in vitro study demonstrated that *CRY1* has the ability to supress activity of NF-kB/NLRP3 signalling cascade via binding to adenylyl cyclase and limiting production of cAMP which in turn leads reduction of protein kinase A activation and subsequent decrease in activation of NF-kB. Our results suggest that macrophage-like cells could be hypersensitive to monosodium urate crystals. Therefore, the increase in *CRY1* level induced by MSU crystals can potentially be a contrary mechanism of cell to an increased NLRP3 activity in order to reduce the release of pro-inflammatory cytokines via NF-kB/NLRP3 axis (Narasimamurthy et al., 2012). Nevertheless, further studies are needed to investigate whether there is an effect of MSU crystals on *CRY1* protein level and also to determine the effect of *CRY1* on NLRP3 inflammasome activity and subsequent cytokine production.

In the present study we demonstrated a time-dependent reduction of *REV-ERBα* in MSU-challenged monocytes. We also detected that circadian oscillation of *REV-ERBα* was blunted in MSU-induced macrophage-like cells ***(Figure 3.2 & 3.6).*** However, we observed a circadian oscillation in REV-ERBα protein levels during 24h period from our western blot analysis. The protein levels of REV-ERBα in both cell types in the presence/absence of MSU crystals were on the rise at 0-12h and on decline at 12-24h with a peak of protein expression at 12h timepoint. Interestingly, MSU treatment did produced an effect on REV-ERBα protein levels in monocytes, but it was not in time-dependent manner as it was observed in mRNA levels ***(Figure 3.25).*** In macrophage-like THP-1 cells, no effect of MSU crystals on REV-ERBα protein level was detected which could be due to variation between mRNA and protein levels of circadian components in the cells. The difference in outcomes from protein analysis compared to mRNA levels suggests that there are variety of steps beyond mere transcriptional control are involved in establishing the protein levels of circadian components (McManus et al., 2015). The REV-ERBα protein auto-inhibits expression of its own RNA so high REV-ERBα protein levels could cause reduced *REV-ERBα* mRNA (Keene, 2010). Moreover, there is a possibility of a reduction in half-life of the protein due to increased rate of degradation as an attempt to regress the sudden change in the clock machinery. The results from this study partially comply with the study by S. Wang et al. In their study researchers also confirmed alteration in mRNA expression of *CRY1* and *REV-ERBα* in dextran sodium sulfate (DSS)-induced primary monocytes and macrophages as well as in vivo model, however, they did not look at the protein level of those core circadian genes (Wang et al., 2018) . Overall, we established that MSU crystal treatment does indeed modify the expression of *CRY1* and *REV-ERBα* clock components in THP-1 monocytes and macrophage-like cells.

In vivo, peripheral clocks are known to be synchronized with the master clock in SCN and influenced by hormonal and metabolic factors. However, our experiment was performed in vitro and therefore serum-shock (the withdrawal of nutrients and growth factor) treatment was used to mimic the Zeitgeber cues in the

in vitro environments. Although, the exact 24-hour period confirmed in vivo could not be replicated in the vitro environment, in theory serum starvation "synchronises" the peripheral clock (Richards & Gumz, 2012). It is believed to occur due to the fact that circadian clock and cell cycle are interlinked. Serum-shock treatment arrests the individual cells at G1 phase and re-feeding the cells with serum rich media triggers the cell cycle to start again which is thought to "re-set" the peripheral clock on the cells (Shin et al., 2008). The serum media in which was used to grow our cells still contain nutrients such as glucose and L-glutamine which are crucial sources of energy for cell culture (Tannockl et al., 1986). Therefore, serum-starvation method cannot completely mimic re-setting of cues in peripheral clocks in vivo as we can't equate serum-shock treatment and re-feeding with day and night cycle. Glucocorticoid treatment is also known to be used as a common method to mimic endogenous re-setting cues by limiting cell's entrance into S phase of the cell cycle (Kiessling et al., 2017). However, glucocorticoid treatment has an anti-inflammatory effect which was not appropriate for the current study as we studied the inflammatory effect of MSU crystals on circadian genes in innate immune cells.

4.3 The NLRP3 inflammasome activity was altered through the effects of heme on *REV-ERBα* and TLR4

Previous loss-of-function studies highlighted that time-of-day variation in leucocyte trafficking and release of pro-inflammatory cytokines are directly mediated by the core circadian genes, including *REV-ERBα* and *BMAL1* in a 24-hour circadian rhythm (Gibbs et al., 2012; Pick et al., 2019). Based on the literature *REV-ERBα* had been identified as transcriptional regulator of inflammatory genes such as NLRP3 (Wang et al., 2020). *REV-ERBα* has been shown to act as a direct regulator of mRNA expression and transcription of the core NLRP3 inflammasome components. Herein, we focus on core circadian component *REV-ERBα* and investigate its effect on the regulation of inflammatory responses in MSU-challenged THP-1 monocytes and macrophages-like cells.

Monosodium urate crystals are known as a causative agent in gouty arthritis, however the underlying mechanisms of MSU-induced inflammation only recently begun to be revealed (Dalbeth & Haskard, 2005; Kingsbury et al., 2011). Accumulating evidence from several studies suggests that MSU-induced inflammation occurs via activation of NLRP3 inflammasome which in turn result in secretion of IL-1β from macrophages and subsequent neutrophil influx into the joint space (Dinarello, 2010). In this study we addressed the effect of MSU crystals on NLRP3 activity in THP-1 monocytes and macrophages-like cells. Our results showed that monocytes and macrophages-like cells pre-treated with MSU crystals had a significant increase in caspase-1 activity compared to untreated cells ***(Figure 3.15).*** After activation and formation of NLRP3 inflammasome, it converts pro-caspase-1 into caspase-1 which we measured in our

results. Therefore, caspase-1 activity can be directly linked to the activity of NLRP3 inflammasome. The study by Jhang et al also showed that THP-1 cells, following treatment with MSU crystals led to a significant induction in NLRP3 inflammasome activation as well as subsequent increase in IL-1B release (Jhang et al., 2015). Notably, in their study the researchers discovered an effect of phorbol 12-myristate 13-acetate (PMA) treatment on NLRP3 inflammasome activity. It appears that THP-1 monocytes treated with PMA initiate an inflammatory response by significantly increasing secretion of IL-1b which is linked to the NLRP3 inflammasome. However, our results did not show a significant increase in NLRP3 activity in PMA treated THP-1 monocytes perhaps due to the fact that we measured NLRP3 activity 72h after PMA treatment and not after 3h exposure to PMA in the study mentioned above. Therefore, the treatment with PMA seems to produce a transient increase in NLRP3 activity over a short period of time and may not affect mature macrophages.

To examine the effects of *REV-ERBa* on regulation of NLRP3 inflammasome activity in vitro, we compared the effects of heme (endogenous agonist of *REV-ERBa*) with or without SR-8278 (pharmacological antagonist of *REV-ERBa*). Heme has an ability to bind directly to the *REV-ERBa* ligand-binding domain (LBD) and thereby enhance the ability of *REV-ERBa* to supress the transcription of target genes by increasing recruitment of co-repressors such as NCoR to target genes (Raghuram et al., 2007; Yin et al., 2010). SR-8278 is a synthetic antagonist of *REV-ERBa* which acts completely opposite to heme therefore it directly binds to *REV-ERBa* LBD and inhibits *REV-ERBa* transcriptional repression of target genes (Kojetin et al., 2011). There were no obvious off-target effects of SR-8278 had been shown in in vitro studies.

First, we investigated the effect of SR-8278 alone on monocytes and macrophages-like cells at two time points. We report that inhibition of *REV-ERBα* by SR-8278 in monocytes and macrophages-like cells had no effect on NLRP3 activity in non-MSU treated cells at both time points ***(Figure 3.16 & 3.17).*** However, in the presence of MSU crystals the inhibitory effect has been seen only in macrophage-like cells at 12-24h timepoint. The treatment with SR-8278 indeed resulted in increase in NLRP3 inflammasome activity perhaps due to inhibition of REV-ERBα activity (Kojetin et al., 2011). These results comply with in vivo muscle dystrophy model where authors showed that REV-ERBα antagonism in vivo induced by SR-8278 significantly increased inflammation and reduced expression of pro-myogenic factor which is required to rebuild muscle tissue (Welch et al., 2017). In contrast to these findings, in the presence of MSU crystals, we observed the opposite effect of SR-8278 on NLRP3 activity in both monocytes and macrophage-like cells only at 0-12h timepoint. As we mentioned before, the caspase-1 (NLRP3) activity was measured at 8-12h for 0-12h timepoint and at 20-24h for 12-24h timepoint. Therefore, these results corelate with our previous finding of REV-ERBα protein levels during 24h time period ***(Figure 3.25).*** We observed an increasing trend in REV-ERBα protein expression during first 0-12 hours with its peak at 12h. The results obtained by Bibbs et al, also demonstrated an upregulation of REV-ERBα during first 0-12h and downregulation during

12-24h in LPS-induced macrophages. Therefore, it is possible that detected decrease in NLRP3 activity during 0-12h is related to an endogenous increase in REV-ERBα protein expression in cells.

Evidence from the literature suggest that heme acts not only as an agonist for REV-ERBα but also as an agonist for TLR4 (Figueiredo et al., 2007; Raghuram et al., 2007). It has been shown to directly activate TLR4-mediated signalling via direct binding of heme-binding proteins (HBP) to TLR4 and thus activating inflammatory pathways including NF-kB/NLRP3 axis or indirectly by generation of reactive oxygen species (ROS) via what is called Fenton reaction of iron and H2O2 (Bozza & Jeney, 2020; Janciauskiene et al., 2020). Therefore, in the present study we used heme as REV-ERBα and TLR4 agonist to investigate whether or not it has an effect on MSU-induced inflammatory response at two different time points. Our results showed a cell-dependent effect of heme in the absence of inflammatory inducer. In the absence of MSU crystals, treatment with heme did not change NLRP3 activity in monocytes at either timepoint, yet heme treatment induced NLRP3 activation in macrophage-like cells at 0-12h and 12-24h timepoints ***(Figure 3.16 & 3.17).*** In the study by Figueredo et al, the authors demonstrated that heme in the absence of LPS stimulation induced secretion of TNF-a and IL-6 by human and mouse derived macrophages via upregulation of TLR4 signalling (Figueiredo et al., 2007). Moreover, the findings from another paper stated that TLR4 signalling requires co-receptor CD14 and thus the concentration of LPS has to be much higher in LPS-challenged monocytes compared to macrophage-like cells to achieve the same level TLR4 pathway signalling (Haziot et al., 1996). Finally, in vitro study by Erdei et al showed heme-mediated NLRP3 inflammasome activation via ROS production and K+ efflux which triggered induction of active IL-1b in human umbilical vein endothelial cells in the absence of LPS-induced inflammation (Erdei et al., 2018). Based on our findings and prior studies, we may only speculate that in the absence of inflammatory inducers, heme-mediated increase in NLRP3 inflammasome activity has a cell-specific characteristic. Specifically, it appears that mature macrophage-like cells with high expression of CD14 are more susceptible for heme to either directly or indirectly activate TLR4-mediated signalling via TLR4 agonism or production of ROS which ultimately results in activation of NF-kB/NLRP3 axis. Nevertheless, further investigation is needed to determine the exact mechanism of action of heme in different cells not stimulated by any inflammatory inducers.

Consistently, with the evidence from the literature on the anti-inflammatory effects of heme, here we report that treatment with heme significantly downregulated NLRP3 inflammasome activation in MSU-stimulated monocytes and macrophage-like cells (Pae & Chung, 2015.; S. Wang et al., 2020; Yin et al., 2010). Heme-mediated inhibition of NLRP3 activity appears to be not cell- or time- dependent, as the same effect has been detected in both MSU-challenged cell types and at 0-12h & 12-24h timepoints. However, it is unclear whether the anti-inflammatory effect of heme is due to regulation of REV-ERBα and thus NF-kB/NLRP3 axis or perhaps due to heme oxygenase-1 activity. In vitro and in vivo models of DSS-induced colitis

revealed that REV-ERBα repress NLRP3 activity mainly at the priming step by suppressing *NLRP3* transcription via binding to its promoter region and therefore preventing activation of NF-kB/NLRP3 axis (Wang et al., 2018). Furthermore, genetic and pharmacological modulation of REV-ERBα activity in human and cultured macrophages confirmed anti-inflammatory regulation of *REV-ERBα*. Loss in *REV-ERBα* expression resulted in activation of NF-kB/NLRP3 signalling cascade and consequently led to release of pro-inflammatory cytokines IL-1b, IL-6 and IL-18. By contrast, regaining of *REV-ERBα* expression led to attenuation of inflammatory response (Gibbs et al., 2012). Interestingly, another anti-inflammatory regulatory mechanism of heme had been previously determined in vitro and in vivo studies. Heme oxygenase-1 demonstrated its potent anti-inflammatory functions in LPS-challenged cultured rat Kupffer cell. Stimulation of cells with heme, following stimulation with LPS significantly upregulated levels of HO-1 which led to enzymatic degradation of heme as well as attenuated the expression of NLRP3 and various pro-inflammatory genes such as IL-1, TNF-a and COX2 (Immenschuh et al., 1999; Lin et al., 2003).

Next, we investigated whether the effects of heme on NLRP3 activation was altered by SR-8278. In the absence of MSU crystals we did not detect an effect on NLRP3 activity in either of the cells after co-treatment with heme+SR-8278 compared to cells treated with heme alone, suggesting that effect of heme was not mediated by REV-ERBα. Interestingly, in the presence of MSU crystals we also did not observe a significant difference in activation of NLRP3 inflammasome between monocytes co-treated with heme+SR-8278 and those treated with heme alone at the 0-12h timepoint, which implied that the effects of heme are not dependent on REV-ERBα activity. However, at the 12-24h timepoint, the activity of NLRP3 was significantly reduced in monocytes co-treated with heme+SR-8278 compared to in monocytes treated with heme alone, indicating that SR-8278 might have potentiated rather than inhibited the suppressive effects of heme on NLRP3 activation. Additionally, protein levels of REV-ERBα were on the incline during 0-12h and on decline during 12-24h **(Figure 3.25).** Therefore, despite the heme-mediated inhibition of NLRP3 activity even in the presence of SR-8278, it appears to be mediated by some other anti-inflammatory mechanisms previously described rather than regulation of REV-ERBα activity (Fontaine et al., 2008; Wang et al., 2018). Its noteworthy to mention that we observed a general reduction in TLR4 protein expression in monocytes during 20-24 hours ***(Figure 3.26)***. These results do not comply with finding of the study by Kojetin et al, where researchers characterized the activity of SR-8278 in a cell-based assay (Kojetin et al., 2011). Treatment of HepG2 cells with SR-8278 and heme resulted in inhibition of heme activity and suppression of *REV-ERBa* expression which led to activation of pro-inflammatory pathways. Surprisingly, our results demonstrated an opposite combined effect of treatment in macrophage-like cells in the presence of MSU crystals. The NLRP3 inflammasome activity was significantly increased in macrophage-like cells co-treated with heme+SR-8278 compared to cells treated with heme alone at both timepoints. Based on the prior studies mentioned before and these results we may theorize that heme exerted

its protective anti-inflammatory effect through REV-ERBα to decrease MSU-induced NLRP3 activity, however it was inhibited by SR-8278 (Fontaine et al., 2008; Wang et al., 2018).

Lastly, we sought to compare the combined effect of heme+SR-8278 and SR-8278 alone in THP-1 monocytes/macrophage-like cells. Intriguingly, we detected an increase in activity of inflammasome in macrophage-like cells at 0-12h timepoint in the presence of MSU crystals. However, there was a significant reduction in NLRP3 activity in macrophage-like cells at 12-24h timepoint ***(Figure 3.16 & 3.17).*** On one hand, our findings suggest that SR-8278 did not inhibit the effect of heme at 12-24h timepoint and rather potentiated it, however despite the heme-dependent reduction in NLRP3 activity, it doesn't seem to be driven through REV-ERBα. On the other hand, an increase in NLRP3 inflammasome activity at 0-12h timepoint is most likely to be mediated by effect of heme on REV-ERBα. However, these data contradict with our protein findings on REV-ERBα and TLR4 levels during 24h period. REV-ERBα protein levels are on the incline during 0-12h and on the decline during 12-24h. Therefore, if heme would mediate its effects through REV-ERBα agonist we would expect to see the opposite results. Additionally, REV-ERBα is known act as a suppressor of TLR4 expression (Fontaine et al., 2008). This was partially in line with the data we obtained on the TLR4 vs REV-ERBα ratio during 24 hours period ***(Figure 3.27).*** We observed a significant time- and MSU treatment- dependent reduction on the relative protein levels of TLR4 to REV-ERBα in macrophage-like cells. Surprisingly, the difference between REV-ERBα and TLR4 protein levels appear to be driven by a reduction of TLR4 protein expression in MSU-treated cells rather than an increase in REV-ERBα expression. If anything, we would expect to see an increase in TLR4 expression in MSU-challenged monocytes and macrophage-like cells. The results from this particular experiment are inconclusive and required further investigation to get a better understanding of the interplay between TLR4 and REV-ERBα expression in myeloid cells.

In the present study we obtained the evidence that REV-ERBα indeed plays an important role as a transcriptional regulator of inflammation, however the exact mechanism of its anti-inflammatory activity is yet to be determined. Our results demonstrated that heme has a controversial role in regulation of inflammatory response as it showed to act as pro- and anti- inflammatory regulator, depending on cell type, time and presence of inflammatory inducers. Based on previous studies by Fontaine et al and Shuai wang et al, we also report that REV-ERBα has capacity to regulate activity of NLRP3 and its activation downregulates the expression of NLRP3 inflammasome activity, however the results from this study show some inconsistencies thus further studies on this matter are necessary (Fontaine et al., 2008; Wang et al., 2018).

4.4 The activity of NLRP3 inflammasome was altered following *BMAL1* overexpression or knockdown

Based on the previous studies and on the findings we obtained on the effect of REV-ERBα on regulation of innate immune response via control of NF-kB/NLRP3 signalling pathway, it was logical to investigate the effect of another core circadian component, *BMAL1* which is shown to be regulated by REV-ERBα (Yin et al., 2010).

The biological clock was shown to control NLRP3 activation and expression, therefore controlling the secretion of pro-inflammatory cytokines such as IL-6, IL-18 and IL-1β in innate immune cells, particularly monocytes and macrophages. The *BMAL1* gene is one of the most critical circadian genes for maintenance of 24-h oscillations and it is known to play a key role in regulation of immune responses. Moreover, BMAL1 has been suggested to act as an anti-inflammatory factor as it showed to directly suppress transcription of pro-inflammatory cytokine genes such as Ccl2 and Ccl8 in monocytes by inducing histone modification in E-box of the *CCL2* promoter (Nguyen et al., 2013). The reduction of *BMAL1* levels in macrophages also demonstrated an induction in expression of several pro-inflammatory cytokines TNF-a, IL-1β and IL-6 (Castanon-Cervantes et al., 2010; Keller et al., 2009.) Moreover, the anti-inflammatory activity of BMAL1 was confirmed in in vivo studies. In the recent study by Feng Li et al, BMAL1-deleted mice demonstrated exacerbated P.acnes-induced inflammation in the skin (Li et al., 2022). The researchers proposed that BMAL1 supresses inflammation via its direct target REV-ERBα, which regulates NF-kB axis to restrain inflammatory response. Furthermore, the role of BMAL1 in neurodegeneration was investigated by Musiek et al who generated mice in which *BMAL1* was deleted in majority of neurons and astrocytes. *BMAL1* knock out animals had an increased expression of inflammatory cytokines, which was in line with chronic neuroinflammation (Musiek et al., 2013). Nonetheless, recent studies also demonstrated completely opposite results where BMAL1 acts as a key pro-inflammatory regulator of immune response. The findings from a study on breast cancer cells showed that BMAL1 recruits CREB binding protein to promote acetylation and phosphorylation of p65, therefore upregulating its transcriptional activity and resulting in high NF-kB activity which leads to secretion of inflammatory cytokines (Wang et al., 2019). Additionally, the other study in microglia cells also demonstrated a reduction of pro-inflammatory gene expression in *BMAL1* deficient mice (Wang et al., 2020). Therefore, the previous studies convey a contradictory role of *BMAL1*, suggesting that the exact mechanism of *BMAL1* on orchestration of immune responses is yet to be determined.

In current study we were first to investigate an effect of *BMAL1* on MSU-challenged THP-1 monocytes/macrophages-like cells as there are no studies had been conducted to investigate this matter.

Based on the results from previous studies as well as the known role of *BMAL1* as a crucial transcriptional factor within clock machinery of the cell, we hypothesized that *BMAL1* plays an important part in orchestration of inflammation-related gene expression in THP-1 monocytes and macrophages-like cells. The results of our caspase-1 inflammasome assay clearly indicate that alteration in *BMAL1* expression affected the extent of NLRP3 inflammasome activity and thereby modulated inflammatory response in both monocytes and macrophage-like cells. First, the effect of MSU crystals was confirmed by comparing MSU treated monocytes and macrophages-like cells and untreated control without modifications of *BMAL1*. The treatment with MSU crystals significantly increased the activity of NLRP3 inflammasome in both cell types compared to GFP and shGFP control ***(Figure 3.1 & 3.2)***. These results were in line with our previous findings on effect of MSU crystals ***(Figure 3.1).*** In *BMAL1*-overexpressing monocytes and macrophage-like cells, a significant reduction in NLRP3 inflammasome activity was observed compared to control cells. Consistent with this we observed the reciprocal effect on NLRP3 activity in *BMAL1*-knockdown THP-1 monocytes and macrophage-like cells. We detected a significant increase in NLRP3 inflammasome activity in THP-1 monocytes and macrophage-like cell. Strikingly, we observed the opposing effect of BMAL1 overexpression and knockdown in non-MSU treated monocytes and macrophage-like cells compare to MSU treated cells. Therefore, the results from the current study are only partially consistent with previous studies. On one hand, our findings suggest that BMAL1 may act as an anti-inflammatory factor in the presence of inflammatory mediator which in our case is MSU crystals. Prior studies demonstrated that BMAL1 abundance suppress NLRP3 inflammasome activation and thereby reduces the release of pro-inflammatory cytokines in LPS-induced inflammation (Timmons et al., 2021; Wang et al., 2018). The anti-inflammatory effect of BMAL1 and its regulation of immune responses had been shown through several mechanisms. Of particular interest is that BMAL1 had been shown to regulate inflammatory responses following activation of TLR4 by modulating the epigenetic activity of enhancer RNA transcription (Oishi et al., 2017). In particular, BMAL1 deletion caused an induced acetylation of lysine 27 of histone 3 which resulted in prolong and enhanced activation of NF-kB target genes such as *Nlrp3* inflammasome gene. Moreover, the researchers found that approximately 36% of *BMAL1* binding sites are also bound by NF-kB, which implies integration of circadian gene BMAL1 into the control of immune response machinery in macrophages (Oishi et al., 2017). Notably, in the recent study by Li et al., 2022 the researchers also demonstrated that BMAL1 regulate inflammation via the NF-kB/NLRP3 axis and proposed that *BMAL1* supress inflammation via direct targeting of *REV-ERBa* which in turn acted as a transcriptional repressor of NF-kB/NLRP3 signalling pathway (Li et al., 2022). On the other hand, our results imply that BMAL1 may play a role of pro-inflammatory regulator and its abundance increases the activity of NLRP3 inflammasome. The neuroinflammation study conducted in microglia cells showed that deficiency in BMAL1 caused reduction in pro-inflammatory cytokine release due to inhibition of NLRP3/NF-kB cascade (Wang et al., 2020). Moreover, the researchers proposed that microglia cells similar to macrophages and can

polarize into the (M2) anti-inflammatory state by inducing IL-10 expression and thereby antagonise pro-inflammatory response. However, these findings do not comply with our results as we detected different results in the same co-cultured cell line. Based on our findings we cannot draw a clear conclusion whether or not BMAL1 acts as pro- or anti- inflammatory regulator as it actions might be context dependent. There is a probability that activity of BMAL1 is dependent of cell type and tissue as its actions highly affected by the cellular microenvironments including cofactors and redox state (Sulli et al., 2019). Overall, multiple mechanisms by which *BMAL1* interacts with NF-kB show an involvement of *REV-ERBa* in the transcriptional regulatory machinery governed by NF-kB. Further investigation is needed to reveal the exact mechanism of regulation of immune response by *BMAL1*.

4.5 The treatment with prednisolone modified NLRP3 inflammasome activity

Glucocorticoids such as prednisone are one of the most common medications for treatment of gout arthritis. Prednisone gained its clinical success due to its effective ani-inflammatory effect which is attributed to its capacity to supress the expression of pro-inflammatory genes such as IL-1β, TNF-α, IL-6 via activation of glucocorticoid receptors and the inhibition of pro-inflammatory transcriptional factor NF-kB by the process known as transrepression (de Bosscher et al., 2014). Glucocorticoids have the ability to increase the expression of the inhibitor of kB (Ikβ). This cytoplasmic chaperone arrests translocation of NF-kB into the nucleus, therefore preventing activation of NLRP3 inflammasome and subsequent release of pro-inflammatory cytokine IL-1β which stimulates the inflammatory cascade (Schäcke et al., 2011). Endogenous glucocorticoids are known to be produced by the adrenal cortex which in turn is under control of the master clock in the SCN as well as peripheral clocks in adrenal gland itself. Moreover, there is evidence form the literature that glucocorticoids play a key role in regulation of peripheral clocks (Pezük et al., 2012) . In the study by Alex Y et al, the authors found that treatment of mesenchymal stem cells with dexamethasone stimulates oscillation of core circadian components (Bernal et al., 2014.). Interestingly, emerging evidence from the literature on rheumatoid arthritis suggest that implementation of chronotherapy into traditional glucocorticoid treatment may result in higher effectiveness of the treatment in patients with RA (Buttgereit et al., 2015; Cutolo, 2016). The data from the large-scale clinical trials documented that modified-release of prednisone in particular a night-time-release formulation achieved great efficacy in prevention of the acute, night upregulation of the inflammatory response (de Andrade et al., 1964). Interestingly, as it has been already mentioned previously, MSU-induced inflammation response in gout is also known to frequently occur during the night or an early morning. Surprisingly, there has been no studies done to investigate whether or not there is a time-dependent effect on MSU-induced inflammatory responses following the glucocorticoid treatment. Based on the evidence from the previous studies on RA, we hypothesised that time of the day

affects the ability of prednisolone (prednisone metabolite) to regulate MSU-induced inflammatory response, particularly NLRP3 inflammasome activity in THP-1 monocytes/macrophages-like cells.

In the present study, we obtained evidence that prednisolone (the active metabolite of prednisone) exhibits time-dependent as well as cell-specific effect on MSU-induced inflammation response in THP-1 monocytes/macrophage-like cells. The treatment with prednisolone significantly decreased the activity of NLRP3 inflammasome at 0-12h timepoint in MSU- treated monocytes compared to vehicle controls ***(Figure 3.21).*** Interestingly, at 12-24h timepoint the complete opposite effect was detected. Monocytes treated with PDN increased the activity of NLRP3 in the presence of MSU crystals compared to MSU-treated controls. Furthermore, we also determined the effect of PDN in monocytes in the absence of MSU crystals. At 0-12h timepoint PDN pre-treated monocytes showed reduction in NLRP3 activity in the absence of MSU crystals. However, at 12-24h timepoint PDN alone (without MSU crystals) increased NLRP3 inflammasome activity compared to vehicle control ***(Figure 3.21).*** In our macrophage-like cells prednisolone treatment showed similar effect on NLRP3 inflammasome activity as in monocytes ***(Figure 3.22).*** Although, we did not expect an increase in NLRP3 activity at 12-24h timepoint in monocytes and macrophage-like cells treated with PDN in the absence of MSU crystals the similar phenomenon had been discovered in previous study (Busillo et al., 2011). Surprisingly, glucocorticoids had been shown to not only induce the expression and activity of NLRP3 but also to sensitize THP-1 monocytes/macrophage-like cells to ATP-mediated release of pro-inflammatory cytokines such as IL-1β, TNF-a and IL-6. Its noteworthy, the authors of this paper also raised the possibility that the cellular microenvironment as well as stage of cell differentiation dictates the actions of cell glucocorticoid receptors from anti- or pro- inflammatory point (Busillo et al., 2011). Furthermore, the findings from another study also demonstrated that in another study by Johnson et al, demonstrated that glucocorticoids may enhance the release of IL-1β and IL-6 in vivo or in vitro models if administered without LPS stimulation (Johnson et al., 2002). Based on the previous studies we speculate that an increase in NLRP3 inflammasome activity occurred due to PDN ability to induce the expression of NLRP3 which consequently led to release of pro-inflammatory cytokines IL-1β, IL-6 and TNF-a. Overall, the effect of PDN in the present study seemingly supporting J. W Yang et al findings, who used LPS-challenged macrophages to investigate the effect of glucocorticoids on NLRP3-inflammasome in vitro.They found that glucocorticoid treatment of cells attenuated LPS-induced inflammation by suppressing NF-kB/NLRP3 signalling pathway and thereby reducing the release of mature IL-1β and IL-18 (Yang et al., 2020). Remarkably, the finding from another study proposed that glucocorticoids induce the expression of an innate immune-related genes such as TLR2 and TLR4 (Chinenov & Rogatsky, 2007). Interestingly, glucocorticoids suppressed the expression of pro-inflammatory genes of the adaptive immune response in the same cells (Galon et al., 2002). Although, the results from these studies appear paradoxical, those finding are fascinating as it has generally been believed that glucocorticoids inhibit activation of TLRs

as well as supress NF-kB inflammatory cascade. As had been mentioned previously REV-ERBα acts as a transcriptional suppressor of NF-kB/NLRP3 signalling pathway. In the study done in human primary hepatocytes demonstrated that treatment with dexamethasone led to 70% reduction in REV-ERBα expression (Pineda Torra et al., 2000). The researchers proposed that there is a negative glucocorticoid response element (nGRE) within REV-ERBα promoter that directly interacts with glucocorticoid receptor and mediated REV-ERBα repression. Therefore, based on the results of previous studies and the unusual results that we had obtained at 12-24h timepoint in monocytes we propose that the circadian oscillations in *REV-ERBα* expression could potentially correlate with the activation of NF-kB/NLRP3 signalling cascade. Thus, further studies have to be conducted to get a deeper understanding on relationships between glucocorticoids and *REV-ERBα* and also to determine the effect of PDN on monocytes and macrophage-like cells in the absence of inflammatory inducers.

4.6 Limitations

In vitro model that we utilized in this study provides a stable, reproducible, and genetically modifiable cell line which mimics disease of human cell system, however this model has a number of caveats to consider. Indeed, the greatest limitation of this study is that THP-1 based model does not recapitulate the whole spectrum of functional characteristics of a primary cell line such as peripheral blood mononuclear cells (PBMC). Although, THP-1 cell model is a validated model for monocytes and macrophages-like cells, these monocytic immortalised cell-line that was derived from a patient with an acute monocytic leukemia and therefore it is not a true representation of human macrophages found in synovial space or gouty tissue. In addition, although we have limited the valid passage of THP-1 cell line to below 20, there is a potential of phenotype drift that might occurred within in vitro culture. Consequently, the experimental repeats might not be as consistent with each other. Finally, the gout research is currently restricted due to the lack of adequate models of chronic gout and also by the difficulties acquiring samples of tophi from patients with gout. Although, in vivo air-pouch model of gout is currently used to investigate the mechanisms of acute gout, this model is not an exact representation of human gouty arthritis. There is a need for a development of an in vivo model to study of tophi formation, investigation of MSU-induced inflammatory response as well as contribution of circadian clock to gout attacks.

However, the malignant background of THP-1 cells might entail different responses compared to primary somatic cells in their natural environment. Hence, due to their distinct developmental origins and phenotypic attributes, the two cell models may not be overlapping across the full response spectrum, including cross-talk with other cell types.

4.7 Future work

Immediate suggestions:

It is important to quantify the levels of pro-inflammatory cytokines including IL-1β, IL-6, TNF-a and IL-18 following NLRP3 inflammasome activation by conducting an ELISA assay. This will provide an insight into the deeper understanding of regulation of inflammation-related gene expression by core circadian components validated in the current study such as *BMAL1, REV-ERBα* and *CRY1* in THP-1 monocytes and macrophages-like cells. In addition, to determine whether CRY1 protein levels are affected by the treatment with MSU crystals, a western blot analysis should be performed. Furthermore, the results from protein analysis of *CRY1* can be used to find whether there is a time-dependent effect of CRY1 protein level and NLRP3 inflammasome activity.

In this study we conducted a series of experiments to investigate the effect of core circadian genes such as *BMAL1* and *REV-ERBα* on the activation of NLRP3 inflammasome. Based on previous studies and our findings, we may speculate that activation of NLRP3 inflammasome is directly related to NF-kB signalling cascade. Therefore, it would be beneficial in the future study to investigate protein levels of activated NF-kB and compared it to levels of p65 in MSU-challenged THP-1 monocytes/macrophages-like cells.

Suggestions for future studies:

Although, the current study provided some meaningful insights into understanding of relation between circadian clock components and MSU-induced inflammation by using THP-1 cell line, these results still must be interpreted with caution as it's not a true representation of human derived myeloid cells. It is important for the future studies to validate the results of this study in primary cell line. Perhaps the next step would be to determine the effect of circadian core components in monocytes and macrophages derived from patient's tissue. However, this would be a hard task as it is difficult to perform a comparison between healthy human macrophages and macrophages from damaged tissue. The human macrophages are very sparse in the healthy tissue, thus its challenging to obtain both healthy and diseased tissue at the same time from a patient with gout. However, the future studies on effect of circadian clock on MSU-induced inflammation could be performed in ex vivo cadaver. Ex vivo cadaver samples from the patients with gout can be used to obtain and compare macrophages from healthy joint and diseased one. As it has been mentioned previously current in vivo model of gout flares does not exactly represent the origin of human tophi formation and cannot be used to investigate chronic gout. Animal species alike humans don't have uricase gene mutation which predispose them to MSU crystals accumulation and subsequent gout attacks. Interestingly, the resent study in larval zebrafish demonstrated a perspective model for studying MSU-induced macrophage immune responses (Hall et al., 2018). The researchers used live imaging to investigate macrophage response to MSU crystals. Accordingly, the same in vivo model could be utilized to study the

effect of circadian clock genes on mechanisms of gouty inflammation. The live imaging would be a great tool to get a deeper understanding into the time-of-day specific effect of circadian components on orchestration of innate immune responses.

4.8 Conclusion

To our knowledge, the current study is the first to uncover the potential effect of circadian components on NLRP3 activation in MSU-challenged THP-1 monocytes/macrophage-like cells model. The results from the present study suggest that alternations in expression of core circadian components including *REV-ERBα* and *CRY1* produce an effect on MSU-induced inflammatory response in THP-1 monocytes/macrophages-like cells. Moreover, the result from this study demonstrated that both REV-ERBα and BMAL1 regulate the activity of NLRP3 inflammasome, however the exact mechanism of their anti-inflammatory activity is yet to be determined. Although further work in this field is necessary, this study provided circumstantial evidence of circadian clock involvement in MSU-induced inflammation. It can serve as a cornerstone for future studies in understanding of relationship between circadian clock in innate immune cells and MSU-induced gouty inflammation.

Appendix A: List of Reagents used

Chemical/ Product	Catalogue Number	Suplier	Method
RPMI 1640 500ML (RPMI 1640 Medium)	11875093	Life Technologies	Cell culture
Penicillin-streptomycin (10,000U/mL)	15140122	Life Technologies	Cell culture
Fetal Bovine Serum (FBS)	MG-FBS0820-500ML-GEN	MediRay	Cell culture
PBS, pH 7.4 10x	10010049	ThermoFisher Scientific	Cell culture
DMSO	1029521000	Merck	Cell culture
phorbol 12-myristate 13-acetate (PMA)	ab120297	Abcam	Cell culture
Lipofectamine RNAimax	13778075	ThermoFisher Scientific	RNA knockdown
Lipofectamine 3000	L3000015	Life technologies	RNA knockdown
esiRNA targeting EGFP (esiRNA1)	EHUEGFP-20UG	Sigma Aldrich	RNA knockdown
esiRNA targeting EGFP (esiRNA1)	EHUEGFP	Sigma Aldrich	RNA knockdown
Ad-GFP-U6-h-ARNTL-shRNA	shADV-201453	Vector Biolabs	Virus
Ad-h-ARNTL	ADV-201453	Vector Biolabs	Virus
Ad-CMV-GFP	ADV-1060	Vector Biolabs	Virus
Cell lysis buffer II	AM8723	ThermoFisher Scientific	cDNA
DNAse I (2U/uL)	AM2222	ThermoFisher Scientific	cDNA
dNTP Mix	RO193	Life Technologies	cDNA
DNAse I buffer (10x)	81706	ThermoFisher Scientific	cDNA

Random primers 3ug/uL	48190011	ThermoFisher Scientific	cDNA
First Strand RT buffer (x5)	28025021	ThermoFisher Scientific	cDNA
DTT	43816	ThermoFisher Scientific	cDNA
MMLV Reverse Transcriptase	28025021	ThermoFisher Scientific	cDNA
DEPC-Treated Water 4x 100ml	750024	Life Technologies	cDNA
Trizol reagent	15596018	Life Technologies	Trizol-cDNA
RNaseOUT	10777019	Life Technologies	Trizol-cDNA
Direct-zol-96 RNA kit	R2054	Ngiao diagnostics	Trizol-cDNA
SuperScript III Reverse Transcriptase	18080085	Life Technologies	Trizol-cDNA
18s primers	W58453100	ThermoFisher Scientific	PCR
SYBR Select Master Mix	4472920	ThermoFisher Scientific	PCR
Random Primers	11034731001	Sigma-Aldrich	PCR

Hs_ARNTL_1 Quantitect primer assay	QT00011844	Bio-Strategy	PCR
Hs_PER1_1_SG Quantitect primer assay	QT00069265	Bio-Strategy	PCR
Hs_PER2_1_SG Quantitect primer assay	QT00011207	Bio-Strategy	PCR
Hs_PER3_1_SG Quantitect primer assay	QT00097713	Bio-Strategy	PCR

Hs_CRY1_SG Quantitect primer assay	QT00025067	Bio-Strategy	PCR
Hs_CRY2_SG Quantitect primer assay	QT00094920	Bio-Strategy	PCR
Hs_NR1D1_1_SG (REV-ERBα) Quantitect primer assay	QT00000413	Bio-Strategy	PCR
Hs_CLOCK_1_SG Quantitect primer assay	QT00054481	Bio-Strategy	PCR
TLR4	QT00047937	Bio-Strategy	PCR
CD14	QT00046382	Bio-Strategy	PCR
CD36	QT00039648	Bio-Strategy	PCR

Promega Capase-Glo-1 Inflammasome assay	PMG9952	In Vitro Technologies	Caspase-1
Prednisolone	ab-142351	Abcam	Caspase-1
Hemin 1g	51280	Sigma Aldrich	Caspase-1
SR-8278, REV-ERBα antagonist	ab146173-5mg	Abcam	Caspase-1
Tween 20	FSBBP337-100	ThermoFisher Scientific	Western
B actin antibody	sc69879	Santa Cruz Biotechnology	Western
GAPDH antibody	G9545-100UL	Sigma	Western
NF-KB P65 antibody 100 UG	MA1186	Life Tech	Western
Phospho NF-KB P65 antibody	MA515160	Life Tech	Western
TLR4 Polyclonal antibody	482300	Life Technologies NZ Ltd	Western
NMDAR2A Polyclonal antibody	RDSPPS012	In Vitro Technologies	Western
Goat anti-rabbit HRP secondary a/b	A16104	ThermoFisher Scientific	Western
Secondary goat anti Mouse (B actin) antibody	ab97046	Abcam	Western
RIPA buffer	89900	ThermoFisher Scientific	Protein preparation

Pierce 660 reagent	22660	ThermoFisher Scientific	Protein preparation
Laemmli Sample Buffer (4x)	1610747	Biorad	Protein preparation
10x Tris/Glycine (Running Buffer)	1610734	Biorad	Western
Methanol	1060092511	Merck	Western
10x Tris/Glycine/SDS (Transfer Buffer)	1610772	Biorad	Western
Precision Plus Dual Colour protein ladder	1610374	Biorad	Western
Skim Milk powder	LP0031B	ThermoFisher Scientific	Western
25x TBS (pH 7.4)	ab64248	Abcam	Western
Clarity(tm) Western ECL Substrate	1705060	Biorad	Western
Criterion™ TGX™ Precast Midi Protein Gels (4-15%, 26 well), 15ul	5671085	Biorad	Western
CyQuant NF Cell Proliferation assay kit	C35006	ThermoFisher Scientific	Cell Number assay
Precision Plus Dual Colour protein ladder	1610374	Biorad	Western
Skim Milk powder	LP0031B	ThermoFisher Scientific	Western
25x TBS (pH 7.4)	ab64248	Abcam	Western
Clarity(tm) Western ECL Substrate	1705060	Biorad	Western
Criterion™ TGX™ Precast Midi Protein Gels (4-15%, 25 well)	5671085	Biorad	Western
CyQuant GR Cell Proliferation assay kit	C7026	ThermoFisher Scientific	Cell Number assay

Appendix B: Buffer and Recipes

1x TBS-Tween Solution

960 mL of MQ water

1 mL of Tween

40 mL of TBS

1x SDS Running Buffer

100 mL 10x Tris/Glycine Native running buffer

900 mL MQ water

1x Transfer Buffer

100 mL 10x Tris/Glycine Transfer buffer

200 mL 100% Methanol

700 mL MQ water

RIPA Lysis Buffer

1 uL sodium fluoride

1 uL sodium orthovanadate

1 uL PMSF

Made up to 100 uL with RIPA Lysis Buffer

Reference list

Alten, R., Gram, H., Joosten, L. A., van den Berg, W. B., Sieper, J., Wassenberg, S., … Jung, T. (2008). The human anti-IL-1β monoclonal antibody ACZ885 is effective in joint inflammation models in mice and in a proof-of-concept study in patients with rheumatoid arthritis. *Arthritis Research and Therapy*, *10*(3), 1–9. doi:10.1186/ar2438

Arthritis Rheumatology - 2014 - Holzinger - Myeloid-Related Proteins 8 and 14 Contribute to Monosodium Urate Monohydrate.pdf. (2014).

Bauer, C., Duewell, P., Mayer, C., Lehr, H. A., Fitzgerald, K. A., Dauer, M., … Schnurr, M. (2010). Colitis induced in mice with dextran sulfate sodium (DSS) is mediated by the NLRP3 inflammasome. *Gut*, *59*(9), 1192–1199. doi:10.1136/gut.2009.197822

Bauernfeind, F. G., Horvath, G., Stutz, A., Alnemri, E. S., MacDonald, K., Speert, D., … Latz, E. (2009). Cutting Edge: NF-κB Activating Pattern Recognition and Cytokine Receptors License NLRP3 Inflammasome Activation by Regulating NLRP3 Expression. *The Journal of Immunology*, *183*(2), 787–791. doi:10.4049/jimmunol.0901363

Bozza, M. T., & Jeney, V. (2020). Pro-inflammatory Actions of Heme and Other Hemoglobin-Derived DAMPs. *Frontiers in Immunology*. Frontiers Media S.A. doi:10.3389/fimmu.2020.01323

Brook, R. A., Forsythe, A., Smeeding, J. E., & Lawrence Edwards, N. (2010). Chronic gout: Epidemiology, disease progression, treatment and disease burden. *Current Medical Research and Opinion*, *26*(12), 2813–2821. doi:10.1185/03007995.2010.533647

Busillo, J. M., Azzams, K. M., & Cidlowski, J. A. (2011). Glucocorticoids sensitize the innate immune system through regulation of the NLRP3 inflammasome. *Journal of Biological Chemistry*, *286*(44), 38703–38713. doi:10.1074/jbc.M111.275370

Buttgereit, F., Smolen, J. S., Coogan, A. N., & Cajochen, C. (2015). Clocking in: Chronobiology in rheumatoid arthritis. *Nature Reviews Rheumatology*. Nature Publishing Group. doi:10.1038/nrrheum.2015.31

Çakirbay, H., Bilici, M., Kavakçi, Ö., Çebi, A., Güler, M., & Tan, Ü. (2004). Sleep quality and immune functions in rheumatoid arthritis patients with and without major depression. *International Journal of Neuroscience*, *114*(2), 245–256. doi:10.1080/00207450490269471

Cao, Z., Guo, Y., Tang, S., Tan, S., Niu, C., Miao, C., & Zhang, W. (2018). Transfection of adenovirus-mediated mircoRNA-126 gene into infant hemangioma endothelial cells in vitro, *11*(3), 1811–1817.

Castanon-Cervantes, O., Wu, M., Ehlen, J. C., Paul, K., Gamble, K. L., Johnson, R. L., … Davidson, A. J. (2010). Dysregulation of Inflammatory Responses by Chronic Circadian Disruption. *The Journal of Immunology*, *185*(10), 5796–5805. doi:10.4049/jimmunol.1001026

Cermakian, N., & Sassone-Corsi, P. (2000). Multilevel regulation of the circadian clock. *Nature Reviews Molecular Cell Biology*, *1*(1), 59–67. doi:10.1038/35036078

Chalfant, J. M., Howatt, D. A., Tannock, L. R., Daugherty, A., & Pendergast, J. S. (2020). Circadian disruption with constant light exposure exacerbates atherosclerosis in male ApolipoproteinE-deficient mice. *Scientific Reports*, *10*(1), 1–11. doi:10.1038/s41598-020-66834-9

Chinenov, Y., & Rogatsky, I. (2007). Glucocorticoids and the innate immune system: Crosstalk with the Toll-like receptor signaling network. *Molecular and Cellular Endocrinology*, *275*(1–2), 30–42. doi:10.1016/j.mce.2007.04.014

Chung, Y. H., Kim, D. H., & Lee, W. W. (2016). Monosodium urate crystal-induced pro-interleukin-1β production is post-transcriptionally regulated via the p38 signaling pathway in human monocytes. *Scientific Reports*, *6*(October), 1–15. doi:10.1038/srep34533

Ciesielska, A., Matyjek, M., & Kwiatkowska, K. (2021). TLR4 and CD14 trafficking and its influence on LPS-induced pro-inflammatory signaling. *Cellular and Molecular Life Sciences*, *78*(4), 1233–1261. doi:10.1007/s00018-020-03656-y

Crawley, W. T., Jungels, C. G., Stenmark, K. R., & Fini, M. A. (2022). U-shaped association of uric acid to overall-cause mortality and its impact on clinical management of hyperuricemia. *Redox Biology*, *51*(February), 102271. doi:10.1016/j.redox.2022.102271

Cronstein, B. N., & Sunkureddi, P. (2013). Mechanistic aspects of inflammation and clinical management of inflammation in acute gouty arthritis. *Journal of Clinical Rheumatology*. doi:10.1097/RHU.0b013e31827d8790

Cruz, C. M., Rinna, A., Forman, H. J., Ventura, A. L. M., Persechini, P. M., & Ojcius, D. M. (2007). ATP activates a reactive oxygen species-dependent oxidative stress response and secretion of proinflammatory cytokines in macrophages. *Journal of Biological Chemistry*, *282*(5), 2871–2879. doi:10.1074/jbc.M608083200

Cui, L. N., Coderre, E., & Renaud, L. P. (2001). Glutamate and GABA mediate suprachiasmatic nucleus inputs to spinal-projecting paraventricular neurons. *American Journal of Physiology - Regulatory Integrative and Comparative Physiology*, *281*(4 50-4), 1283–1289. doi:10.1152/ajpregu.2001.281.4.r1283

Cutolo, M. (2016). Glucocorticoids and chronotherapy in rheumatoid arthritis. *RMD Open*. BMJ Publishing Group. doi:10.1136/rmdopen-2015-000203

Dalbeth, N., & Haskard, D. O. (2005). Mechanisms of inflammation in gout. *Rheumatology*. doi:10.1093/rheumatology/keh640

Dalbeth, Nicola, Dowell, T., Gerard, C., Gow, P., Jackson, G., Shuker, C., & te Karu, L. (2018). Gout in aotearoa New Zealand: The equity crisis continues in plain sight. *New Zealand Medical Journal*, *131*(1485), 8–12.

Davidsson, L., Rudin, A. D., Klose, F. P. S., Buck, A., Björkman, L., Christenson, K., & Bylund, J. (2020). In vivo transmigrated human neutrophils are highly primed for intracellular radical production induced by monosodium urate crystals. *International Journal of Molecular Sciences*, *21*(11). doi:10.3390/ijms21113750

de Andrade, J. R., Mccormick, J. N., & Hill, A. G. S. (1964). *SMALL DOSES OF PREDNISOLONE IN THE MANAGEMENT OF RHEUMATOID ARTHRITIS*. *Ann. Rheum. Dis.*

de Bosscher, K., Beck, I. M., Dejager, L., Bougarne, N., Gaigneaux, A., Chateauvieux, S., … Haegeman, G. (2014). Selective modulation of the glucocorticoid receptor can distinguish between transrepression of NF-κB and AP-1. *Cellular and Molecular Life Sciences*, *71*(1), 143–163. doi:10.1007/s00018-013-1367-4

Dehlin, M., Jacobsson, L., & Roddy, E. (2020). Global epidemiology of gout: prevalence, incidence, treatment patterns and risk factors. *Nature Reviews Rheumatology*, *16*(7), 380–390. doi:10.1038/s41584-020-0441-1

Delerive, P., Monté, D., Dubois, G., Trottein, F., Fruchart-Najib, J., Mariani, J., … Staels, B. (2001). The orphan nuclear receptor RORα is a negative regulator of the inflammatory response. *EMBO Reports*, *2*(1), 42–48. doi:10.1093/embo-reports/kve007

Dimitrov, S., Benedict, C., Heutling, D., Westermann, J., Born, J., & Lange, T. (2009). Cortisol and epinephrine control opposing circadian rhythms in T cell subsets. *Blood*, *113*(21), 5134–5143. doi:10.1182/blood-2008-11-190769

Dinarello, C. A. (2010). How interleukin-1β induces gouty arthritis. *Arthritis and Rheumatism*. doi:10.1002/art.27663

Diseases, M., & Section, A. (1960). IDENTIFICATION OF U R A T E CRYSTALS IN GOUTY SYNOVIAL FLUID * In addition to inspection of the fluid by ordinary light microscopy , in- spection by polarized light microscopy was employed . A uricase digestion test was also devised and performed on all c, 452–460.

Duewell, P., Kono, H., Rayner, K. J., Sirois, C. M., Bauernfeind, F. G., Abela, G. S., … Latz, E. (2010). Activated By Cholesterol Crystals That Form Early in Disease. *Nature*, *464*(7293), 1357–1361. doi:10.1038/nature08938.NLRP3

Erdei, J., Tóth, A., Balogh, E., Nyakundi, B. B., Bányai, E., Ryffel, B., … Jeney, V. (2018). Induction of NLRP3 inflammasome activation by heme in human endothelial cells. *Oxidative Medicine and Cellular Longevity*, *2018*. doi:10.1155/2018/4310816

Evavold, C. L., & Kagan, J. C. (2019). Inflammasomes: Threat-Assessment Organelles of the Innate Immune System. *Immunity*, *51*(4), 609–624. doi:10.1016/j.immuni.2019.08.005

Figueiredo, R. T., Fernandez, P. L., Mourao-Sa, D. S., Porto, B. N., Dutra, F. F., Alves, L. S., … Bozza, M. T. (2007). Characterization of heme as activator of toll-like receptor 4. *Journal of Biological Chemistry*, *282*(28), 20221–20229. doi:10.1074/jbc.M610737200

Figueiredo, R. T., Fernandez, P. L., Mourao-Sa, D. S., Porto, B. N., Dutra, F. F., Alves, L. S., … Bozza, M. T. (2007). Characterization of heme as activator of toll-like receptor 4. *Journal of Biological Chemistry*, *282*(28), 20221–20229. doi:10.1074/jbc.M610737200

Fontaine, C., Rigamonti, E., Pourcet, B., Duez, H., Duhem, C., Fruchart, J. C., … Staels, B. (2008). The nuclear receptor Rev-erbα is a Liver X Receptor (LXR) target gene driving a negative feedback loop on select LXR-induced pathways in human macrophages. *Molecular Endocrinology*, *22*(8), 1797–1811. doi:10.1210/me.2007-0439

Galon, J., Franchimont, D., Hiroi, N., Frey, G., Boettner, A., Ehrhart-Bornstein, M., … Bornstein, S. R. (2002). Gene profiling reveals unknown enhancing and suppressive actions of glucocorticoids on immune cells. *The FASEB Journal*, *16*(1), 61–71. doi:10.1096/fj.01-0245com

Gibbs, J. E., Blaikley, J., Beesley, S., Matthews, L., Simpson, K. D., Boyce, S. H., … Loudon, A. S. I. (2012). The nuclear receptor REV-ERBα mediates circadian regulation of innate immunity through selective regulation of inflammatory cytokines. *Proceedings of the National Academy of Sciences of the United States of America*, *109*(2), 582–587. doi:10.1073/pnas.1106750109

Gong, T., Liu, L., Jiang, W., & Zhou, R. (2020). DAMP-sensing receptors in sterile inflammation and inflammatory diseases. *Nature Reviews Immunology*, *20*(2), 95–112. doi:10.1038/s41577-019-0215-7

Grebe, A., Hoss, F., & Latz, E. (2018). NLRP3 inflammasome and the IL-1 pathway in atherosclerosis. *Circulation Research*, *122*(12), 1722–1740. doi:10.1161/CIRCRESAHA.118.311362

Haimovich, B., Calvano, J., Haimovich, A. D., Calvano, S. E., Coyle, S. M., & Lowry, S. F. (2010). In vivo endotoxin synchronizes and suppresses clock gene expression in human peripheral blood leukocytes. *Critical Care Medicine*, *38*(3), 751–758. doi:10.1097/CCM.0b013e3181cd131c

Hall, C. J., Sanderson, L. E., Lawrence, L. M., Pool, B., van der Kroef, M., Ashimbayeva, E., … Crosier, P. S. (2018). Blocking fatty acid-fueled mROS production within macrophages alleviates acute gouty inflammation. *Journal of Clinical Investigation*, *128*(5), 1752–1771. doi:10.1172/JCI94584

Haziot, A., Ferrero, E., Kö, F., Hijiya, N., Yamamoto, S., Silver, J., & Stewart, C. L. (1996). *Resistance to Endotoxin Shock and Reduced Dissemination of Gram-Negative Bacteria in CD14-Deficient Mice*. *Immunity* (Vol. 4).

Hirota, T., Lee, J. W., John, P. C. S., Sawa, M., Iwaisako, K., Noguchi, T., … Kay, S. A. (2013). NIH Public Access, *337*(6098), 1094–1097. doi:10.1126/science.1223710.Identification

Hirota, T., Okano, T., Kokame, K., Shirotani-Ikejima, H., Miyata, T., & Fukada, Y. (2002). Glucose down-regulates Per1 and Per2 mRNA levels and induces circadian gene expression in cultured rat-1 fibroblasts. *Journal of Biological Chemistry*, *277*(46), 44244–44251. doi:10.1074/jbc.M206233200

Hornung, V., Bauernfeind, F., Halle, A., Samstad, E. O., Kono, H., Rock, K. L., … Latz, E. (2008). Silica crystals and aluminum salts activate the NALP3 inflammasome through phagosomal destabilization. *Nature Immunology*, *9*(8), 847–856. doi:10.1038/ni.1631

Huo, M., Huang, Y., Qu, D., Zhang, H., Wong, W. T., Chawla, A., … Tian, X. Y. (2017). Myeloid Bmal1 deletion increases monocyte recruitment and worsens atherosclerosis. *FASEB Journal*, *31*(3), 1097–1106. doi:10.1096/fj.201601030R

Immenschuh, S., Tan, M., & Ramadori, G. (1999). Nitric oxide mediates the lipopolysaccharide dependent upregulation of the heine oxygenase-1 gene expression in cultured rat Kupffer cells. *Journal of Hepatology*, *30*, 61–69.

Janciauskiene, S., Vijayan, V., & Immenschuh, S. (2020). TLR4 Signaling by Heme and the Role of Heme-Binding Blood Proteins. *Frontiers in Immunology*. Frontiers Media S.A. doi:10.3389/fimmu.2020.01964

Jhang, J. J., Cheng, Y. T., Ho, C. Y., & Yen, G. C. (2015). Monosodium urate crystals trigger Nrf2- and heme oxygenase-1-dependent inflammation in THP-1 cells. *Cellular and Molecular Immunology*, *12*(4), 424–434. doi:10.1038/cmi.2014.65

Johnson, J. D., O'Connor, K. A., Deak, T., Stark, M., Watkins, L. R., & Maier, S. F. (2002). Prior stressor exposure sensitizes LPS-induced cytokine production. *Brain, Behavior, and Immunity*, *16*(4), 461–476. doi:10.1006/brbi.2001.0638

Kanbara, A., & Seyama, I. (2011). Effect of urine pH on uric acid excretion by manipulating food materials. *Nucleosides, Nucleotides and Nucleic Acids*, *30*(12), 1066–1071. doi:10.1080/15257770.2011.596498

Kc, R., Li, X., Forsyth, C. B., Voigt, R. M., Summa, K. C., Vitaterna, M. H., … Im, H. J. (2015). Osteoarthritis-like pathologic changes in the knee joint induced by environmental disruption of circadian rhythms is potentiated by a high-fat diet. *Scientific Reports*, *5*(October), 1–7. doi:10.1038/srep16896

Keene, J. D. (2010). Minireview: Global regulation and dynamics of ribonucleic acid. *Endocrinology*. doi:10.1210/en.2009-1250

Keller, M., Mazuch, J., Abraham, U., Eom, G. D., Herzog, E. D., Volk, H.-D., … Maier, B. (2015). *A circadian clock in macrophages controls inflammatory immune responses*.

Kelley, N., Jeltema, D., Duan, Y., & He, Y. (2019). The NLRP3 Inflammasome: An Overview of Mechanisms of Activation and Regulation. *International Journal of Molecular Sciences*, *20*(13), 1–24.

Kiessling, S., Beaulieu-Laroche, L., Blum, I. D., Landgraf, D., Welsh, D. K., Storch, K. F., … Cermakian, N. (2017). Enhancing circadian clock function in cancer cells inhibits tumor growth. *BMC Biology*, *15*(1). doi:10.1186/s12915-017-0349-7

Kingsbury, S. R., Conaghan, P. G., & McDermott, M. F. (2011). The role of the NLRP3 inflammasome in gout. *Journal of Inflammation Research*. doi:10.2147/JIR.S11330

Kojetin, D., Wang, Y., Kamenecka, T. M., & Burris, T. P. (2011). Identification of SR8278, a synthetic antagonist of the nuclear heme receptor REV-ERB. *ACS Chemical Biology*, *6*(2), 131–134. doi:10.1021/cb1002575

Kojetin, D., Wang, Y., Kamenecka, T. M., & Burris, T. P. (2011). Identification of SR8278, a synthetic antagonist of the nuclear heme receptor REV-ERB. *ACS Chemical Biology*, *6*(2), 131–134. doi:10.1021/cb1002575

Kolz, M., Johnson, T., Sanna, S., Teumer, A., Vitart, V., Perola, M., … Gieger, C. (2009). Meta-analysis of 28,141 individuals identifies common variants within five new loci that influence uric acid concentrations. *PLoS Genetics*, *5*(6). doi:10.1371/journal.pgen.1000504

Kondratova, A. A., & Kondratov, R. v. (2012). The circadian clock and pathology of the ageing brain. *Nature Reviews Neuroscience*. doi:10.1038/nrn3208

Kopmels, B., Mariani, J., Delhaye-Bouchaud, N., Audibert, F., Fradelizi, D., & Wollman, E. E. (1992). Evidence for a Hyperexcitability State of Staggerer Mutant Mice Macrophages. *Journal of Neurochemistry*, *58*(1), 192–199. doi:10.1111/j.1471-4159.1992.tb09295.x

Kowalska, E., & Brown, S. A. (2007). Peripheral clocks: Keeping up with the master clock. *Cold Spring Harbor Symposia on Quantitative Biology*, *72*, 301–305. doi:10.1101/sqb.2007.72.014

Kuhlman, S. J., Craig, L. M., & Duffy, J. F. (2018). Introduction to chronobiology. *Cold Spring Harbor Perspectives in Biology*, *10*(9), 1–10. doi:10.1101/cshperspect.a033613

Kuo, C. F., Grainge, M. J., Zhang, W., & Doherty, M. (2015). Global epidemiology of gout: Prevalence, incidence and risk factors. *Nature Reviews Rheumatology*, *11*(11), 649–662. doi:10.1038/nrrheum.2015.91

Landis, R. C., Yagnik, D. R., Florey, O., Philippidis, P., Emons, V., Mason, J. C., & Haskard, D. O. (2002). Safe disposal of inflammatory monosodium urate monohydrate crystals by differentiated macrophages. *Arthritis and Rheumatism*, *46*(11), 3026–3033. doi:10.1002/art.10614

Lee, J. S., Hmama, Z., Mui, A., & Reiner, N. E. (2004). Stable gene silencing in human monocytic cell lines using lentiviral-delivered small interference RNA: Silencing of the p110α isoform of phosphoinositide 3-kinase reveals differential regulation of adherence induced by 1α,25-dihydroxycholecalciferol and b. *Journal of Biological Chemistry*, *279*(10), 9379–9388. doi:10.1074/jbc.M310638200

Li, F., Lin, L., He, Y., Sun, G., Dong, D., & Wu, B. (2022). BMAL1 regulates Propionibacterium acnes -induced skin inflammation via REV-ERBα in mice . *International Journal of Biological Sciences*, *18*(6), 2597–2608. doi:10.7150/ijbs.71719

Li, Y., & Androulakis, I. P. (2021). Light entrainment of the SCN circadian clock and implications for personalized alterations of corticosterone rhythms in shift work and jet lag. *Scientific Reports*, *11*(1), 1–19. doi:10.1038/s41598-021-97019-7

Lin, H. Y., Juan, S. H., Shen, S. C., Hsu, F. L., & Chen, Y. C. (2003). Inhibition of lipopolysaccharide-induced nitric oxide production by flavonoids in RAW264.7 macrophages involves heme oxygenase-1. *Biochemical Pharmacology*, *66*(9), 1821–1832. doi:10.1016/S0006-2952(03)00422-2

Liu, R., O'Connell, M., Johnson, K., Pritzker, K., Mackman, N., & Terkeltaub, R. (2000). Extracellular signal-regulated kinase 1/extracellular signal-regulated kinase 2 mitogen-activated protein kinase signaling and activation of activator protein 1 and nuclear factor κB transcription factors play central roles in interleukin-8 expression sti. *Arthritis and Rheumatism*, *43*(5), 1145–1155. doi:10.1002/1529-0131(200005)43:5<1145::AID-ANR25>3.0.CO;2-T

Liu, X., Yu, R., Zhu, L., Hou, X., & Zou, K. (2017). Bidirectional Regulation of Circadian Disturbance and Inflammation in Inflammatory Bowel Disease. *Inflammatory Bowel Diseases*, *23*(10), 1741–1751. doi:10.1097/MIB.0000000000001265

Mandal, A. K., & Mount, D. B. (2015). The molecular physiology of uric acid homeostasis. *Annual Review of Physiology*, *77*(January 2015), 323–345. doi:10.1146/annurev-physiol-021113-170343

Mao, L., Kitani, A., Strober, W., & Fuss, I. J. (2018). The role of NLRP3 and IL-1β in the pathogenesis of inflammatory bowel disease. *Frontiers in Immunology*. Frontiers Media S.A. doi:10.3389/fimmu.2018.02566

Mariotte, A., de Cauwer, A., Po, C., Abou-Faycal, C., Pichot, A., Paul, N., … Georgel, P. (2020). A mouse model of MSU-induced acute inflammation in vivo suggests imiquimod-dependent targeting of Il-1β as relevant therapy for gout patients. *Theranostics*, *10*(5), 2158–2171. doi:10.7150/thno.40650

Martinon, F., Pétrilli, V., Mayor, A., Tardivel, A., & Tschopp, J. (2006). Gout-associated uric acid crystals activate the NALP3 inflammasome. *Nature*, *440*(7081), 237–241. doi:10.1038/nature04516

McAlpine, C. S., & Swirski, F. K. (2016). Circadian influence on metabolism and inflammation in atherosclerosis. *Circulation Research*, *119*(1), 131–141. doi:10.1161/CIRCRESAHA.116.308034

McManus, J., Cheng, Z., & Vogel, C. (2015). Next-generation analysis of gene expression regulation-comparing the roles of synthesis and degradation. *Molecular BioSystems*. Royal Society of Chemistry. doi:10.1039/c5mb00310e

Mendonça-Natividade, F. C., Lopes, C. D., Ricci-Azevedo, R., Sardinha-Silva, A., Pinzan, C. F., Alegre-Maller, A. C. P., … Roque-Barreira, M. C. (2019). Receptor heterodimerization and co-receptor engagement in TLR2 activation induced by MIC1 and MIC4 from Toxoplasma gondii. *International Journal of Molecular Sciences*, *20*(20). doi:10.3390/ijms20205001

Mieda, M. (2020). The central circadian clock of the suprachiasmatic nucleus as an ensemble of multiple oscillatory neurons. *Neuroscience Research*, *156*, 24–31. doi:10.1016/j.neures.2019.08.003

Muller, W. A. (2012). Regulate Globally, Act Locally: Adrenergic Nerves Promote Leukocyte Recruitment. *Immunity*, *37*(2), 189–191. doi:10.1016/j.immuni.2012.08.004

Musiek, E. S., Lim, M. M., Yang, G., Bauer, A. Q., Qi, L., Lee, Y., … FitzGerald, G. A. (2013). Circadian clock proteins regulate neuronal redox homeostasis and neurodegeneration. *Journal of Clinical Investigation*, *123*(12), 5389–5400. doi:10.1172/JCI70317

Narasimamurthy, R., Hatori, M., Nayak, S. K., Liu, F., Panda, S., & Verma, I. M. (2012). Circadian clock protein cryptochrome regulates the expression of proinflammatory cytokines. *Proceedings of the National Academy of Sciences of the United States of America*, *109*(31), 12662–12667. doi:10.1073/pnas.1209965109

Nguyen, K. D., Fentress, S. J., Qiu, Y., Yun, K., Cox, J. S., & Chawla, A. (2013). Circadian gene Bmal1 regulates diurnal oscillations of Ly6Chi inflammatory monocytes. *Science*, *341*(6153), 1483–1488. doi:10.1126/science.1240636

Nicholls, A., Snaith, M. L., & Scott, J. T. (1973). Effect of Oestrogen Therapy on Plasma and Urinary Levels of Uric Acid. *British Medical Journal*, *1*(5851), 449. doi:10.1136/bmj.1.5851.449

Nowarski, R., Jackson, R., Gagliani, N., de Zoete, M. R., Palm, N. W., Bailis, W., … Flavell, R. A. (2015). Epithelial IL-18 Equilibrium Controls Barrier Function in Colitis. *Cell*, *163*(6), 1444–1456. doi:10.1016/j.cell.2015.10.072

Nuki, G., & Simkin, P. A. (2006). A concise history of gout and hyperuricemia and their treatment. *Arthritis Research and Therapy*, *8*(SUPPL. 1), 1–5. doi:10.1186/ar1906

Oishi, Y., Hayashi, S., Isagawa, T., Oshima, M., Iwama, A., Shimba, S., … Manabe, I. (2017). Bmal1 regulates inflammatory responses in macrophages by modulating enhancer RNA transcription. *Scientific Reports*, *7*(1). doi:10.1038/s41598-017-07100-3

Okubo, N., Minami, Y., Fujiwara, H., Umemura, Y., Tsuchiya, Y., Shirai, T., … Yagita, K. (2013). Prolonged bioluminescence monitoring in mouse ex vivo bone culture revealed persistent circadian rhythms in articular cartilages and growth plates. *PLoS ONE*, *8*(11). doi:10.1371/journal.pone.0078306

Pae, H.-O., & Chung, H.-T. (2010). *REVIEW ARTICLE Heme Oxygenase-1: Its Therapeutic Roles in Inflammatory Diseases*.

Pagel, R., Bär, F., Schröder, T., Sünderhauf, A., Künstner, A., Ibrahim, S. M., … Sina, C. (2017). Circadian rhythm disruption impairs tissue homeostasis and exacerbates chronic inflammation in the intestine. *FASEB Journal*, *31*(11), 4707–4719. doi:10.1096/fj.201700141RR

Pan, X., Bradfield, C. A., & Hussain, M. M. (2016). Global and hepatocyte-specific ablation of Bmal1 induces hyperlipidaemia and enhances atherosclerosis. *Nature Communications*, *7*, 1–15. doi:10.1038/ncomms13011

Patke, A., Young, M. W., & Axelrod, S. (2020). Molecular mechanisms and physiological importance of circadian rhythms. *Nature Reviews Molecular Cell Biology*, *21*(2), 67–84. doi:10.1038/s41580-019-0179-2

Peng Zhao, Su, X., Ge, T., & Fan, J. (2016). Effect of Soy Sauce on Serum Uric Acid Levels in Hyperuricemic Rats and Identification of Flazin as a Potent Xanthine Oxidase Inhibitor HHS Public Access. *Physiology & Behavior*, *176*(1), 139–148. doi:10.1002/art.39115.Food

Pezük, P., Mohawk, J. A., Wang, L. A., & Menaker, M. (2012). Glucocorticoids as entraining signals for peripheral circadian oscillators. *Endocrinology*, *153*(10), 4775–4783. doi:10.1210/en.2012-1486

Pharmacotherapy - 2013 - Tran - Role of Interleukin-1 Inhibitors in the Management of Gout.pdf. (2013).

Piccini, A., Carta, S., Tassi, S., Lasiglié, D., Fossati, G., & Rubartelli, A. (2008). ATP is released by monocytes stimulated with pathogen-sensing receptor ligands and induces IL-1β and IL-18 secretion in an autocrine way. *Proceedings of the National Academy of Sciences of the United States of America*, *105*(23), 8067–8072. doi:10.1073/pnas.0709684105

Pick, R., He, W., Chen, C. S., & Scheiermann, C. (2019). Time-of-Day-Dependent Trafficking and Function of Leukocyte Subsets. *Trends in Immunology*. Elsevier Ltd. doi:10.1016/j.it.2019.03.010

Pourcet, B., & Duez, H. (2020). Circadian Control of Inflammasome Pathways: Implications for Circadian Medicine. *Frontiers in Immunology*. Frontiers Media S.A. doi:10.3389/fimmu.2020.01630

Pourcet, B., Zecchin, M., Ferri, L., Beauchamp, J., Sitaula, S., Billon, C., … Duez, H. M. (2018). Circadian Activity of NLRP3 In fl ammasome to Reduce the, 1449–1464. doi:10.1053/j.gastro.2017.12.019

Preitner, F., Bonny, O., Laverrière, A., Rotman, S., Firsov, D., da Costa, A., … Thorens, B. (2009). Glut9 is a major regulator of urate homeostasis and its genetic inactivation induces hyperuricosuria and urate nephropathy. *Proceedings of the National Academy of Sciences of the United States of America*, *106*(36), 15501–15506. doi:10.1073/pnas.0904411106

Preitner, N., Damiola, F., Luis-Lopez-Molina, Zakany, J., Duboule, D., Albrecht, U., & Schibler, U. (2002). The orphan nuclear receptor REV-ERBα controls circadian transcription within the positive limb of the mammalian circadian oscillator. *Cell*, *110*(2), 251–260. doi:10.1016/S0092-8674(02)00825-5

Puttonen, S., Oksanen, T., Vahtera, J., Pentti, J., Virtanen, M., Salo, P., & Kivimäki, M. (2010). Is shift work a risk factor for rheumatoid arthritis? The Finnish Public Sector study. *Annals of the Rheumatic Diseases*, *69*(4), 679–680. doi:10.1136/ard.2008.099184

Qing, Y. F., Zhang, Q. B., Zhou, J. G., & Jiang, L. (2014). Changes in toll-like receptor (TLR)4-NFκB-IL1β signaling in male gout patients might be involved in the pathogenesis of primary gouty arthritis. *Rheumatology International*, *34*(2), 213–220. doi:10.1007/s00296-013-2856-3

Ragab, G., Elshahaly, M., & Bardin, T. (2017). Gout: An old disease in new perspective – A review. *Journal of Advanced Research*. Elsevier B.V. doi:10.1016/j.jare.2017.04.008

Raghuram, S., Stayrook, K. R., Huang, P., Rogers, P. M., Nosie, A. K., McClure, D. B., … Rastinejad, F. (2007). Identification of heme as the ligand for the orphan nuclear receptors REV-ERBα and REV-ERBβ. *Nature Structural and Molecular Biology*, *14*(12), 1207–1213. doi:10.1038/nsmb1344

Ramsahai, J. M., King, E., Niven, R., Tavernier, G., Wark, P. A. B., & Simpson, J. L. (2020). Serum prednisolone levels as a marker of oral corticosteroid adherence in severe asthma. *BMC Pulmonary Medicine*, *20*(1), 1–8. doi:10.1186/s12890-020-01263-y

Raspé, E., Duez, H., Mansén, A., Fontaine, C., Fiévet, C., Fruchart, J. C., … Staels, B. (2002). Identification of Rev-erbα as a physiological repressor of apoC-III gene transcription. *Journal of Lipid Research*, *43*(12), 2172–2179. doi:10.1194/jlr.M200386-JLR200

Revu, S., Wu, J., Henkel, M., Rittenhouse, N., Menk, A., Delgoffe, G. M., … McGeachy, M. J. (2018). IL-23 and IL-1β Drive Human Th17 Cell Differentiation and Metabolic Reprogramming in Absence of CD28 Costimulation. *Cell Reports*, *22*(10), 2642–2653. doi:10.1016/j.celrep.2018.02.044

Richards, J., & Gumz, M. L. (2012). Advances in understanding the peripheral circadian clocks. *The FASEB Journal*, *26*(9), 3602–3613. doi:10.1096/fj.12-203554

Ridker, P. M., MacFadyen, J. G., Thuren, T., & Libby, P. (2020). Residual inflammatory risk associated with interleukin-18 and interleukin-6 after successful interleukin-1b inhibition with canakinumab: Further rationale for the development of targeted anti-cytokine therapies for the treatment of atherothrombosis. *European Heart Journal*, *41*(23), 2153–2163. doi:10.1093/eurheartj/ehz542

Robinson, I., & Reddy, A. B. (2014). Molecular mechanisms of the circadian clockwork in mammals. *FEBS Letters*. Elsevier. doi:10.1016/j.febslet.2014.06.005

Ruan, W., Yuan, X., & Eltzschig, H. K. (2021). Circadian rhythm as a therapeutic target. *Nature Reviews Drug Discovery*, *20*(4), 287–307. doi:10.1038/s41573-020-00109-w

Schäcke, H., Döcke, W.-D., & Asadullah, K. (2016). *Mechanisms involved in the side effects of glucocorticoids*.

Schlesinger, N. (2013). Clinical features of gout. *Gout*, *63*(4), 70–77. doi:10.2217/EBO.13.10

Schwartz, S. A. (2006). Disease of Distinction. *Explore: The Journal of Science and Healing*, *2*(6), 515–519. doi:10.1016/j.explore.2006.08.007

Shearman, L. P., Sriram, S., Weaver, D. R., Maywood, E. S., Chaves, I., Zheng, B., … Reppert, S. M. (2000). Interacting molecular loops in the mammalian circadian clock. *Science*, *288*(5468), 1013–1019. doi:10.1126/science.288.5468.1013

Shin, J. S., Hong, S. W., Lee, S. L. O., Kim, T. H., Park, I. C., An, S. K., … Lee, M. S. (2008). Serum starvation induces G1 arrest through suppression of Skp2-CDK2 and CDK4 in SK-OV-3 cells. *International Journal of Oncology*, *32*(2), 435–439. doi:10.3892/ijo.32.2.435

Singh, J. A. (2013). Racial and gender disparities among patients with gout. *Current Rheumatology Reports*, *15*(2), 1–15. doi:10.1007/s11926-012-0307-x

Solt, L. A., Wang, Y., Banerjee, S., Hughes, T., Kojetin, D. J., Lundasen, T., … Burris, T. P. (2012). Regulation of circadian behaviour and metabolism by synthetic REV-ERB agonists. *Nature*, *485*(7396), 62–68. doi:10.1038/nature11030

Song M, Emilsson L, Bozorg SR, Nguyen LH, Joshi AD, Staller K, et al. (2020). Total plasma heme concentration increases after red blood cell transfusion and predicts mortality in critically ill medical patients. HHS Public Access. *Lancet Gastroenterol Hepatol*, *5*(6), 537–547. doi:10.1111/trf.15218.Total

Stawski, R. S., Almeida, D. M., Lachman, M. E., & Rosnick, C. B. (2015). In vivo suppression of NK cell cytotoxicity by stress and surgery: glucocorticoids have a minor role compared to catecholamines and prostaglandins. NIH Public Access. *NIH Public Access*, *61*(6), 515–525. doi:10.1016/j.bbi.2013.12.007.In

Steffens, S., Winter, C., Schloss, M. J., Hidalgo, A., Weber, C., & Soehnlein, O. (2017). Circadian Control of Inflammatory Processes in Atherosclerosis and Its Complications. *Arteriosclerosis, Thrombosis, and Vascular Biology*, *37*(6), 1022–1028. doi:10.1161/ATVBAHA.117.309374

Sulli, G., Lam, M. T. Y., & Panda, S. (2019). Interplay between Circadian Clock and Cancer: New Frontiers for Cancer Treatment. *Trends in Cancer*. Cell Press. doi:10.1016/j.trecan.2019.07.002

Summa, K. C., Voigt, R. M., Forsyth, C. B., Shaikh, M., Cavanaugh, K., Tang, Y., … Keshavarzian, A. (2013). Disruption of the Circadian Clock in Mice Increases Intestinal Permeability and Promotes Alcohol-Induced Hepatic Pathology and Inflammation. *PLoS ONE*, *8*(6). doi:10.1371/journal.pone.0067102

Swanson, K. v., Deng, M., & Ting, J. P. Y. (2019). The NLRP3 inflammasome: molecular activation and regulation to therapeutics. *Nature Reviews Immunology*, *19*(8), 477–489. doi:10.1038/s41577-019-0165-0

Takiue, Y., Hosoyamada, M., Kimura, M., & Saito, H. (2011). The effect of female hormones upon urate transport systems in the mouse kidney. *Nucleosides, Nucleotides and Nucleic Acids*, *30*(2), 113–119. doi:10.1080/15257770.2010.551645

Tannockl, I. F., Steele', D., & Roberts2, J. (1986). Influence of reduced concentration of L-glutamine on growth and viability of cells in monolayer, in spheroids, and in experimental tumours. *Br. J. Cancer* (Vol. 54).

Tedgui, A., & Mallat, Z. (2006). Cytokines in atherosclerosis: Pathogenic and regulatory pathways. *Physiological Reviews*, *86*(2), 515–581. doi:10.1152/physrev.00024.2005

Timmons, G. A., Carroll, R. G., O'Siorain, J. R., Cervantes-Silva, M. P., Fagan, L. E., Cox, S. L., … Curtis, A. M. (2021). The Circadian Clock Protein BMAL1 Acts as a Metabolic Sensor In Macrophages to Control the Production of Pro IL-1β. *Frontiers in Immunology*, *12*. doi:10.3389/fimmu.2021.700431

Tsuchiya, Y., Akashi, M., & Nishida, E. (2003). Temperature compensation and temperature resetting of circadian rhythms in mammalian cultured fibroblasts. *Genes to Cells*, *8*(8), 713–720. doi:10.1046/j.1365-2443.2003.00669.x

Vajjhala, P. R., Mirams, R. E., & Hill, J. M. (2012). Multiple binding sites on the pyrin domain of ASC protein allow self-association and interaction with NLRP3 protein. *Journal of Biological Chemistry*, *287*(50), 41732–41743. doi:10.1074/jbc.M112.381228

Wang, J., Li, S., Li, X., Li, B., Li, Y., Xia, K., … Wu, H. (2019). Circadian protein BMAL1 promotes breast cancer cell invasion and metastasis by up-regulating matrix metalloproteinase9 expression. *Cancer Cell International*, *19*(1). doi:10.1186/s12935-019-0902-2

Wang, S., Li, F., Lin, Y., & Wu, B. (2020). Targeting REV-ERBα for therapeutic purposes: Promises and challenges. *Theranostics*. Ivyspring International Publisher. doi:10.7150/thno.43834

Wang, S., Lin, Y., Yuan, X., Li, F., Guo, L., & Wu, B. (2018). REV-ERBα integrates colon clock with experimental colitis through regulation of NF-κB/NLRP3 axis. *Nature Communications*, *9*(1). doi:10.1038/s41467-018-06568-5

Wang, S., Lin, Y., Yuan, X., Li, F., Guo, L., & Wu, B. (2018). REV-ERBα integrates colon clock with experimental colitis through regulation of NF-κB/NLRP3 axis. *Nature Communications*, *9*(1). doi:10.1038/s41467-018-06568-5

Wang, X. L., Wolff, S. E. C., Korpel, N., Milanova, I., Sandu, C., Rensen, P. C. N., … Yi, C. X. (2020). Deficiency of the Circadian Clock Gene Bmal1 Reduces Microglial Immunometabolism. *Frontiers in Immunology*, *11*. doi:10.3389/fimmu.2020.586399

Welch, R. D., Billon, C., Valfort, A. C., Burris, T. P., & Flaveny, C. A. (2017). Pharmacological inhibition of REV-ERB stimulates differentiation, inhibits turnover and reduces fibrosis in dystrophic muscle. *Scientific Reports*, *7*(1). doi:10.1038/s41598-017-17496-7

Yang, J. W., Mao, B., Tao, R. J., Fan, L. C., Lu, H. W., Ge, B. X., & Xu, J. F. (2020). Corticosteroids alleviate lipopolysaccharide-induced inflammation and lung injury via inhibiting NLRP3-inflammasome activation. *Journal of Cellular and Molecular Medicine*, *24*(21), 12716–12725. doi:10.1111/jcmm.15849

Yang, L., Chu, Y., Wang, L., Wang, Y., Zhao, X., He, W., … Gao, C. (2015). Overexpression of CRY1 protects against the development of atherosclerosis via the TLR/NF-κB pathway. *International Immunopharmacology*, *28*(1), 525–530. doi:10.1016/j.intimp.2015.07.001

Yang, X., Downes, M., Yu, R. T., Bookout, A. L., He, W., Straume, M., … Evans, R. M. (2006). Nuclear Receptor Expression Links the Circadian Clock to Metabolism. *Cell*, *126*(4), 801–810. doi:10.1016/j.cell.2006.06.050

Yin, L., Wu, N., & Lazar, M. A. (2010). Nuclear receptor Rev-erbalpha: a heme receptor that coordinates circadian rhythm and metabolism. *Nuclear Receptor Signaling*. doi:10.1621/nrs.08001

Y-L So, A., Bernal, T. U., Pillsbury, M. L., Yamamoto, K. R., & Feldman, B. J. (2009). *Glucocorticoid regulation of the circadian clock modulates glucose homeostasis*.

Yu, D., Fang, X., Xu, Y., Xiao, H., Huang, T., Zhang, Y., … Gao, J. (2019). Rev-erbα can regulate the NF-κB/NALP3 pathway to modulate lipopolysaccharide-induced acute lung injury and inflammation. *International Immunopharmacology*, *73*(May), 312–320. doi:10.1016/j.intimp.2019.04.035

Zhang, W. Z. (2021). Why does hyperuricemia not necessarily induce gout? *Biomolecules*, *11*(2), 1–11. doi:10.3390/biom11020280

Zheng, S. C., Zhu, X. X., Xue, Y., Zhang, L. H., Zou, H. J., Qiu, J. H., & Liu, Q. (2015). Role of the NLRP3 inflammasome in the transient release of IL-1β induced by monosodium urate crystals in human fibroblast-like synoviocytes. *Journal of Inflammation (United Kingdom)*, *12*(1), 4–12. doi:10.1186/s12950-015-0070-7